CR-167909

HUGHES

HUGHES AIRCRAFT COMPANY

ELECTRON DYNAMICS DIVISION

3100 West Lomita Boulevard, Torrance, California 90509, Tel 517-6000, TWX 910-347-7321

W-09170

FINAL REPORT

PYROLITIC GRAPHITE COLLECTOR DEVELOPMENT PROGRAM

CONTRACT NO. NAS3-22505

PREPARED FOR

NATIONAL AERONAUTICS AND SPACE ADMINISTRATION
LEWIS RESEARCH CENTER
CLEVELAND, OHIO 44135

FEBRUARY 1982

HUGHES AIRCRAFT COMPANY
ELECTRON DYNAMICS DIVISION
3100 WEST LOMITA BOULEVARD
P.O. BOX 2999
TORRANCE, CALIFORNIA 90509

FINAL REPORT

PYROLITIC GRAPHITE COLLECTOR DEVELOPMENT PROGRAM

CONTRACT NO. NAS3-22505

FEBRUARY 25, 1982

Prepared by: W. J. Wilkins

W. J. Wilkins
Project Manager

Approved by: J. A. Christensen

J. A. Christensen, Manager
Power Tube Department

HUGHES AIRCRAFT COMPANY
ELECTRON DYNAMICS DIVISION
3100 WEST LOMITA BOULEVARD
TORRANCE, CALIFORNIA 90509

UNCLASSIFIED

SECURITY CLASSIFICATION OF THIS PAGE (When Data Entered)

REPORT DOCUMENTATION PAGE		READ INSTRUCTIONS BEFORE COMPLETING FORM
1. REPORT NUMBER CR 167909	2. GOVT ACCESSION NO.	3. RECIPIENT'S CATALOG NUMBER
4. TITLE (and Subtitle) Final Report Pyrolytic Graphite Collector Development Program		5. TYPE OF REPORT & PERIOD COVERED Final 6. PERFORMING ORG. REPORT NUMBER W-09170
7. AUTHOR(s) William J. Wilkins		8. CONTRACT OR GRANT NUMBER(s) NAS3-22505
9. PERFORMING ORGANIZATION NAME AND ADDRESS Hughes Aircraft Company Electron Dynamics Division 3100 West Lomita Blvd., P.O. Box 2999 Torrance, California 90509		10. PROGRAM ELEMENT, PROJECT, TASK AREA & WORK UNIT NUMBERS
11. CONTROLLING OFFICE NAME AND ADDRESS NASA Lewis Research Center (Code 6241) 21000 Brookpark Road Cleveland, Ohio 44131		12. REPORT DATE February 25, 1982 13. NUMBER OF PAGES
14. MONITORING AGENCY NAME & ADDRESS(if different from Controlling Office)		15. SECURITY CLASS. (of this report) UNCLASSIFIED 15a. DECLASSIFICATION/DOWNGRADING SCHEDULE N/A

16. DISTRIBUTION STATEMENT (of this Report)

17. DISTRIBUTION STATEMENT (of the abstract entered in Block 20, if different from Report)

18. SUPPLEMENTARY NOTES

19. KEY WORDS (Continue on reverse side if necessary and identify by block number)

Pyrolytic Graphite
Multistage Depressed Collector Electrode

20. ABSTRACT (Continue on reverse side if necessary and identify by block number)

Pyrolytic graphite promises to have significant advantages as a material for multistage depressed collector electrodes. Among these advantages are lighter weight, improved mechanical stiffness under shock and vibration, reduced secondary electron back-streaming for higher efficiency, and reduced outgassing at higher operating temperatures.

This report discusses the essential properties of pyrolitic graphite and the necessary design criteria for its use in MDC's. This includes the study of

DD FORM 1 JAN 73 1473 EDITION OF 1 NOV 65 IS OBSOLETE

UNCLASSIFIED

SECURITY CLASSIFICATION OF THIS PAGE (When Data Entered)

suitable electrode geometries and methods off attachment to other metal and ceramic collector components consistent with typical electrical, thermal, and mechanical requirements.

Electron Dynamics Division
3100 West Lomita Boulevard

ABSTRACT

Pyrolytic graphite promises to have significant advantages as a material for multistage depressed collector electrodes. Among these advantages are lighter weight, improved mechanical stiffness under shock and vibration, reduced secondary electron back-streaming for higher efficiency, and reduced outgassing at higher operating temperatures.

This report discusses the essential properties of pyrolitic graphite and the necessary design criteria for its use in MDC's. This includes the study of suitable electrode geometries and methods off attachment to other metal and ceramic collector components consistent with typical electrical, thermal, and mechanical requirements.

TABLE OF CONTENTS

LIST OF ILLUSTRATIONS

LIST OF ILLUSTRATIONS (CONTINUED)

LIST OF ILLUSTRATIONS (CONTINUED)

LIST OF ILLUSTRATIONS (CONTINUED)

LIST OF TABLES

1.0 INTRODUCTION

This report is prepared by the Electron Dynamics Division (EDD) of Hughes Aircraft Company (HAC) for submission to National Aeronautics and Space Administration (NASA) Lewis Research Center, (LRC), Cleveland, Ohio, in accordance with Contract NAS 3-22505. It contains information related to the development of necessary mechanical, thermal and fabrication processes for a pyrolytic graphite (PG) multistage depressed collector (MDC).

Pyrolytic graphite promises to have significant advantages as a material for multistage depressed collector electrodes. Among these advantages are lighter weight, improved mechanical stiffness under shock and vibration, reduced secondary electron back-streaming for higher efficiency, and reduced outgassing at higher operating temperatures. Successful utilization of pyrolytic graphite in collectors could improve the power, efficiency, weight, heat dissipation of future microwave transmitters. Some European companies have already developed pyrolytic graphite collectors under government funded contracts. Figure 1.0-1 shows a pyrolytic graphite specimen shaped like a typical MDC electrode.

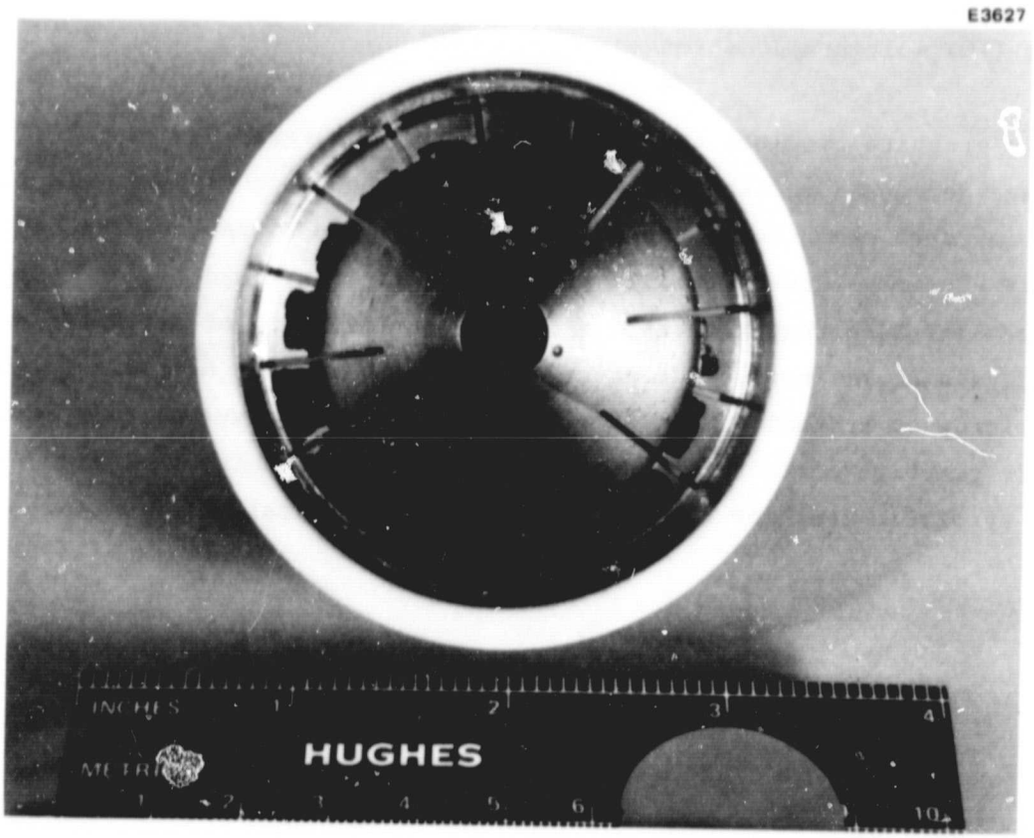

Figure 1.0-1 Pyrolytic graphite electrode assembly.

2.0 THERMAL/MECHANICAL DESIGN

2.1 BACKGROUND

Improved traveling wave tube (TWT) efficiency can be realized by implementing multistage collector electrodes depressed to different voltages. Conduction and liquid cooled TWT multistage collectors, traditionally contain copper electrodes isolated from ground potential by ceramic. The entire assembly is brazed together for optimum heat conduction from the electrode to the outside surface of the collector.

Reference 2.3-29 describes a space TWT used in a commercial communications satellite utilizing a collector cooled by radiation. Hughes EDD has produced space qualified tubes with this type of collector. The radiation-cooled collector contains molybdenum electrodes clamped together which radiate to the inside surface of the collector can, which in turn radiates to deep space on its outside surface. This type of collector is not brazed and thus avoids the internal stresses produced as a result of brazing.

These two styles of internal collector cooling offer their own unique advantages and disadvantages in construction, operation and reliability. These questions will be covered in the discussions on the technical and manufacturing feasibility of the two design concepts. The two collector types were designed for maximum reliability by minimizing operating temperatures and mechanical stresses inherent in their different construction. The paramount effort of this study was to compare the two styles of design in the area of reliability.

Improved TWT efficiency can be realized by reducing secondary electron emission from the electrodes in addition to having a multistage collector. Reference 2.3-28 investigated the use of low molecular weight materials such as carbon to achieve reduced secondary electron emission. References 2.3-35 and 2.3-36 report on the two different collector approaches, one using internal conduction and the other using internal radiation, on 12 GHz broadcast TWT's utilizing low molecular weight collector electrodes.

The leading candidate for a low electron emission electrode is pyrolytic graphite. This material has excellent thermal conductivity in one direction as well as being much stronger than other carbon materials. Pyrolytic graphite was investigated for both mechanical and thermal capacities in both types of collector designs.

The overall intent of the thermal and mechanical evaluation of the multistage collector with low secondary emission is to assure its reliability over its expected life. Hughes EDD has vast experience with both types of multistage collector design and analysis. Structural and thermal computer programs using material properties obtained during the research program were the key tool in evaluating the optimum collector design.

2.2 TYPICAL MDC CONCEPTS

This task surveyed different conceptual designs which would incorporate low secondary electron emission electrodes in an MDC. The study examined two different configurations, attachment schemes, and material selections to assure that the optimum design is not overlooked. Each concept was judged according to the criteria established in Task 3 (See Figure 2.2-1). This evaluation considered and emphasized ease of manufacture, structural and thermal integrity of the design, and cost. From this evaluation, a list of potentially viable solutions was generated along with a qualitative estimate of the relative promise of each design. This listing provides a meaningful guide to all subsequent tasks. Specific areas of investigation were limited to concepts directly related to one of the candidate design. This assisted in unifying all tasks and aided in completing the total effort in a timely and cost effective manner.

EDD proposed as a prime candidate for the final MDC design the all-brazed collector design as shown in Figure 2.2-2. This design is compatible with liquid, air, conduction and radiation cooling systems. The main structural member and vacuum barrier is a thin metallic outer can. The internal electrodes are insulated from this can by brazed alumina ceramic pieces. These insulators are circular arc segments rather than complete rings to reduce potentially high brazing stresses yet maintain a maximum contact area with the electrodes for

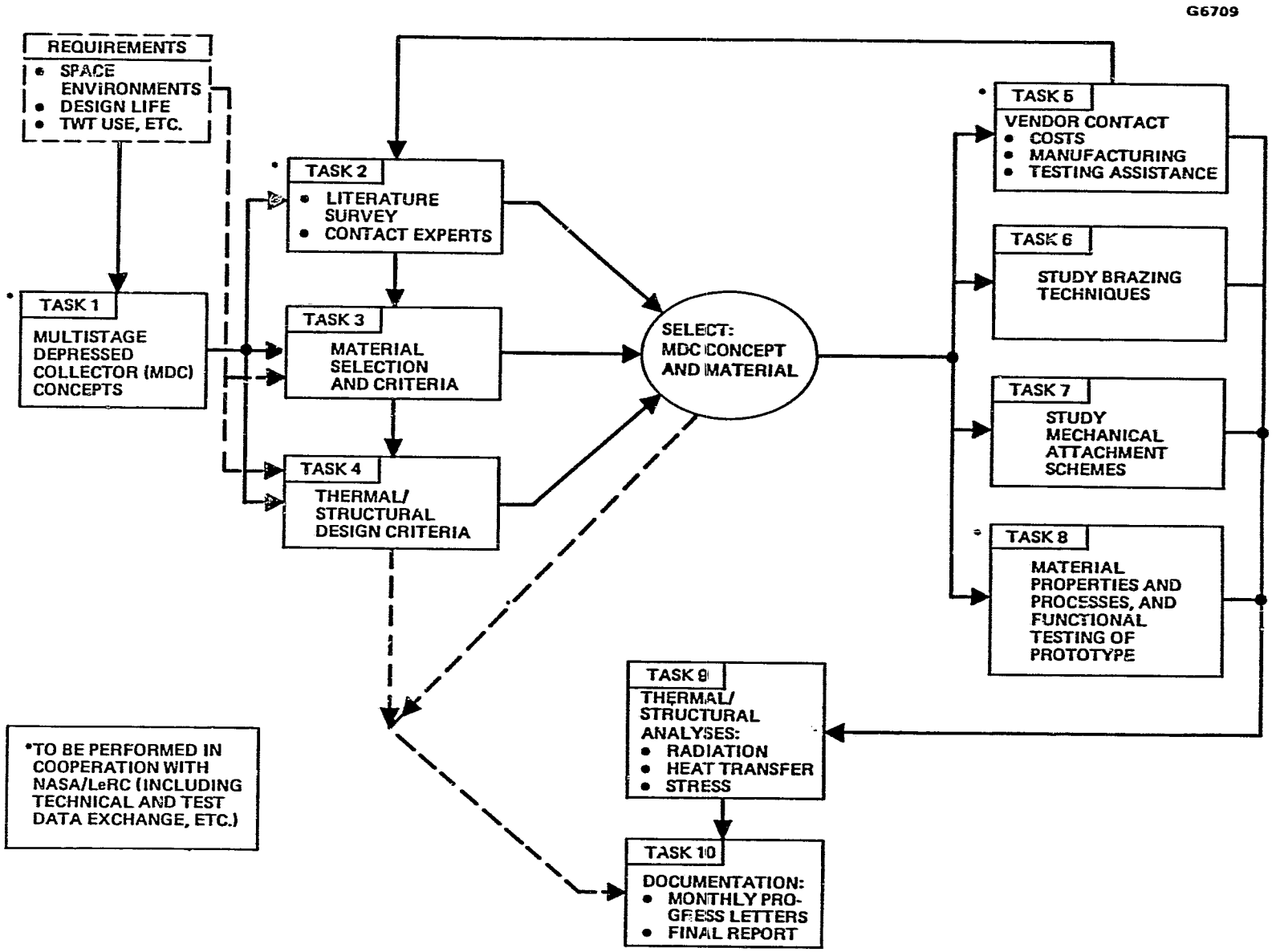

Figure 2.2-1 Flowchart of EDD proposed tasks and inter-relationships.

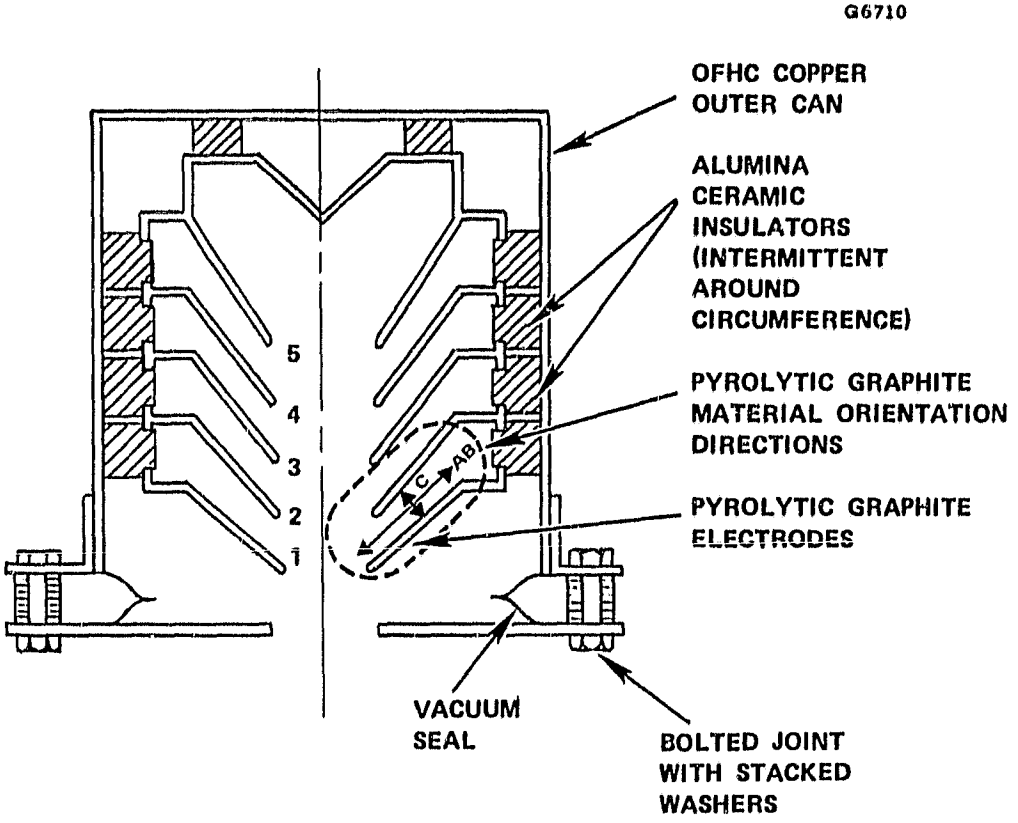

Figure 2.2-2 EDD proposed multistage depressed collector study configuration, using pyrolytic graphite electrodes.

optimum heat transfer. The spacing between the electrodes is controlled by the precision ground ceramics.

For radiation cooled applications heat conduction back into the TWT from the collector is inhibited by the stacked washer joint, and the wishbone-shaped vacuum seal. The multiple contact interfaces in the bolted joint insures high thermal impedance to any heat wanting to travel through it. The required vacuum seal is comprised of two thin, brazed, metallic rings. The thinness of the pieces and relatively long radial distance makes this a good thermal choke.

MDC cooling can also be accomplished via forced air or liquid flowing over the ground metal can or by conduction to a heat sink.

2.3 LITERATURE SURVEY

An extensive literature survey was conducted by HEDD. The intent was to summarize state-of-the-art knowledge about the thermostructural behavior of various graphites, with particular attention to pyrolytic graphite (PG). Results of this survey will be summarized in Sections 2.4 and 2.5, which formulated the material selection criteria and thermostructural design criteria. Over forty technical reports, vendor brochures and technical papers were examined.

The principal data banks on graphites (including PG) in the U.S. are concentrated in the following organizations (and their key individuals):

Organization	Address and Phone	Contact(s)
1. Aerospace Corporation	P.O. Box 92957 Los Angeles, CA 90009 (213) 648-5897	Dr. R.A. Meyer Dr. J.D. Buch Dr. D.J. Chang Dr. J.L. White E.Y. Robinson J.E. Zimmer J.D. McClelland
2. PDA Engineering	1740 Garry Ave. Suite 201 Santa Ana, CA 92705 (714)556-2800	Dr. J. Greg Crose Dr. E.L. Stanton

3.	Southern Methodist University Civil Mechanical Engineering Dept.	Dallas, Texas 75275	Dr. R.M. Jones
4.	Science Applications, Inc.	18872 Bardeen Ave. Irvine, CA 92715 (714) 955-3130	Dr. W.C. Loo Julius Jortne K.M. Kratsch
5.	Southern Research Institute (S.R.I.)	Birmingham, AL 35205	H. Stuart Starre Colt D. Pears
6.	Weiler Research, Inc.	2675 Bayshore Frontage Road, Suite 524 Mountain View, CA	Dr. Frank C. We
7.	Air Force Materials Laboratory (AFML)	Wright-Patterson Air Force Base, Ohio 45433	Dr. Nick J. Porg Dr. Stephen W. Ts
8.	Aerotherm Division Acurex Corporation	485 Clyde Ave. Mountain View, CA 94042	D.L. Baker
9.	Naval Surface Weapons Center (NSWC)	White Oak Laboratory, CA-43 Silver Spring, MD 20910	Dr. R. Edward R. Feldhuhn
10.	Oak Ridge National Lab (ORNL)	P.O. Box X Oak Ridge, TN 37830	W.P. Eatherly G.M. Slaughter D.A. Canonico R.G. Donnelly N.C. Cole
11.	General Electric Co., RESD	P.O. Box 8555 Philadelphia, PA 19101	K.J. Hall A. Levine R. Everswle
12.	Ford Aerospace & Communications Corp.	Ford Road Newport Bch., CA 92663	J. Perry
13.	Super Temp Operations, B.F. Goodrich	11120 S. Norwalk Blvd. Santa Fe Springs, CA 90670 (213) 944-6244	Don H. Leeds Betty J. Wood

This list of names resembles a "Who's Who in the U.S. Reentry Vehicle Technology". This fact is not surprising, since much of the current data base on graphite and carbon/carbon materials was generated for various nosetip programs in the past twelve years. Certainly, among this group of organizations and individuals, they know almost everything that is to be known about the material characterization, thermostructural analyses, and manufacturability of various graphites. Many of these individuals were contacted, and they referred us to hundreds of reports on graphites -- many of limited use and applicability for the NASA LeRC/HEDD multistage depressed collector (MDC) program. HEDD felt it would be more appropriate to review some of this information, summarize key material concepts and features, and note some important factors to be considered in the material solution criteria and thermostructural design criteria. Needless to say, this report is a beginning toward a better understanding of the proper use of graphite-type materials in TWT collectors.

Part of the literature surveyed is contained in References 2.3-1 to 2.3-35. The best up-to-date summary of various thermal and mechanical properties of graphite is Buch (Reference 1). It compares the properties of pyrolytic graphite against many other carbon and graphitic materials. Many of these comparative charts will be given in Task 3. The best report on nonlinear multiaxial modeling of graphitic and carbon-carbon materials is Jones (Reference 5), co-developer of the so-called Jones-Nelson model. ATJ-S is probably the best characterized graphite material (References 2.3-1, 2.3-4, 2.3-5, 2.3-6, 2.3-7, 2.3-9, 2.3-10, 2.3-11, 2.3-12). Like PG, ATJ-S is "transversely isotropic", meaning it has the same properties in every direction in the ab-plane, but different properties in the transverse c-direction. The organization which has performed the most comprehensive testing on carbon and graphite materials is Southern Research Institute (So. R.I.) in Birmingham, Alabama (References 2.3-7, 2.3-10). Among all the companies listed in the preceding table, two - Aerospace Corporation and PDA Engineering - probably possess the most extensive experience in the understanding of the carbon/graphite materials and their thermostructural analyses. The best and most comprehensive reference on PG is Reference 2.3-13 from Super-Temp (along with their two related brochures, References 2.3-14 and 2.3-15).

Some general comments can be made about our search for properties for graphites, and about PG in particular:

- Much is known about their thermal and mechanical properties.

- Very little (to nothing) is known about their electrical properties, including secondary electron emission characteristics.

- Nothing was found about the brazing of PG to ceramics and metals. Some work at ONRL on brazing graphite to ceramic (References 2.3-17, 2.3-18) have been encouraging.

- The general consensus of the experts was that for the temperature encountered in TWT collectors, PG electrodes should easily survive the thermal stresses, strains, and vibration environments with no problems. Their consensus advice was to concentrate all our attention on the PG-ceramic joint -- brazed, mechanical attachment, metal gaskets, silicon carbide alloying, etc. One expert (Dr. Crose at PDA) suggested using outside and inside carbon-carbon rings which are shrink-fit together to clamp the PG-ceramic joint and effect a vacuum seal.

Many people have compared the graphite family of materials to an undisciplined but extremely gifted child. It has the potential to accomplish things which no other material would even attempt, but is always getting into trouble. The real problem, with graphite as with the child, is not that they are bad; it's that nobody seems to understand them. Graphites, much like elastomeric potting compounds in TWTs, may serve their functions well - if the designer knows their capabilities and limitations, and uses them properly.

2.4 MATERIAL SELECTION CRITERIA AND ANALYSIS

2.4.1 Graphite Materials - General

Carbon materials and concepts may be generically classified as shown in Figure 2.4-1 (Reference 2.3-1). All carbon and graphitic materials contain flaws, cracks, impurities, in addition to the basically anisotropic behavior. We must first define some important mechanical (structural) data in order to differentiate among different graphitic materials. Reference 2.3-10 contains a list of such variables and their units (Table 2.4-1). Even though some of the properties included in Table I are necessary only for nosetip thermostructural and ablation analyses, the table serves the purpose of pointing out important properties and their use in material selection.

For graphitic materials, the biaxial tensile strength (rather than uniaxial) is important, as well as the failure strain. Needless to say, for thermal stress problems, the coefficient of thermal expansion (d) - which will be different in different directions - is exceedingly important to know. The density (p) is needed to compute thermal, mechanical, and vibrational response. For steady-state thermal conduction, we need to know the thermal conductivity (k). For transient thermal response, we also need the specific heat (Cp). TWTs are subjected to continuous thermal cycling during their 10-year design life. Graphitic materials are usually brittle, but also exhibit nonlinear stress-strain behavior. Unfortunately, no information exists on fatigue strength (especially under thermal loads) for PG and other graphites. For thermal stress analysis purposes, some order of priority can be assigned to the data required in the analysis:

Structural Data		Thermal Data	
Elastic modulus*			
(as function of temperature)	1	Thermal conductivity	1
Coefficient of thermal expansion	1	Emissivity	2
Poisson's ratio	2	Specific heat	2
Shear modulus	2		
Strain to failure	1		

*May be different for tension and compression! (Number indicates the order of priority for data accuracy)

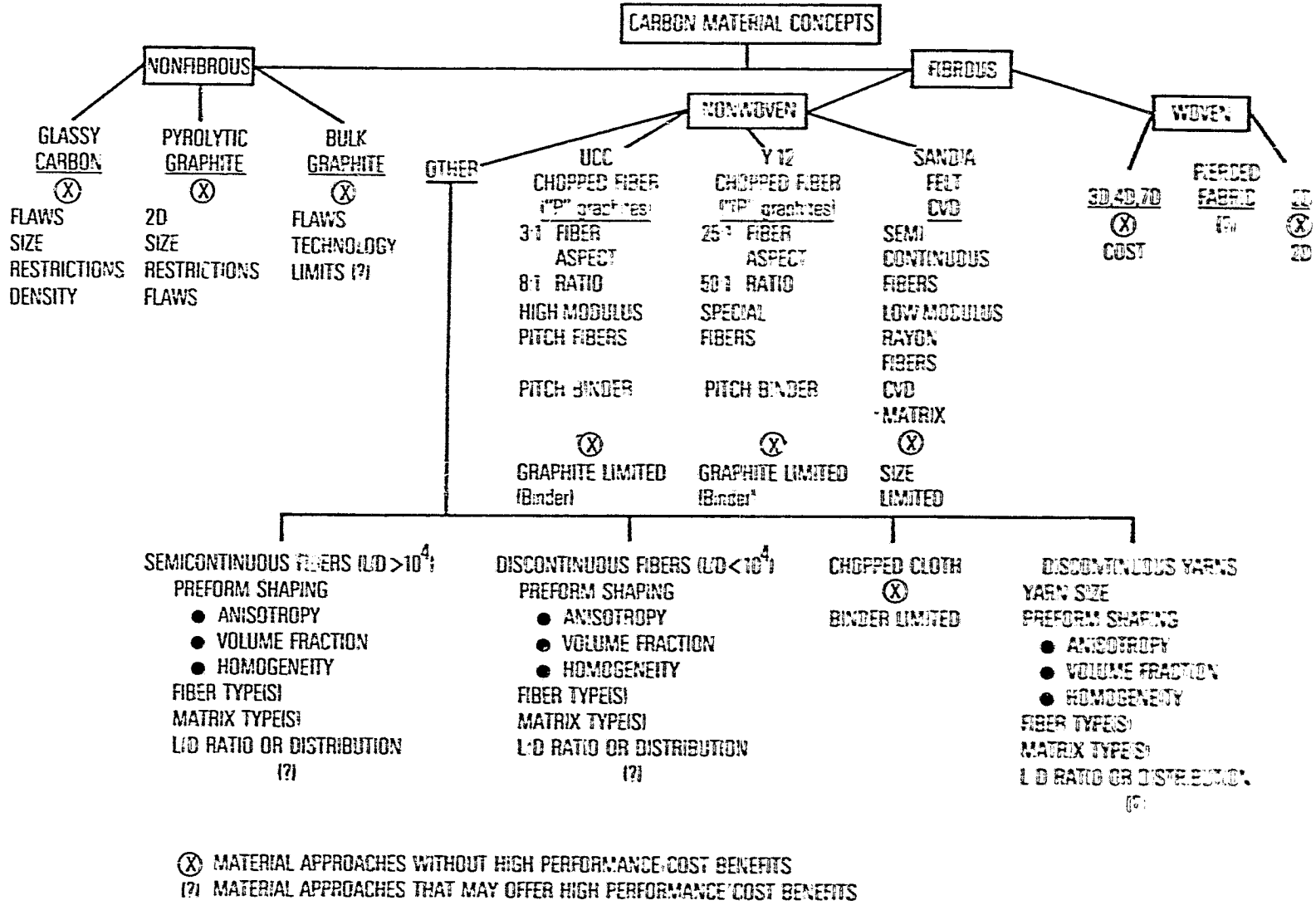

Figure 2.4-1 Carbon material concepts.

TABLE 2.4-1

DESIGN DATA MATRIX

Property	Symbol	Unit	Use
Mechanical (Structural) Data			
Elastic Constants determined under tensile compression and shear loading.	See Appendix C for symbol and unit.		Prediction of stress state of a deformed body, i.e., thermal stress prediction. Shell/ring structural response to special effects environment. Normal to surface stress wave analyses.
Strength tensile and compressive loading - tensile strength important	σ_{ult}	psi	Used in failure criteria to compare predicted thermal stress levels with actual loading capability of material.
Biaxial Tensile Strength	-	psi	Used in failure criteria.
Failure strain tensile loading	ε_{ult}	percent	Used in failure criteria to compare predicted thermal strain levels with actual total strain capability of material. Used in assessing maximum allowable inpulse, for ring capability

TABLE 2.4-1 (Continued)

Property	Symbol	Unit	Use
Thermal Expansion Coefficient in symmetry defined direction.	α	in./in./^{o}F	Predictions of thermal stress state of body Shell/Ring structural response to special effects environment. Used as part of Gruneisen constant (as volume thermal expansion coefficient) in normal to surface stress wave analyses
Thermal Property Data			
Density	ρ	lb/ft^3	Computation of thermal response, transient mechanical, vibrational, weapons effects, ablation mass loss, and heat of ablation.
Thermal Conductivity	k	Btu/ft-sec-F^{o}	Computation of the temperature distribution for thermal protection and thermal gradient for thermostructural response, affects material-environment thermal balance.
Specific Heat	Cp(t)	Btu/lb-F^{o}	Computation of transient re-entry heating thermal response and heat soak thermal response to special environment.

TABLE 2.4-1 (Continued)

Property	Symbol	Unit	Use
Emittance	$\varepsilon_H(t)$	(dimension less)	
Total Hemispherical			Computation of total re-radiated heat flux ($\varepsilon_H T_S 4$) from surface of vehicle by use of computed surface temperature T_S
Spectral Emittance (Normal)	$\varepsilon(\lambda, \tau)$		Computation of radiated flux at each wavelength interval (for IR signature analysis) or absorbed radiation from boundary layer; angular dependence can be estimated if not available but can be a sensitive function of surface condition and roughness.
Graphite Thermal Modeling Properties			
Vapor Pressure	P_V	$lb/in.^2$	A key parameter which affects the rate of ablation; may appear in analytical model describing ablation process.
Heat of Ablation	Q^+	Btu/lb	A defined expression used to measure ablation resistance; will appear in some form in analytical model.

TABLE 2.4-1 (Continued)

Property	Symbol	Unit	Use
Ablation Species	(Chemical symbols)		An analytical model: where identified, these can contribute to boundary layer species; provide a more realistic model.
Boundary Layer Species	(Chemical symbols)		Used in analytical model to relate material performance to boundary layer heating environment; may include species ablating from specimen
Ablation Test Data			
Surface Roughness	Δ_X	microinches	Decisive information required in applying mechanical erosion analytical model to a given material.
Model Dimensions	X	inches	Fundamental data required to generate analytical results in predictive model.
Filler/Binder Ratio	Expressed as percentage		An input to thermomechanical erosion model. To this end filler and binder may be specified in order to obtain ratio.

TABLE 2.4-1 (Continued)

Property	Symbol	Unit	Use
Surface Temperature	T_S	^oR	Basic data; can be used to compare with predictions or may be used as input in appropriately modified analytical models.
Surface Recession	S	in./sec $lb/sec-ft^2$	Basic information for generating heats of ablation. Intimately related to the analytical predictions.
Internal Temperatures	T_y	^oR	Internal temperature response is useful to compare to analytical prediction, to generate some thermal property data and to serve as input in modified analytical models.
Dimensional Growth	ΔS	inches	Although not presently incorporated into analytical models, its presence must be assessed in order to correctly interpret recession and apply it to the analytical model.
Shape Change History			Shape changes can drastically alter the interactions between material and environment. Characteristics of shape change must be considered in analysis.

TABLE 2.4-1 (Continued)

Property	Symbol	Unit	Use
Test Time	t	sec	Considered with recession, serves as one method of determining heat of ablation.
Heat Transfer Rate (cold wall)	q_{cw}	Btu/sec-ft^2	Normally measured in testing, this is a basic input to analytical models.
Heat Transfer Rate Distribution		Btu/sec-ft^2	Frequently useful as a contributor to shape change, this data may be applied to the analytical model
Model Stagnation Pressure	P_S	Atmos, lb/in^2	Basic information required to properly evaluate material performance with analytical model
Stagnation (Recovery) Enthalpy	h_s or h_r	Btu/lb	A basic parameter in the analytical model, it is determined experimentally from other data.
Mass Flow Working Medium	m	lb/sec	Experimental parameter often used for calculating heat of ablation. Also useful in assessing flow as laminar, turbulent.

TABLE 2.4-1 (Continued)

Property	Symbol	Unit	Use
Flow Area at Model	A	$m^2 ft^2$	An experimental facility consideration useful only when comparing theoretical prediction with experiment
Exit Pressure	P_e	$lb/in.^2$	Important in calculating experimental flow properties when relating theory to experiment

If one uses a margin of safety criterion, it has been shown by many researchers performing sensitivity analyses that the most sensitive thermal stress influencing parameters are elastic modulus, thermal expansion coefficient, and thermal conductivity with strain to failure as the comparator. An alternate way to show the different sensitivity relationships is given in Figures 2.4-2, 2.4-3, and 2.4-4 (Reference 2.3-10). Therefore, for graphitic materials, it is important to know the minimum strain to failure very accurately. Note also that for graphite materials, the compressive modulus is usually lower than the tensile modulus. Any finite element code used for the thermostructural analysis must be able to account for this material nonlinearity. Experience in testing many types of graphites has shown that, due to wide data scatter and the omnipresent microcracks, flaws, and nodules, it is prudent to use a factor of safety of 2. This means that any calculated stress or strain should be multiplied by 2 before it is compared against the ultimate stress or the failure strain to obtain a margin of safety.

Most graphites have a density in the range of 1.70-1.91 g/cc. However, pyrolytic graphite has a density of 2.20 g/cc. This compares with the density of OFHC copper of 9.08 g/cc. PG is thus about one-fourth as heavy as OFHC copper.

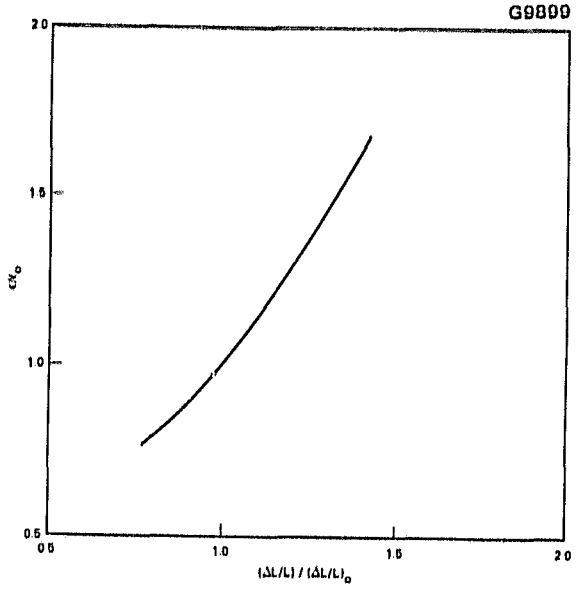

Figure 2.4-2 Sensitivity of thermal strain to thermal expansion ($\Delta L/L$).

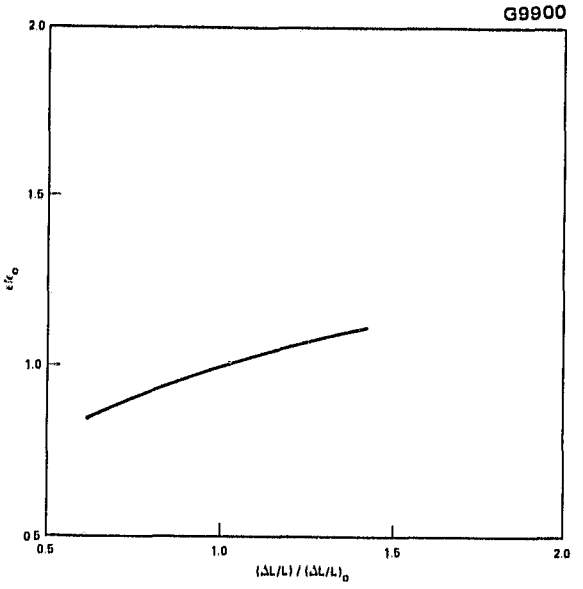

Figure 2.4-3 Sensitivity of thermal strain to modulus.

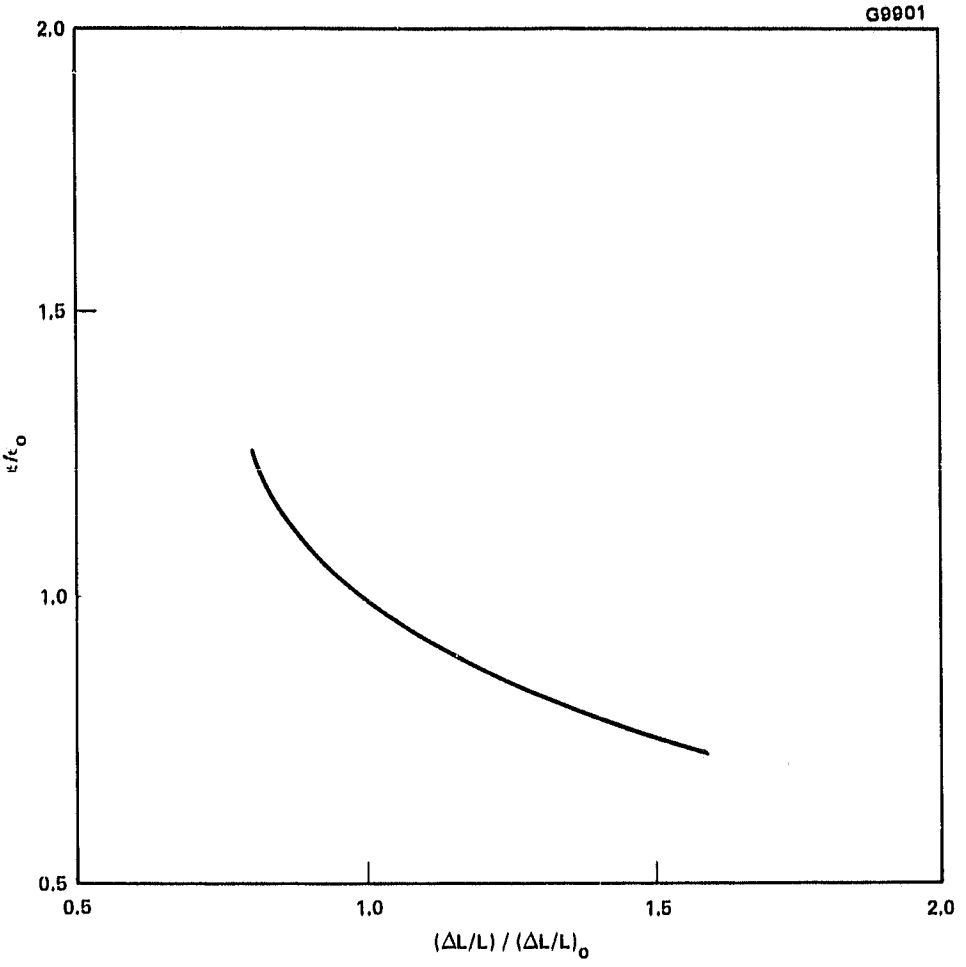

Figure 2.4-4 Sensitivity of thermal strain to conductivity.

2.4.2 Comparison of PG and Other Carbon and Graphitic Materials

Buch (Reference 2.3-1) presents the most comprehensive property-by-property comparison of PG to other carbon and graphite materials:

	Fig.
• Volumetric thermal expansion	2.4-6
• PG anisotropy of thermal expansion vs. temperature	2.4-7
• ATJ-S and 994-2 of thermal expansion vs. temperature	2.4-8
• Glastic modulus vs. temperature for a 3-D carbon composite and a bulk graphite	2.4-9
• Relative stiffness (modulus) vs. temperature in several carbon composites and graphites	2.4-10
• Relative moduli of PG vs. temperature	2.4-13
• Elastic anisotropy vs. temperature for PG and a bulk graphite	2.4-14
• Elastic modulus vs. temperature for isotropic and moderately anisotropic carbon forms	2.4-15
• Free thermal expansion (1500°C) vs. elastic modulus (25°C) for carbon forms	2.4-19
• Free thermal expansion (2750°C) vs. elastic modulus (25°C) for carbon forms	2.4-20
• Free thermal expansion (2750°C) vs. elastic modulus (2750°C) for carbon forms	2.4-21
• Free thermal expansion (2000°C) vs. elastic modulus (25°C) for UCC chopped fiber-based graphites and other carbon forms	2.4-22
• Free thermal expansion (2750°C) vs. failure strain (25°C) for various carbon forms	2.4-23
• Load vs. crack openning for pre-cracked four-point bonding of graphites and carbon composites	2.4-28

Although all these plots are not all directly relevant to our study, they present a clear picture of PG properties versus other carbon forms. Some of Buch's comments in his comprehensive study are interesting. The volumetric thermal expansion (Figure 2.4-5) represents three times the average linear thermal expansion (irrespective of direction), and illustrates that the microstructural arrangement of the graphite drystals play a dominant role in this 25-1500°C temperature range. Note that PG ranks very highly in this parameter (about 4.4%), nearly as much as the pure graphite single crystal. The tendency of highly ordered forms of carbon (e.g. PG) to exhibit isotropy with elevated temperatures will be reinforced with elastic moduli data.

For thermostructural applications, the major factor is the temperature dependence of the elastic modulus in determining the resulting thermochcmical strains. The elastic anisotropics of the continuously nucleated and substrate nucleated forms of PG (Figure 2.4-11) shw that PG tends to isotropic elastic behavior at very high temperatures.

For thermostructural loadings, the dominant failure variable is strain, and the emphasis should be on relatively low temperature failure strain. PG, in the plane of deposition, is a low expansion material with low failure strain (Figure 2.4-17). Taken as a class of materials, the carbon forms presented exhibit approximately a 2:1 ratio of thermal expansion to failure strain. PG shows a 3:1 ratio. Buch concludes that "there is an unavoidable correlation between the free thermal strain (expansion) and failure strain of all carbon forms."

In regard to crack propagation, crack and defect tolerance, Buch states that "at present, there are insufficient data and/or thecretical models to predict the crack propagation characteristics of carbon-based composites as a general class. There are no concise design approaches to treating the significances of crack propagation characteristics."

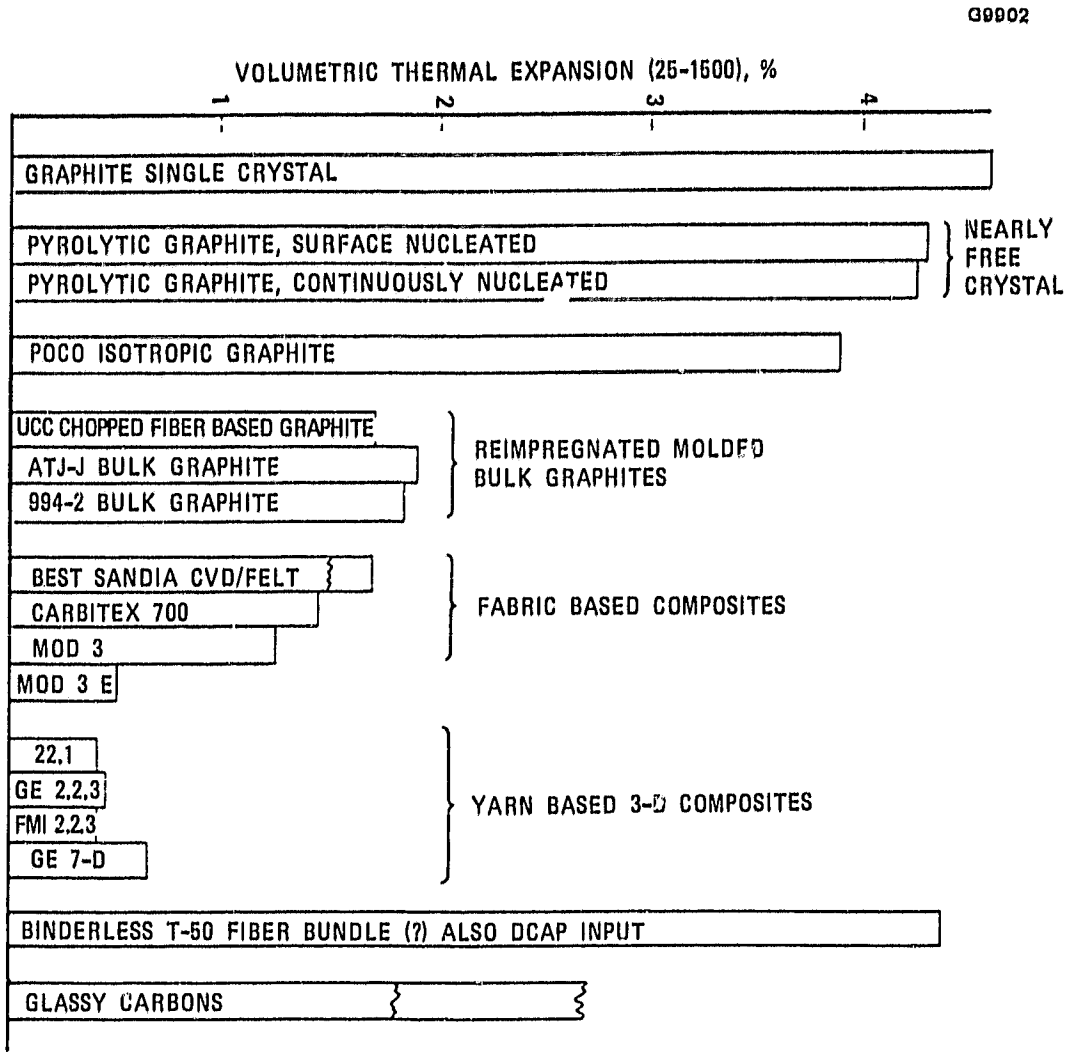

Figure 2.4-5 Volumetric thermal expansions (25-1500C) for various carbon forms.

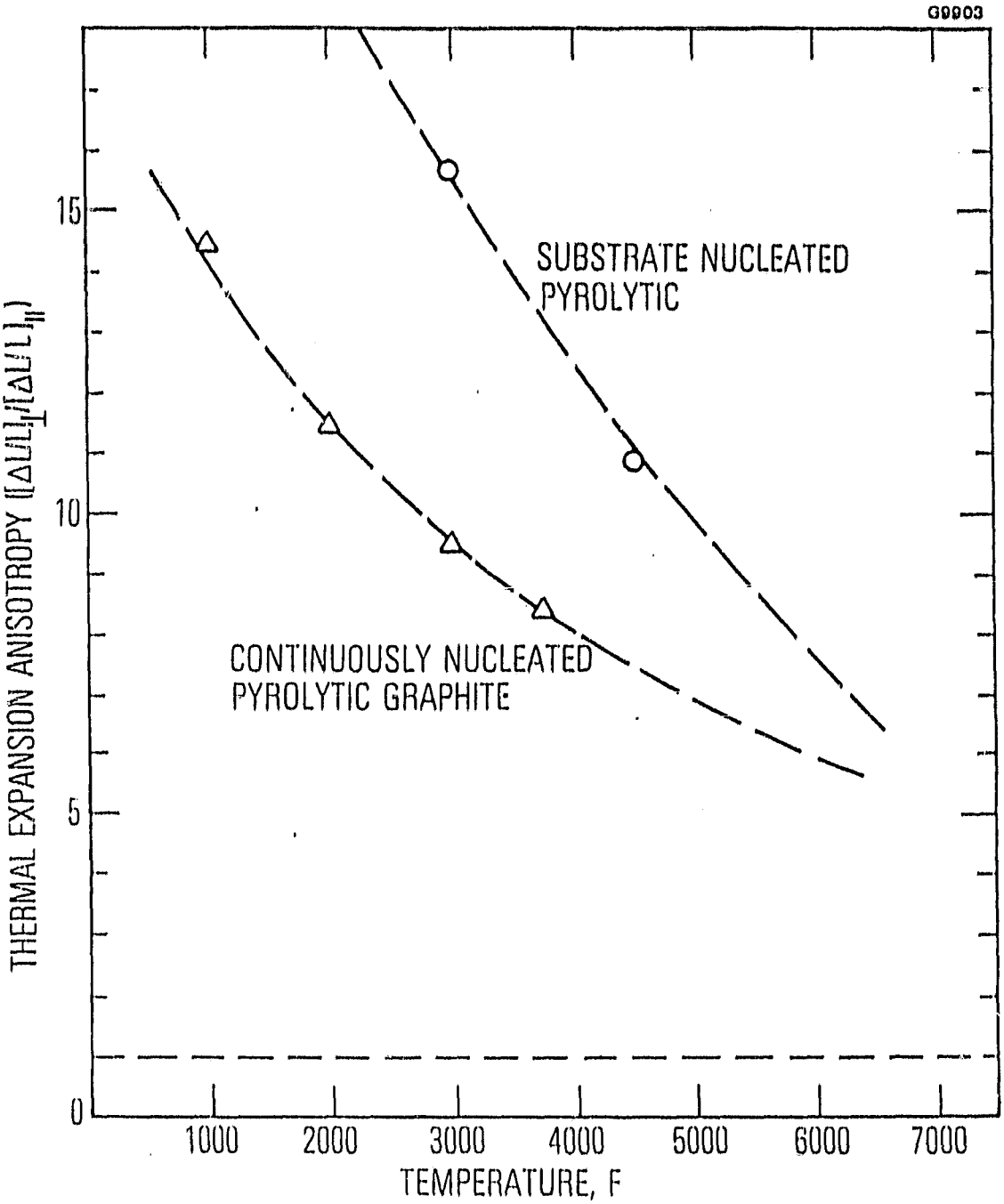

Figure 2.4-6 Anisotropy of thermal expansion vs temperature for pyrolytic graphics.

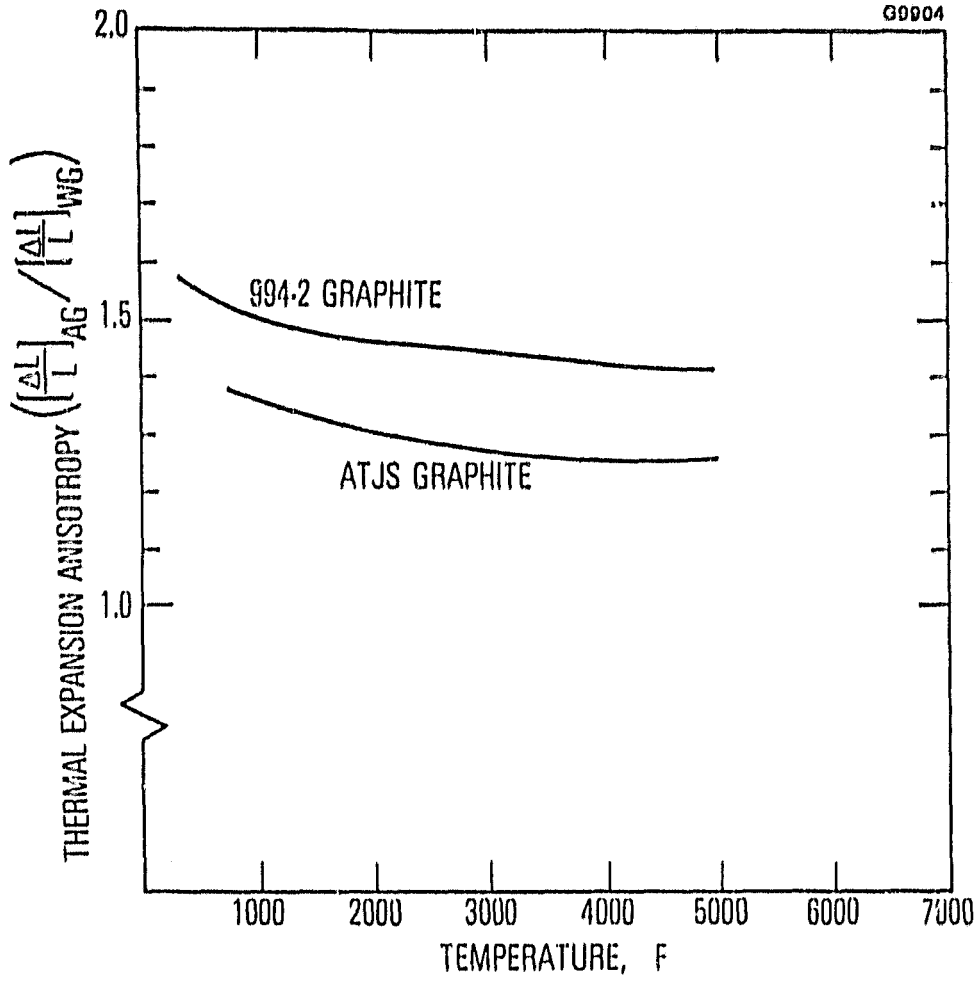

Figure 2.4-7 Anisotropy of thermal expansion vs temperature for bulk graphites.

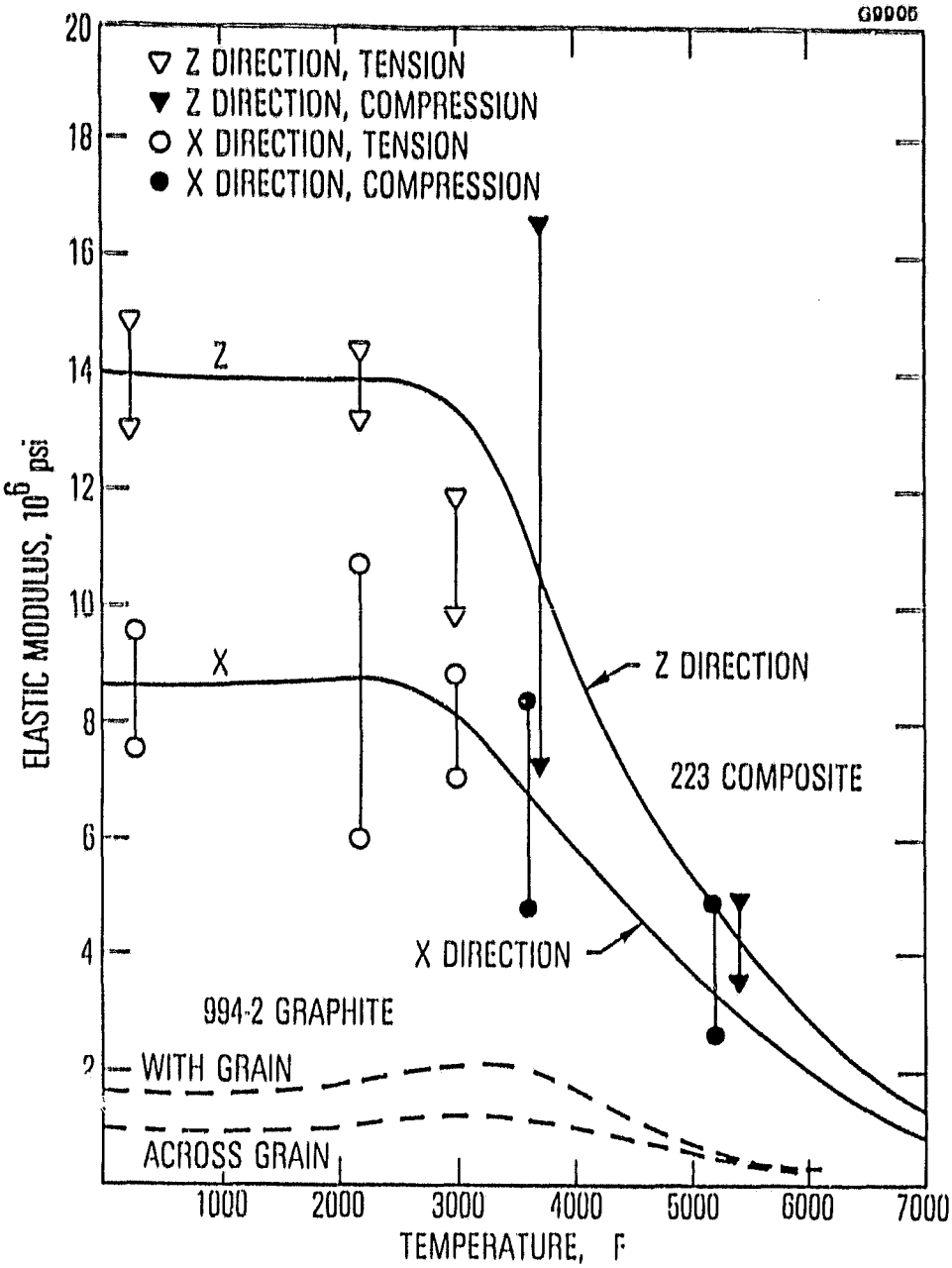

Figure 2.4-8 Elastic modulus vs temperature for a 3-D carbon composite and a bulk graphite.

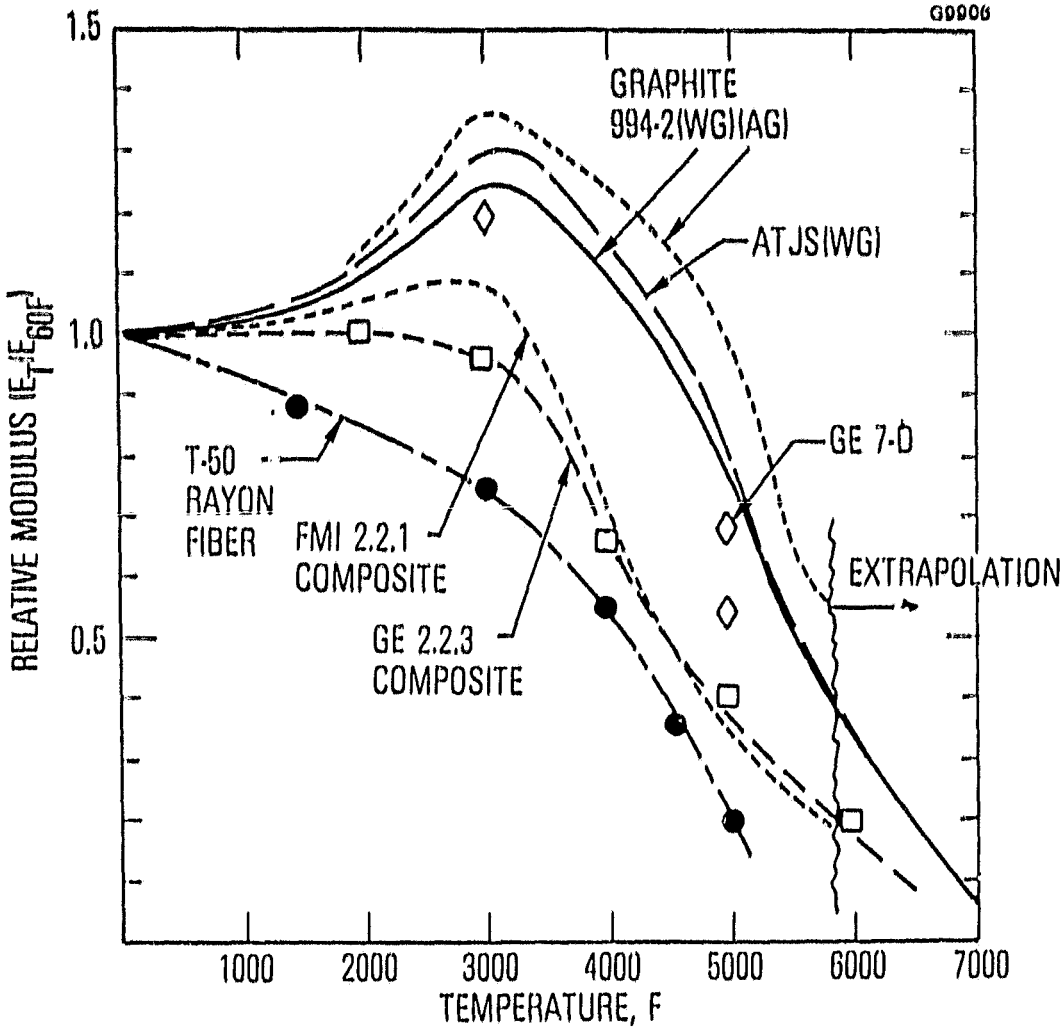

Figure 2.4-9 Relative stiffness (modulus) vs temperature in several carbon composites and graphites.

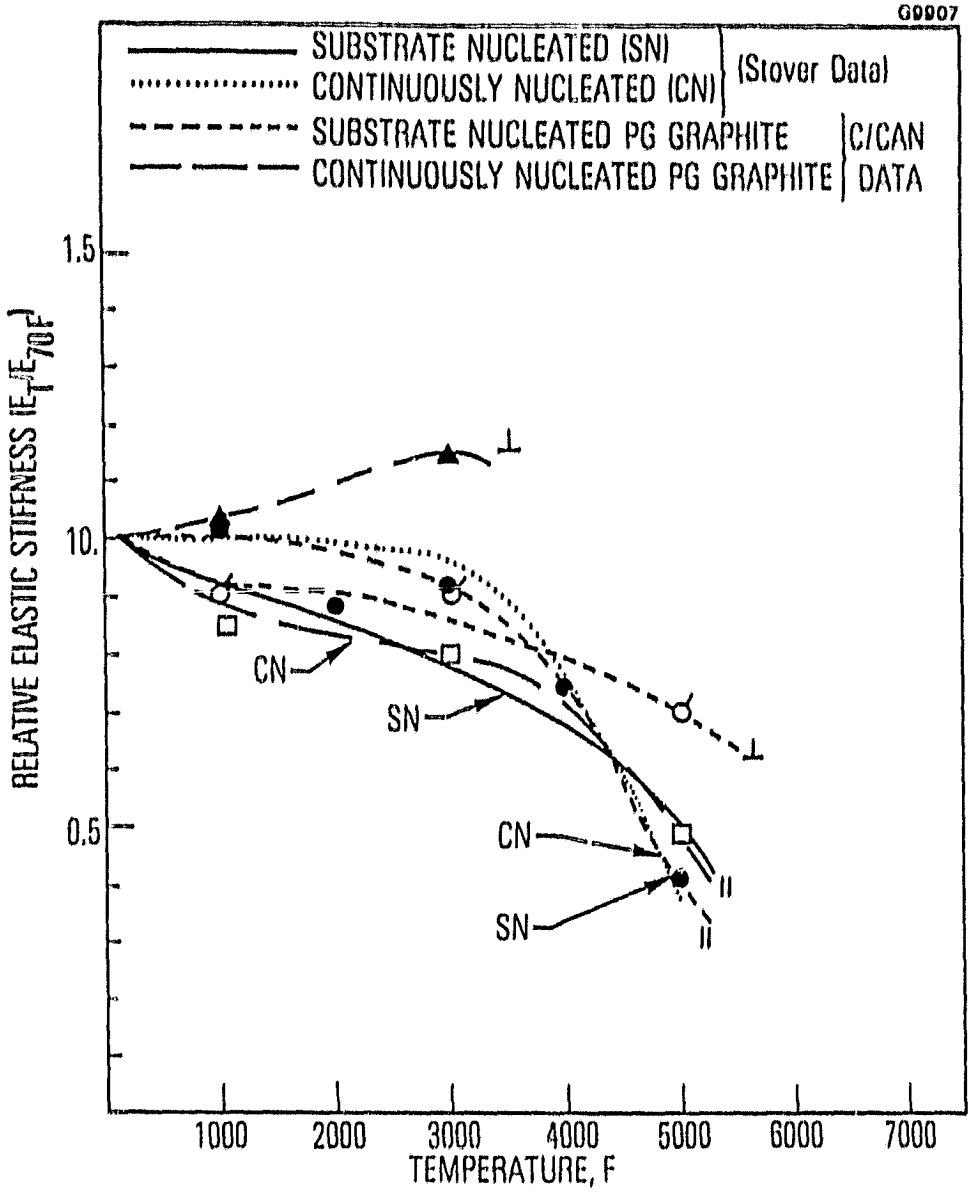

Figure 2.4-10 Relative moduli of pyrolytic graphites vs temperature.

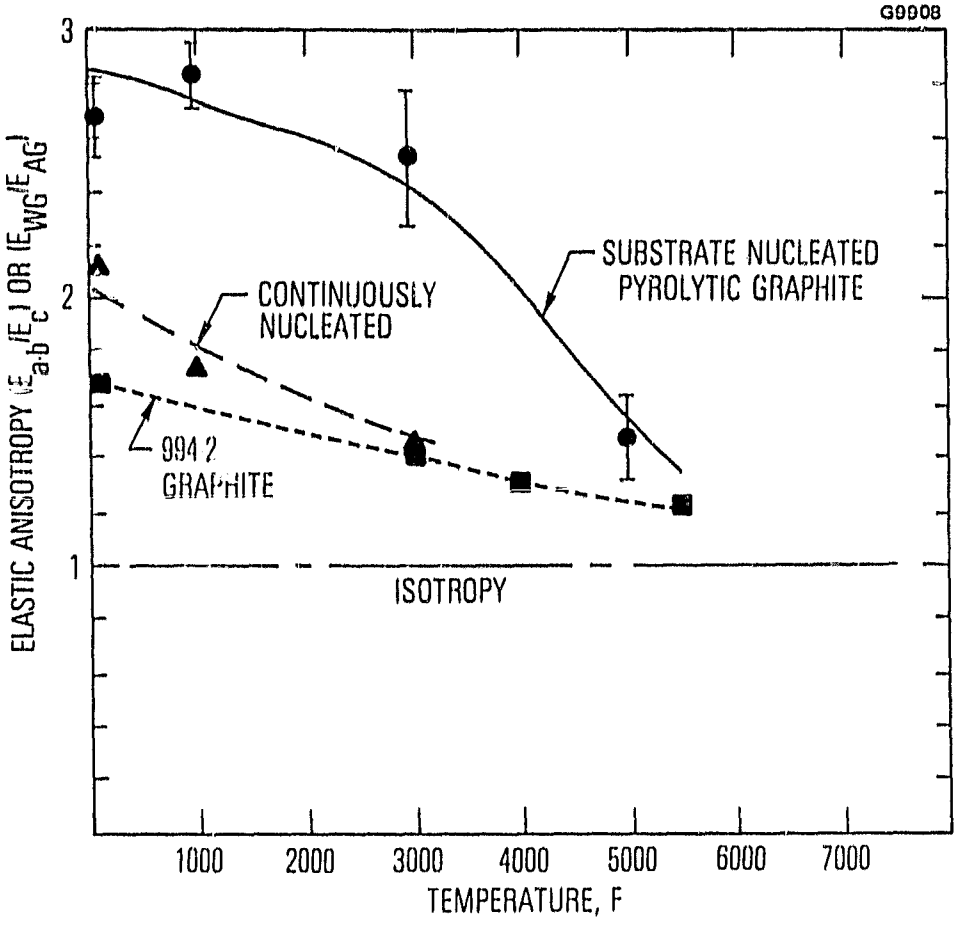

Figure 2.4-11 Elastic anisotropy vs temperature for pyrolytic graphites and a bulk graphite.

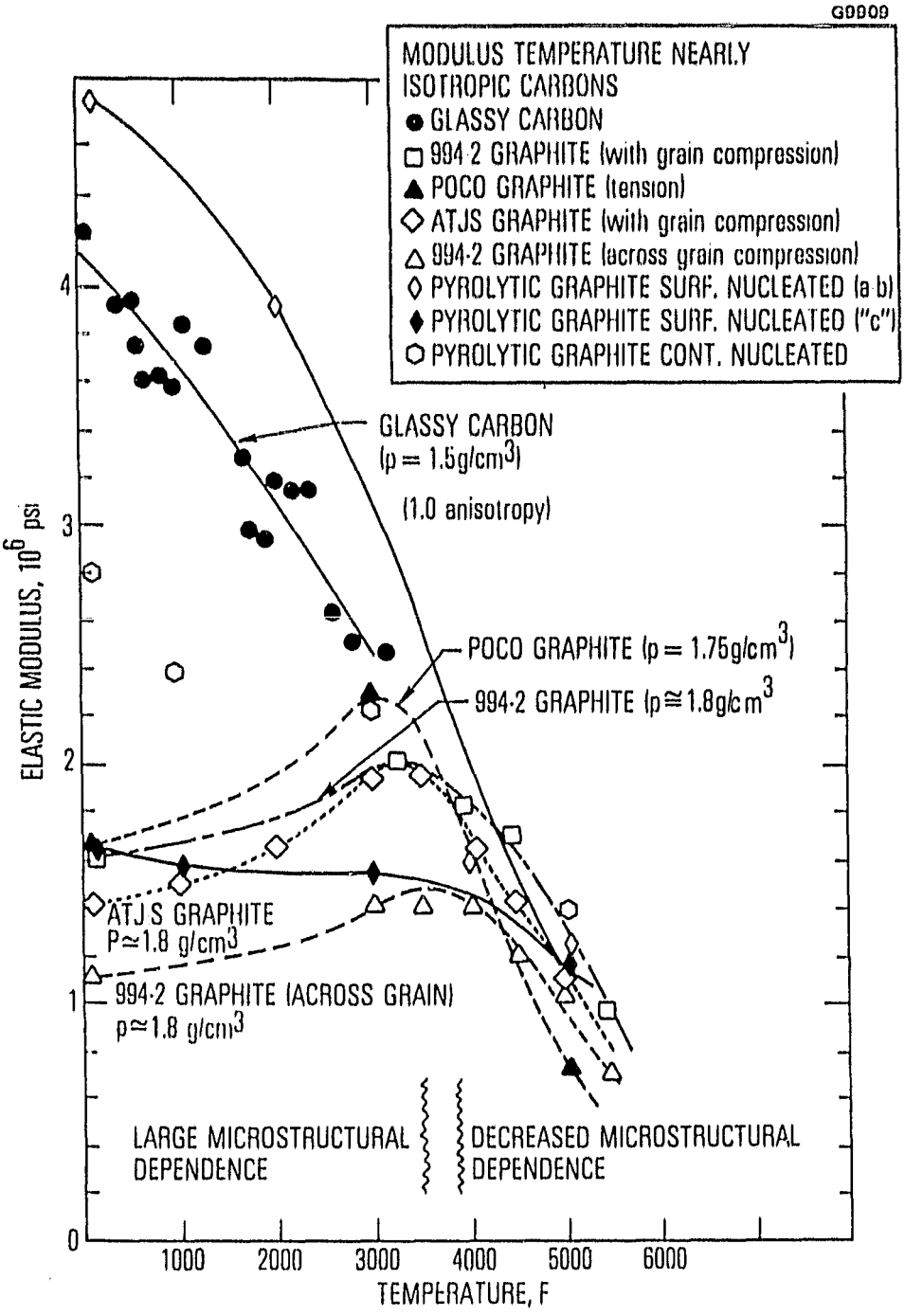

Figure 2.4-12 Elastic modulus vs temperature for isotropic and moderately anisotropic carbon forms.

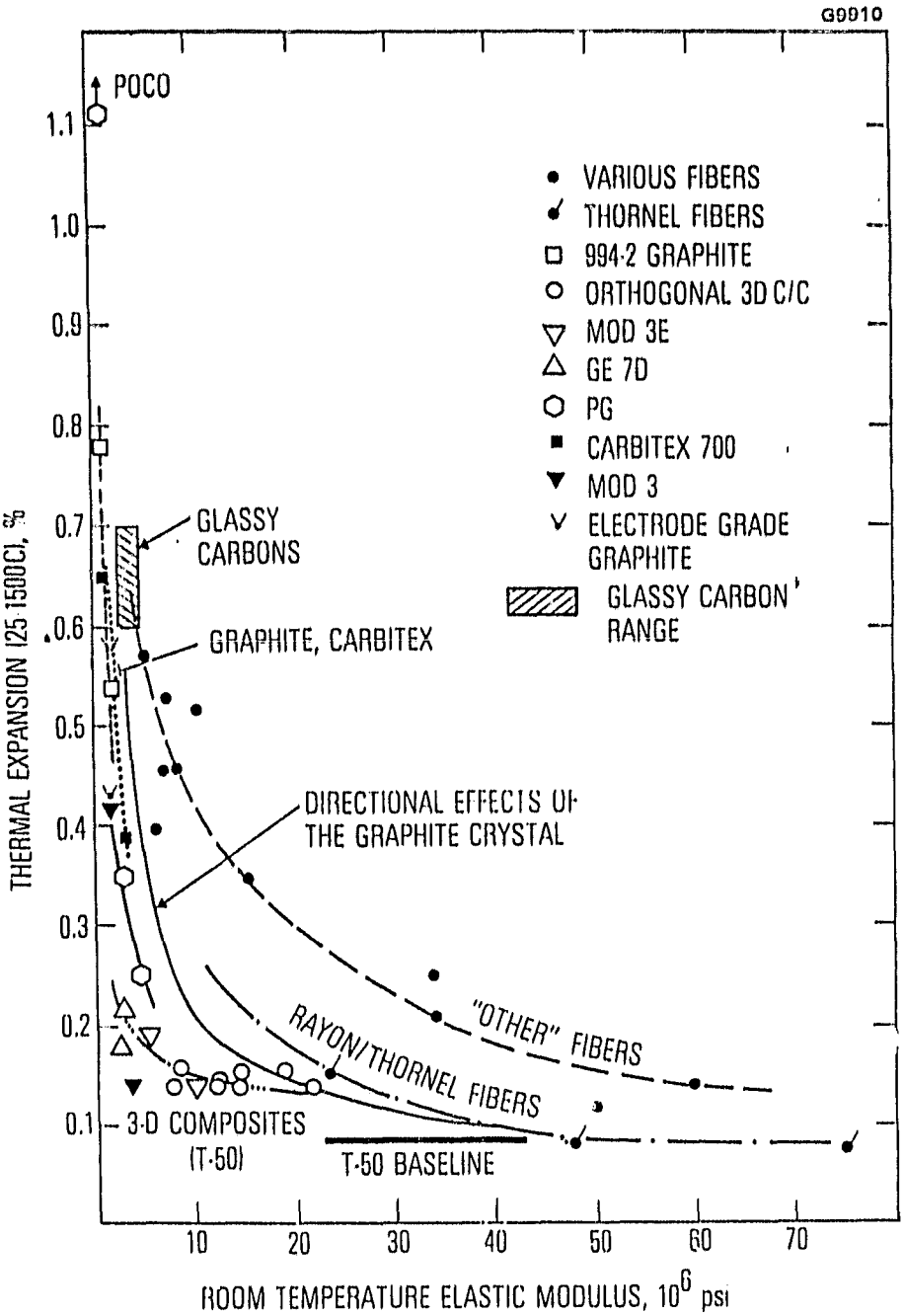

Figure 2.4-13 Free thermal expansion (1500 C) vs elastic modulus (25 C) for carbon forms.

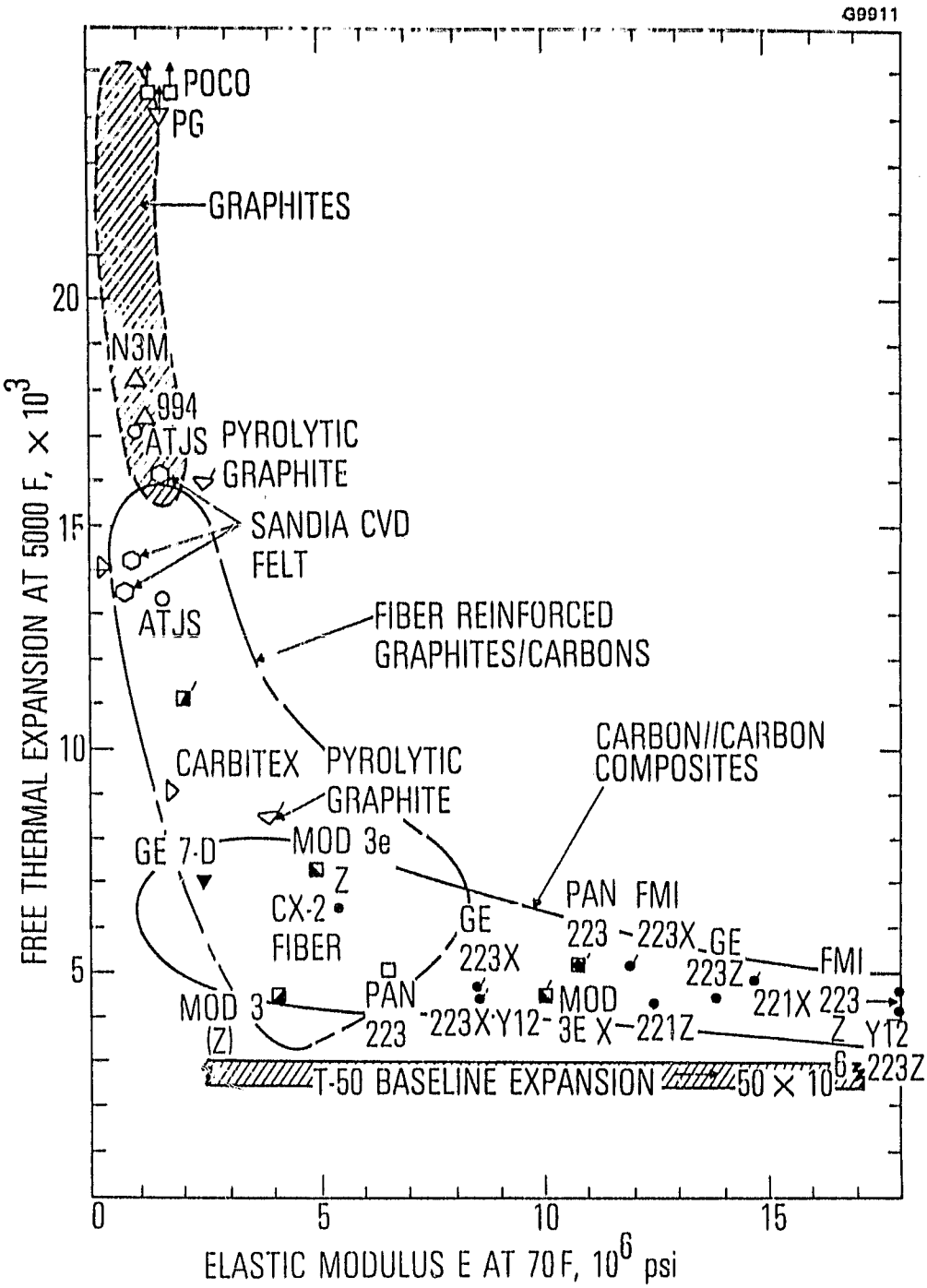

Figure 2.4-14 Free thermal expansion (2750 C) vs elastic modulus (25 C) for carbon forms.

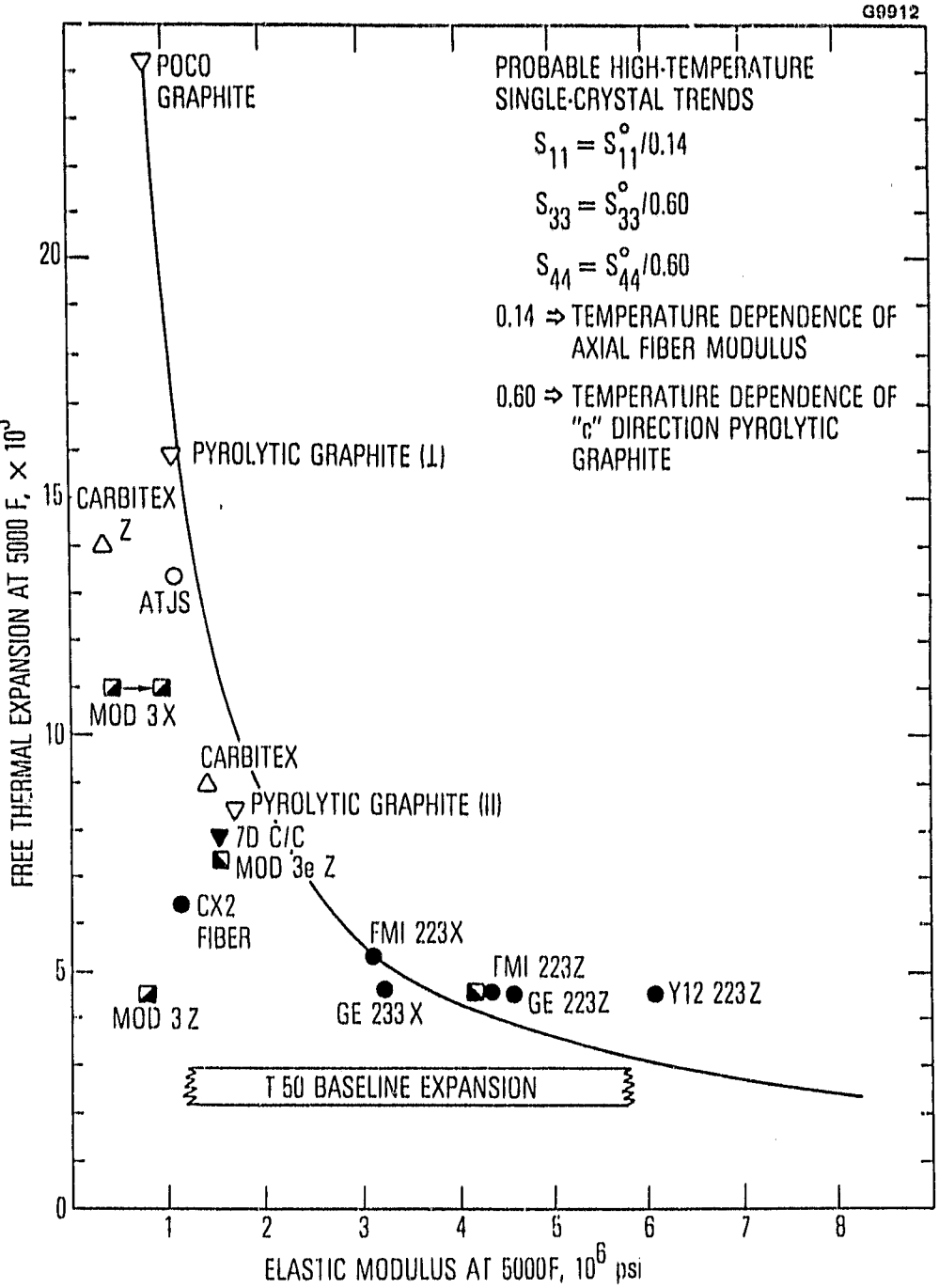

Figure 2.4-15 Free thermal expansion (2750 C) vs elastic modulus (2750 C) for carbon forms.

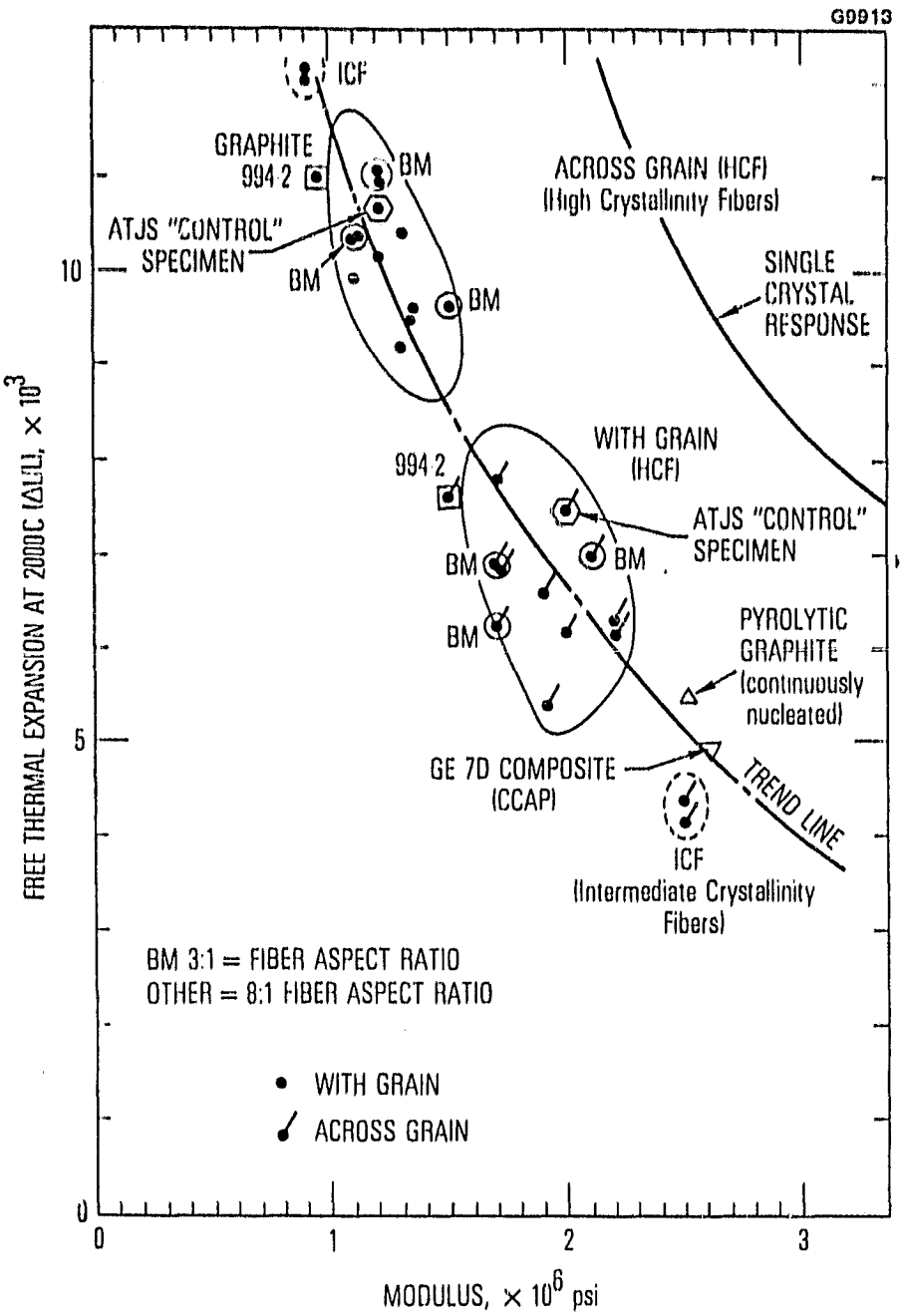

Figure 2.4-16 Free thermal expansion (2000 C) vs elastic modulus (25 C) for UCC chopped fiber-based graphites and other carbon forms.

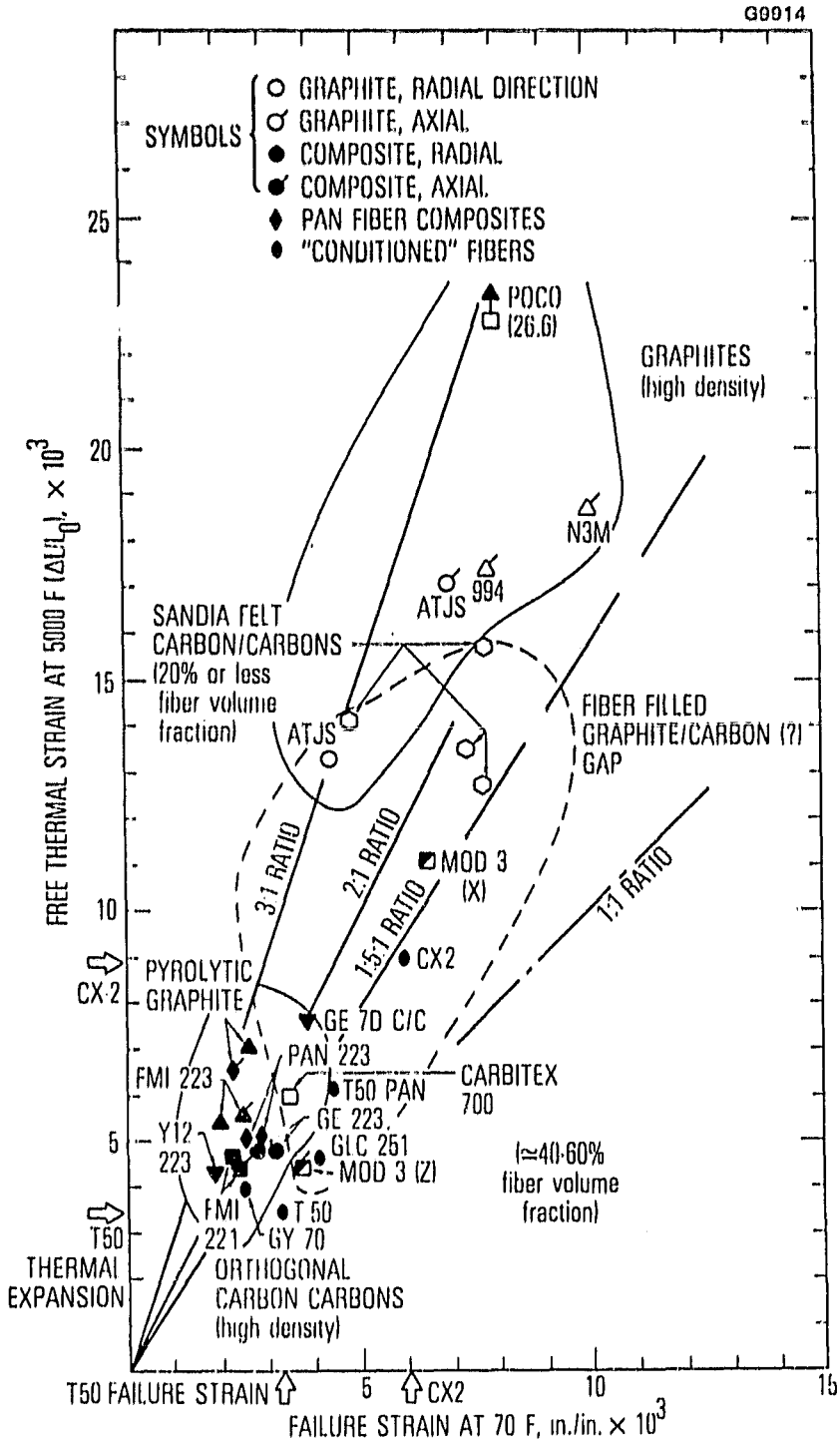

Figure 2.4-17 Free thermal expansion (2750 C) vs failure strain (25 C) for various carbon forms.

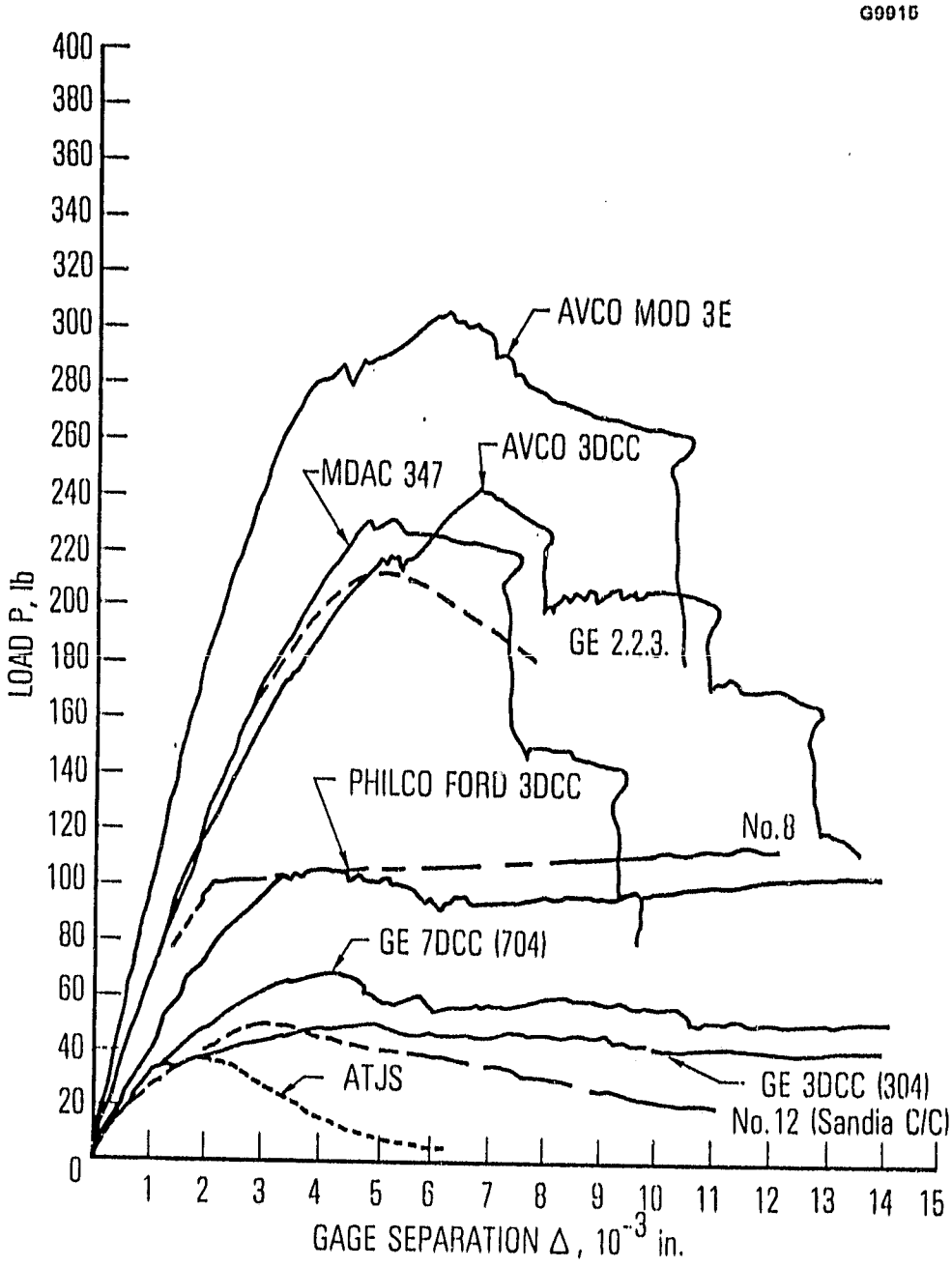

Figure 2.4-18 Load vs crack opening for precracked four-point bending of graphites and carbon composites.

2.4.3 Pyrolytic Graphite Properties

In our literature search and material selection process, nothing was found which indicates that PG would be a poor candidate for use in MDC collectors or that it has undesirable thermomechanical properties. To improve quality control, many researchers have suggested rigorous nondestructive screening and inspection tests, to be imposed in addition to the usual vendor quality checks. An example of such a list of inspection tests is Table 2.4-2 (Reference 2.3-10). In addition to this list, radiography and a penetrant test are often used on graphitic materials. These tests should be seriously considered if graphite electrodes are used on a large scale in TWT collectors.

The best references on PG properties are References 2.3-13 - 2.3-16. Smith and Leeds (Reference 2.3-13) from Super-Temp present the most complete and comprehensive survey of PG, the material and its mechanical, thermal, electrical, and chemical properties. Table 2.4-3 illustrates some typical PG properties, and where possible, the comparable properties for isotropic OFHC copper.

TABLE 2.4-2

PURPOSE OF CHARACTERIZATION

AND INSPECTION TESTS

Nondestructive Tests	Purpose
Visual inspection and alcohol	Detect gross surface defects such as cracks and pits
Bulk density	Characterization of material, determination of variability
X-Ray	Detect internal defects such as voids, cracks oriented parallel with x-ray beam.
Ultrasonic pulse-echo C-scan mapping	Detect internal defects oriented favorably (90 degrees) to sound beam. Determine areas of billets suitable for test specimens.
Sound velocity measurement, two inch centers, two directions	Determine density variability within billet, anisotropy within billet, billet to billet variation (dynamic modulus dependent).
Radiation gaging	Determine localized density at numerous points within billet.
Eddy current testing (biaxial specimens)	Detect tight cracks, through and partial thickness.
Hardness test	Characterize material, indication of density and heat treatment of billet, for billet to billet variations and end to end variations in one billet.

TABLE 2.4-3

TYPICAL PYROLITIC GRAPHITE PROPERTIES

Property	Units	PG	OFHC Copper (isotropic)
1. Density	g/cc	2.20 ± 0.02	9.08
2. Modulus of elasticity (R.T.)	psi		
• Tension		4.29×10^6 (ab) 1.55×10^6 (c)	18×10^6 -
• Compression		4.19×10^6 (ab) 1.58×10^6 (c)	18×10^6 -
3. Tensile Strength (R.T.)	psi		
• ab-plane • c-direction		14,000 400	27,000 -
4. Compressive Strength (R.T.)	psi		
• ab-plane • c-direction		10,000 45,000	40,000 -
5. Coefficient of Thermal Expansion	in/in/$^\circ$C		
• ab-plane		0.72×10^{-6}	17×10^{-6}
• c-direction		21.6×10^{-6}	-
6. Thermal Conductivity	Btu/ft/ft^2/hr/$^\circ$F		
• ab-plane		R.T. 200 2000°C 70 ± 20	226 (68°F)
• c-direction		R.T. 1.0 2000°C 0.6 ± 0.2	193 (1000°F)

TABLE 2.4-3 (CONTINUED)

Property	UNITS	PG	(OFHC Copper (isotropic)
7. Poisson's ratio			
• ν_{ab}		-0.15	0.328
• ν_{ac}		0.90	-
• ν_{ca}		0.35	-
8. Sheer modulus	psi		
• G_a (translaminar)		2.55×10^6	6.6×10^6
• G_c (interlaminar)		0.10×10^6	-

2.5 THERMOSTRUCTURAL DESIGN CRITERIA AND ANALYSES

2.5.1 Thermostructural Properties

Given a MDC configuration which features pyrolytic graphite electrodes, any thermostructural analysis approach should consider the following important factors:

1. Temperature-dependent stress-strain behavior.

2. Time dependence - higher strain rates and higher heating rates involved

3. Differences between tensile and compressive stress-strain behavior - different E_t and E_c.

4. Nonlinear stress-strain curve behavior.

5. Transversely isotropic material - with r-θ (ab) plane as the plane of isotropy.

6. Biaxial softening - development of slightly higher strains in biaxial tension than in uniaxial tension.

7. Residual stresses - in any closed shape, caused by cooling from the deposition temperature os 4,000°F for PG coupled with anisotropic thermal expansion.

Dr. Robert M. Jones (Reference 2.3-5) of SMU gives perhaps the most complete treatise on the nonlinear multiaxial modeling of graphitic and carbon-carbon materials. Some of his material and comments are included here for completeness; the reader is referred to Reference 2.3-5 for a complete discourse. An integral part of every stress analysis is the stress-strain relationship or material model; Jones gives the most up-to-date and complete treatment of the subject, of all the literature surveyed. Two significant deficiencies of current (1976) material

modeling are (1) biaxial softening and (2) different modulus under tensile loading than under compressive loading.

2.5.1.1 Biaxial Softening - Figure 2.5-1 illustrates the biaxial softening phenomenon, where slightly larger strains are developed in biaxial tension than in uniaxial tension. The behavior of generally decreasing Poisson's ratio is in contradiction to what might be anticipated onthe basis of conventional Poisson effects (where ν increases). This phenomenon was first observed by Fortner for ATJ-S graphite, and is attributed to plastic volume changes resulting from internal tearing or microcracking. Jones and Nelson then developed a so-called Jones-Nelson material model for description of the deformation behavior of ATJ-S under biaxial tension. This model is used in the SAAS III program (Reference 26), developed by Jones (now at SMU) and Cross (now at PDA) when both were at Aerospace Corporation in 1971. The Jones-Nelson material model was used in SAAS III to predict strains for Fortner's biaxial test specimen shown in Figure 2.5-2. The correlation of the predicted SAAS strains with Fortner's experimentally observed strains is shown in Figure 2.5-3, for room temperature behavior at a constant principle stress of 3550 psi. The Jones-Nelson predictions are within 3% of the equal biaxial tension strains and are identical to the two uniaxial tension cases. Actually, the Jones-Nelson model is more a general model for nonlinear behavior of orthotropic materials than just a biaxial softening model. Therefore, this model should be considered for use in modeling other graphite materials, such as PG.

2.5.1.2 Different Moduli in Tension and Compression - Many composite and graphitic materials behave differently under tensile and compressive loads, and PG is no exception. Both the elastic moduli (stiffnesses) and the strengths in principal material property directions of these orthotropic materials are different for tensile loading than for compressive loading. This characteristic behavior is shown schematically in the stress-strain curve of Figure 2.5-4. This phenomenon, which is nonlinear, causes a material like PG to be more difficult to analyze (and hence design) than an isotropic material like OFHC copper or alumina ceramic. Note that in the PG property table (Task 2), in the ab-plane, PG has a slightly lower compressive modulus than the tensile modulus and a

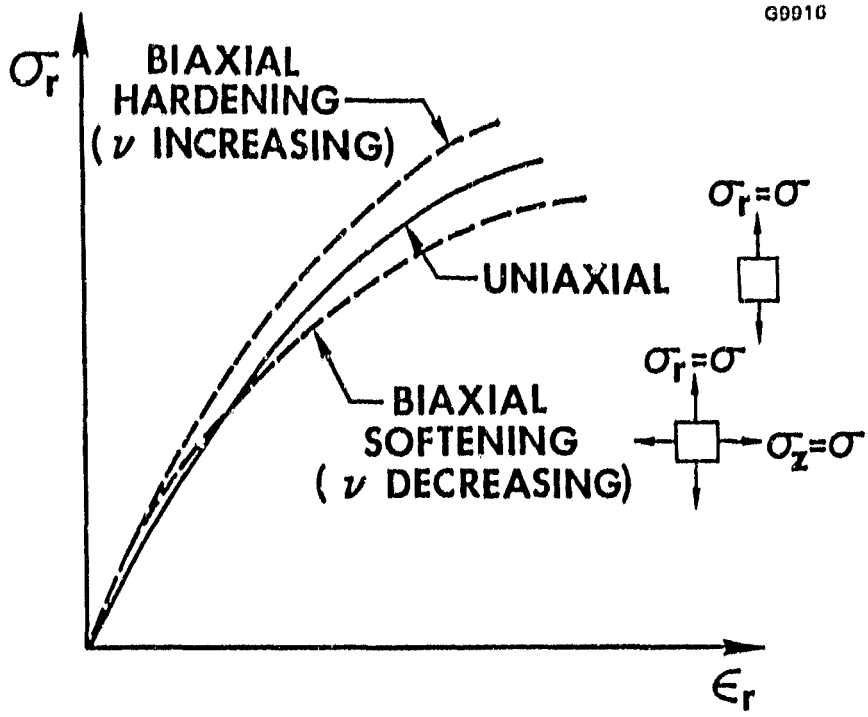

Figure 2.5-1 Biaxial softening of graphite.

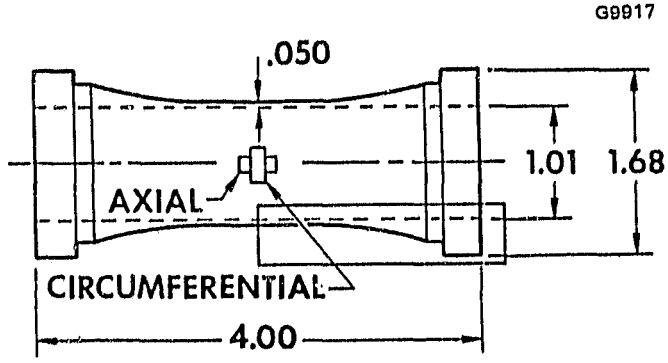

Figure 2.5-2 Hollow graphite biaxial specimen.

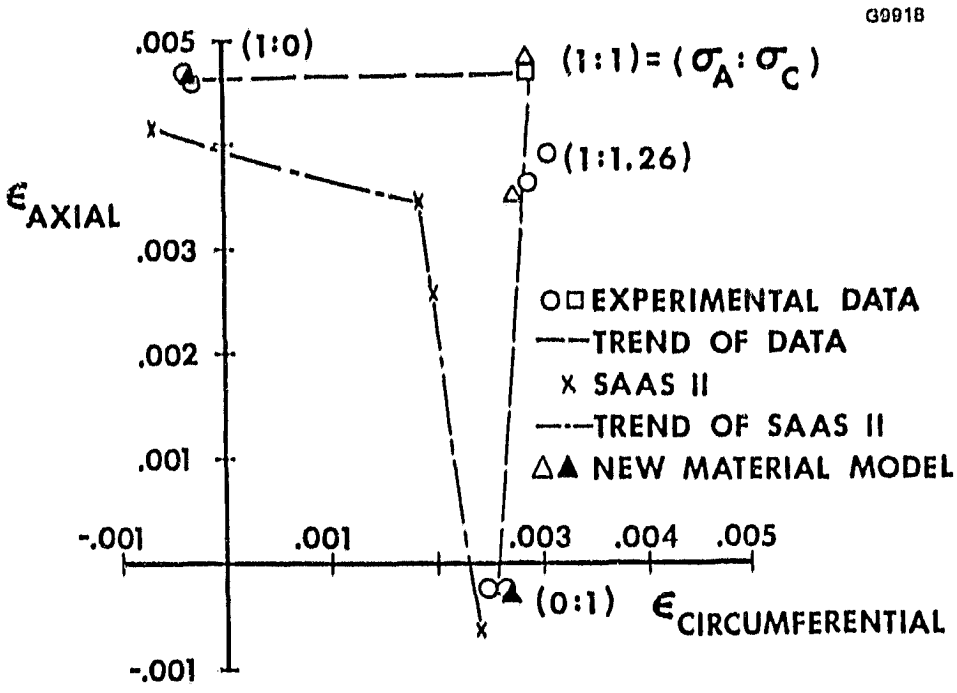

Figure 2.5-3 Biaxial strain response of a hollow ATJ-S graphite specimen at room temperature (70°F) and 3550 psi principal stress.

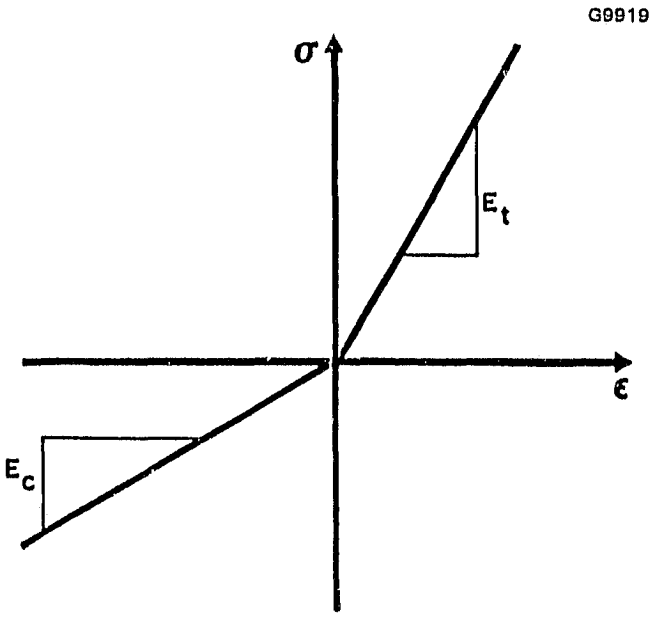

Figure 2.5-4 Stress-strain curve for a material with different moduli in tension and compression.

significantly lower room-temperature compressive strength (10,000 psi) than the tensile strength (14,000 psi). However, in the c-direction, this trend is reversed! A finite-element structural analysis code used to analyze the PG electrodes in TWT collectors, in order to avoid inaccurate stress-strain answers, must be able to account for this nonlinear behavior. This nonlinearity, even though it may be small, may mean the difference between cracking or delaminating a PG electrode, and we cannot ignore this effect *a priori*. Fortunately, SAAS III can handle this material behavior, and is therefore proposed for the MDC thermostructural analysis effort.

Table 2.5-1 illustrates how this different moduli in tension and compression behavior occurs in several types of fibrous or granular carbon and composite materials. No adequate physical explanation for this puzzling phenomenon has been offered.

Figure 2.5-5 shows that while a bilinear stress-strain model (in SAAS) can be used to approximate the apparent behavior, it is only a rough simulation of the actual behavior of such types of materials. A nonlinear transition region exists, and is particularly troublesome because the measurement of strains near zero stress is difficult to perform accurately. For most materials (and PG is no exception), the existing mechanical property data (and their data scatter) are insufficient to justify the use of a more complex material model than a bilinear one such as used in SAAS III. This bilinear model, however, contains one disadvantage (inaccuracy) because a slope (modulus) discontinuity occurs at the origin stress-strain curve. When the different moduli in tension and compression characteristic is combined with the biaxial softening characteristic, the Jones-Nelson model still leads to a fairly good correlation between predicted and experimental biaxial strains.

In general, graphites are macroscopically homogeneous, transversely isotropic, and generally fail in a brittle manner. Their stress-strain curves are nonlinear to failure, and vary with temperature.

TABLE 2.5-1

TENSION AND COMPRESSION MODULI RELATIONSHIPS
FOR SEVERAL COMMON COMPOSITE MATERIALS

Material	Fibrous or Granular	Representative Moduli Relationship
Glass/Epoxy	Fibrous	$E_t = 1.2E_c$
Boron/Epoxy	Fibrous	$E_c = 1.2E_t$
Graphite/Epoxy	Fibrous	$E_t = 1.4E_c$
Carbon/Carbon	Fibrous	$E_t = 2.5E_c$
ZTA Graphite	Granular	$E_c = 1.2E_t$
ATJ-S Graphite	Granular	$E_t = 1.2E_c$

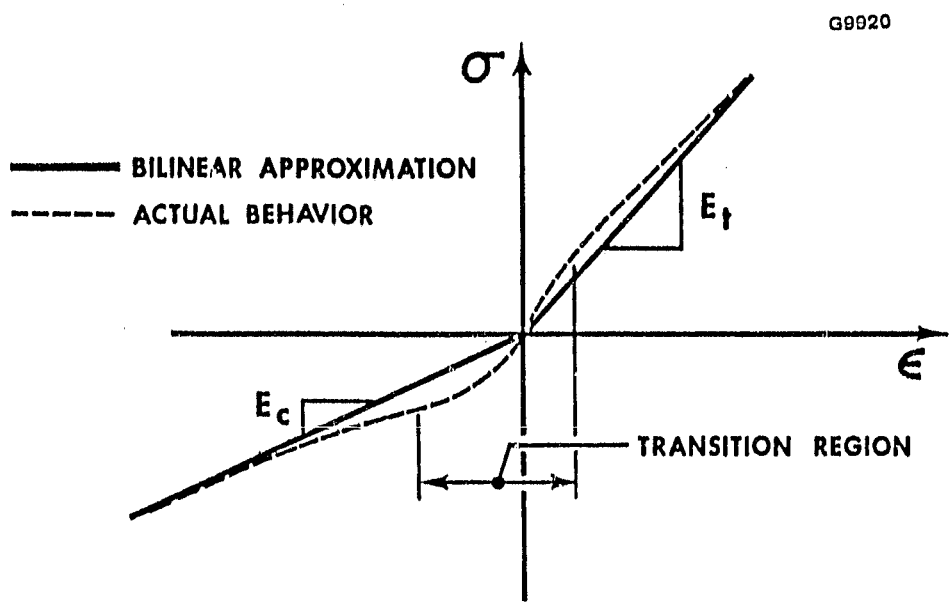

Figure 2.5-5 Comparison of bilinear model with actual behavior.

2.5.1.3 Jones-Nelson Nonlinear Material Model - This section gives a concise description of the Jones-Nelson material model (the reader is referred to Reference 2.3-5 for details). Basically, the premise of the model is that the mechanical properties of a material (for example, Young's modulus in any direction, Poisson's ratio, shear modulus) are expressed in terms of the strain energy of the body with the approximate equation

$$(\text{Mechanical Property})_i = Ai \left[1 - Bi \left(\frac{U}{U_{oi}}\right)^{Ci}\right]$$

where: Ai are the elastic values of the material property; the Bi and Ci are related to the initial curvature and rate of change of curvature, respectively, of the stress-strain curve; and U is the strain energy density of an equivalent elastic system at each stage of nonlinear deformation:

$$U = 1/2(\sigma_r \xi_r + \sigma_z \xi_z + \sigma_o \xi_o + \tau_{rz} \gamma_{rz})$$

The strain energy density U is normalized by U_o so that Bi and Ci are dimensionless. (The stress and strain quantities are related as shown in the next section).

The stress-strain relations and the mechanical property versus energy equations are a set of indeterminate relatives which are solved with the iteration procedure shown in Figure 2.5-6. Much of the work in implementing the Jones-Nelson nonlinear material model is in calculating appropriate values of A, B, and C in the above equation. For example, using ATJ-S σ-ξ curve and E-U curve at 70°F, the following constraints are obtained for ATJ-S:

$$A = 2 \times 10^6 \text{ psi}, \quad B = 0.182, \quad C = 0.337, \quad U_o = 1.0 \text{ psi}$$

Details are given in Reference 2.3-5.

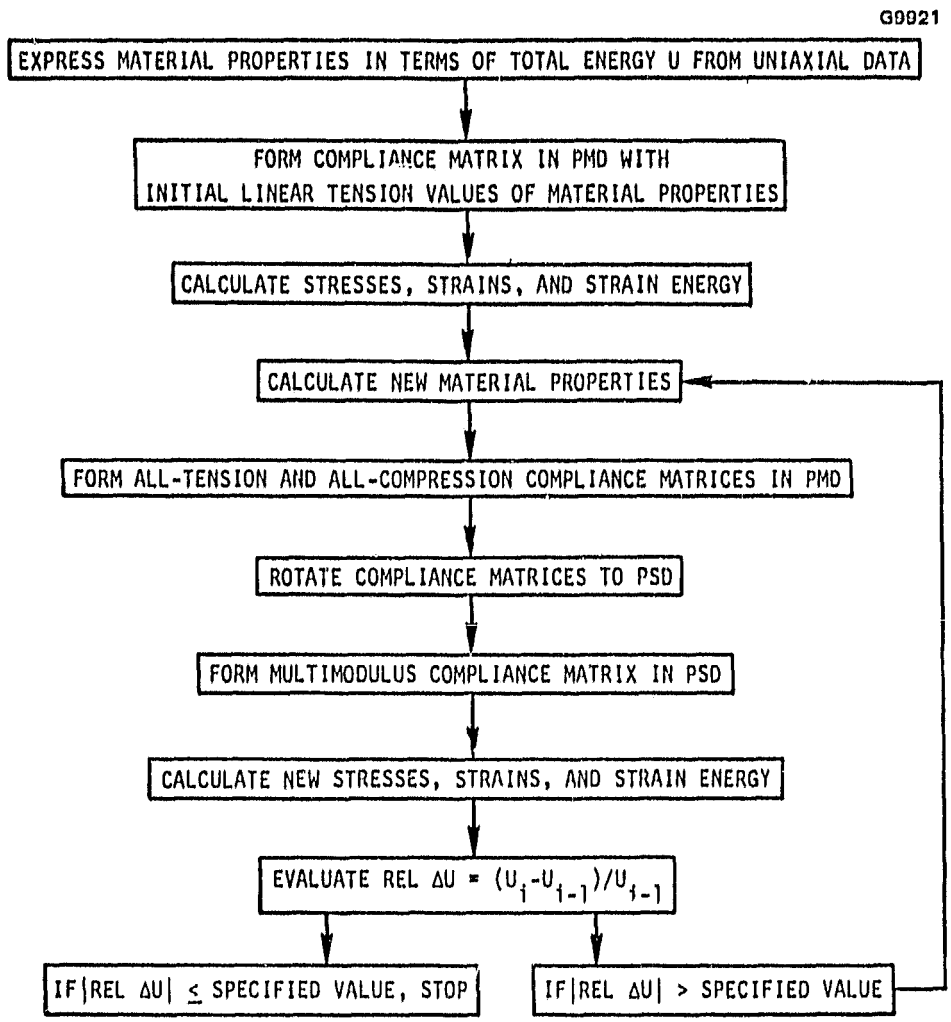

PMD = PRINCIPAL MATERIAL DIRECTIONS

PSD = PRINCIPAL STRESS DIRECTIONS

Figure 2.5-6 Iteration procedure for nonlinear multimodulus materials.

2.5.1.4 Stress-Strain Equations - The basic problem is the stress analysis of nonlinear elastic bodies whose stress-strain behavior is described with, for the example of an orthotropic axisymmetric body under axisymmetric load, the equations:

$$\begin{bmatrix} \xi_r \\ \xi_z \\ \xi_\theta \\ \gamma_{rz} \end{bmatrix} = \begin{bmatrix} \frac{1}{E_r} & -\frac{\nu_{rz}}{E_r} & -\frac{\nu_{r\theta}}{E_r} & 0 \\ -\frac{\nu_{rz}}{E_r} & -\frac{1}{E_z} & -\frac{\nu_{z\theta}}{E_z} & 0 \\ \frac{\nu_{r\theta}}{E_r} & -\frac{\nu_{r\theta}}{E_z} & -\frac{1}{E_\theta} & 0 \\ 0 & 0 & 0 & \frac{1}{G_{rz}} \end{bmatrix} \begin{pmatrix} \sigma_r \\ \sigma_z \\ \sigma_\theta \\ \tau_{rz} \end{pmatrix}$$

where the directions denoted with the subscripts r, z, and θ are principal material directions. The material properties in the compliance matrix are:

E_r = Young's modulus in the r direction

E_z = Young's modulus in the z direction

E_θ = Young's modulus in the θ direction

$\nu_{rz} = -\varepsilon_z/\varepsilon_r$ for the loading $\sigma_r = \sigma$ (all other stresses zero)

$\nu_{r\theta} = -\varepsilon_\theta/\varepsilon_r$ for the loading $\sigma_r = \sigma$ (all other stresses zero)

$\nu_{z\theta} = -\varepsilon_\theta/\varepsilon_z$ for the loading $\sigma_z = \sigma$ (all other stresses zero)

G_{rz} = Shear modulus in the rz plane

The reciprocal relations of orthotropic elasticity are:

$$\frac{\nu_{rz}}{E_r} = \frac{\nu_{zr}}{E_z}$$

$$\frac{\nu_{r\theta}}{E_r} = \frac{\nu_{\theta r}}{E_\theta}$$

$$\frac{\nu_{z\theta}}{E_z} = \frac{\nu_{\theta z}}{E_\theta}$$

and can be used to express alternate definitions for the Poisson's ratios in terms of the seven independent material properties inthe stress-strain equations expressed in matrix form above. The material properties are a function of stress level because the material is nonlinear elastic. However, the unloading behavior or any subsequent reloading behavior of the body is not considered.

2.5.1.5 Correlation with Thermal Stress Disk - Jones (Reference 2.3-5) described how the Jones-Nelson nonlinear material model and SAAS III were applied successfully to a set of thermal stress disk experiments at SoRI. The annular disk cross sections considered are shown in Figure 2.5-7; they are not unlike the geometry of our MDC PG electrodes being considered. In this SoRI test, the annular disk is rapidly heated at its outside diameter, resulting in an outside to inside diameter temperature gradient. Both tensile and compressive stresses were generated. The failures invariably occurred in the region of tensile stress (near inner diameter). The correlation between prediction and experiment was good.

2.5.1.6 Discussion and Recommendations for MDC Study - All the foregoing information serves to suggest the following HEDD recommendations on the material

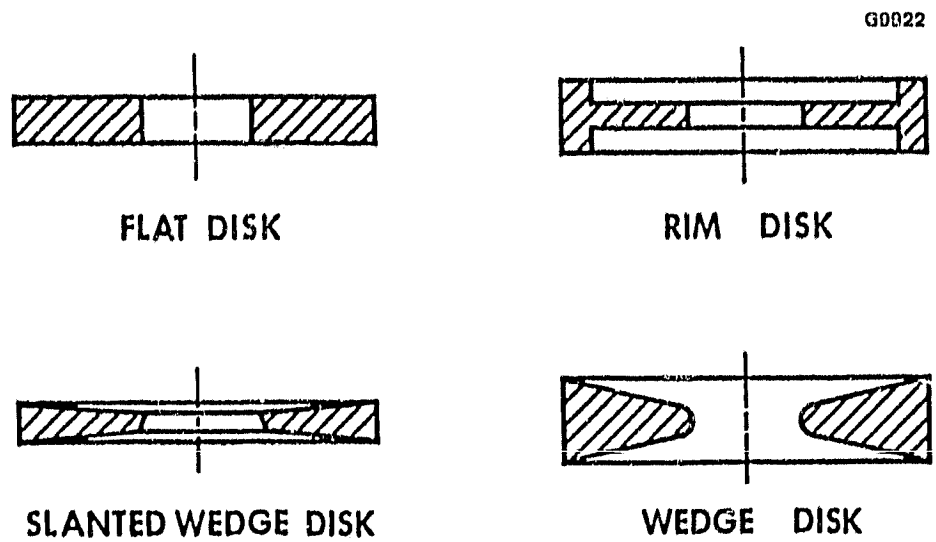

Figure 2.5-7 Annular disk cross sections.

2.5.1.6 Discussion and Recommendations for MDC Study - All the foregoing information serves to suggest the following HEDD recommendations on the material selection and thermostructural design/analysis in the MDC study:

1. Use pyrolytic graphite as the electrode material. It has good secondary electron emission characteristics, and no known detrimental thermal/mechanical properties.

2. Use a factor of safety of 2 for thermostructural analyses.

3. For delamination - All and crack-free parts, adopt the Super-Temp recommendation of a (t/r) ratio of 0.07 in designing the electrodes.

4. It is of utmost importance to obtain a good PG stress-strain curve - test if necessary. This is required for a Jones-Nelson nonlinear material model in future thermostructural analyses.

5. Use the SAAS III finite element code to perform the thermostructural analyses, which will account for the known difference in tensile and compression moduli. Use a fine mesh at the PG-ceramic joint, in order to better predict the stresses.

   (Advanced versions of the SAAS III code which accounts for the Jones-Nelson model are available at SMU and PDA).

6. Preliminary Land calculations show that the PG electrodes should withstand the anticipated thermal and vibration environments satisfactorily. The expected thermal strains ($\alpha\Delta\tau$) are in the 10^{-4} in./in. range, while PG failure strains are in the 10^{-3} to 10^{-2} range. Therefore, concentrate all the efforts and funds on the PG-ceramic joint.

2.5.2 Pyrolytic Graphite Collector Electrode Braze Cooldown Stress Analysis

2.5.2.1 Introduction - The electrical efficiency of a TWT depends in some degree on the ability to effectively collect the spent electron beam at a voltage as close to the cathode voltage as is possible. A multistage collector consisting of electrodes at distinct voltages is typically used to provide this gain in efficiency. The efficiency of the collector itself is also improved when the secondary emissions from the secondary emissions from the electrodes are reduced. Multistage collectors usually consist of disc shaped copper electrodes surrounded by a ceramic cylinder. A step-like shape inside the ceramic cylinder allows each electrode to be electrically separated from each other. A modification to the solid copper electrodes has been suggested; this is the use of pyrolytic graphite material which has low secondary emission characteristics.

The exact shape of the electrodes is determined principally by the TWT's electrical characteristics. The size of the ceramic cylinder is primarily dictated by the number of stages and required thermal dissipation. The required metal to graphite joints for this design will be made via brazing with a braze alloy at approximately 850°C. But the outer diameter of the electrodes is effectively limited by the amount of residual stresses resulting from the brazing operation. In addition, it is important to insure that no collector component size or shape contributes to high stresses in itself or in neighboring components after assembly. To this end, an analytical study has been performed evaluating residual components' stresses after brazing. It is especially important to investigate the localized stresses in the actual metal to graphite braze joint.

Two detailed braze cooldown analyses were performed using finite element analysis techniques. Although not requiring a very large model, this analysis did require simulating braze cooldown which necessitated a code with temperature dependent anisotropic material properties. ANSYS is a large scale, general purpose, finite element code which features each of these capabilities. Inputting the appropriate geometry, material properties, and temperature drop, ANSYS can solve for the thermal stresses. A unique restart capability allows ANSYS to accurately simulate braze cooldown. Using these capabilities, residual

stresses in the collector components as well as in the area of the actual metal to graphite joint can be calculated.

The results of this analysis indicate that residual stresses in both collector components and at the metal to graphite joint are acceptable. The outer diameter and thickness of the pyrolytic graphite electrode should be studied in more detail to determine the optimum configuration for brazing and operation.

The following report summarizes the analytical methodology, the computer code, and the critical assumptions used in arriving at this conclusion. Results showing various components' residual stresses as well as residual stresses close to the metal to graphite joint are presented.

The report given in Section 2.5.3 summarizes the work performed earlier this year. This work determined which materials should be used in brazing a collector assembly using pyrolytic graphite. The stresses incurred in the actual braze joint were investigated for a "T" type joint in plane stress, plane strain and axisymmetric analyses.

2.5.2.2 General Analytical Technique - This analysis utilized the varied capabilities of the ANSYS computer code. ANSYS is a large scale, general purpose finite element code used for the solution of many classes of complex engineering problems. For this application, ANSYS's ability to calculate stresses from thermally induced strains was used.

Metals display significantly different physical properties at elevated temperatures than they do at room temperature. Since a material like copper will plastically deform at a lower stress at 800°C than at 400°C, characteristics like this must be taken into account in the analysis. The computer analysis of the cooling from the 850°C braze temperature to room temperature cannot be analytically simulated in one step because ofthe varying material properties. ANSYS has the ability to use a prestressed or prestrained stiffness matrix of a previous solution and, by using this attribute, a fairly accurate simulation of braze cooldown is made. In this analysis a temperature decrease step of

approximately 200°C is chosen, the model is solved, and the resulting stiffness matrix is stored. The model is then restarted for the next temperature decrease of 200°C using the stored stiffness matrix from the previous run as the initial conditions for each element. In this manner the material properties can be assumed to be approximately constant within the 200°C temperature decrease in each temperature iteration, but can still vary from step to step. That is, the stored stiffness matrix provides a preload to the model which is the cumulative result of the previously solved temperature steps.

The braze cooldown method described required an iterative solution through the multiple temperature steps. The allowance for the copper to deform plastically requires an iterative solution for each thermal load step. The resultant analysis is necessarily very costly from a computer viewpoint. The solution time for a model is approximately a cubic function of the number of model nodes. In order for an analysis of this type to not be prohibitively expensive, it is necessary to model components with a minimum of nodes. The requirement to investigate both the collector component stresses, as well as stresses in both the copper and graphite, adjacent to the metal to graphite braze joint, was best served by making one large three dimensional model. The variation of material properties through the thickness and the introduction of slots in the electrode made a two-dimensional model impossible.

The stresses calculated in this analysis represent the collector components modelled to nominal first-estimate dimensions; namely thickness and diameter. The assembly was assumed to be stress-free at the 850°C brazing temperature. Stresses in the collector were calculated at the room temperature completion of the cooldown process. The margins of safety for each component were calculated using the ultimate strength of the materials, due to a cooldown of this type and magnitude, occurring only once during the collector's lifetime. Consideration was not given to any alloying effect the braze material might have on the copper or graphite. No effort was made to include creep or stress relaxation of the copper in the computer solution. A great deal of stress annealing will also occur during the TWT bake-out processing operation, which is done at approximately 500°C. Low temperature cycling as with operation,

will also tend to reduce the residual stresses. Therefore, the calculated stresses are only accurate soon after the braze cooldown, and will be considerably diminished by the time the TWT is put into normal operation.

2.5.2.3 Collector Model - The general design concept used for a pyrolytic graphite electrode within a collector assembly is shown in Figure 2.5-8. The graphite is brazed to an outer copper ring which in turn is brazed to an alumina ceramic. Since the two dimensional analyses as given in Section 2.5.3, determined that the hoopdirectional stresses were high during brazing; stress relieving slots were cut into the graphite and copper electrodes as shown in Figure 2.5-9. The generated finite element structural model of the collector is shown in Figure 2.5-10. This model consisted of 816 nodes forming 444 solid elements. All components which were made from copper were allowed to plastically deform. The thermal step used to step-down from 850°C to room temperature was 200°C.

The analyzed collector consisted of graphite electrodes, a copper ring, and a ceramic (alumina) cylinder. The assembly is brazed together in one operation. The model consists of all of these pieces. The slots cut into the graphite and copper were included where significant stress concentrations were expected to occur.

In the areas of the models where the graphite and metal parts were joined, no effort was made to modify material properties ofthe metal to allow for possible alloying with the braze alloy. There was also no effort to compensate for the strength or stiffness of the graphite through its metallization depth. This is justified because the resultant effects on the stresses would probably be very small.

The model considered a 22.5 degree arc of the total collector assembly as shown in Figure 2.5-11. The boundary conditions applied allowed the slotted material to move in the circumferential direction. At locations where the materials are a continuous goop, the circumferential displacements were held fixed. In addition to the above boundary conditions, the model was held in one axial location on the ceramic to prevent rigid body motion.

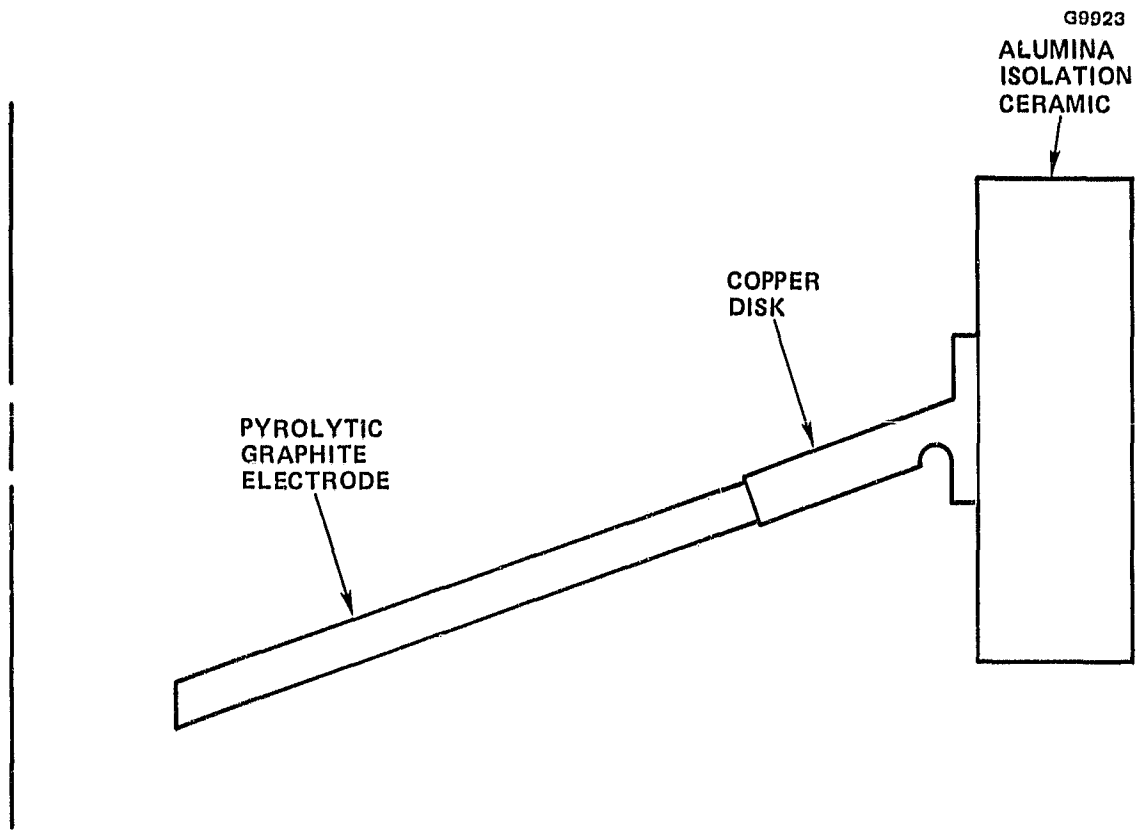

Figure 2.5-8 Pyrolytic graphite collector electrode configuration.

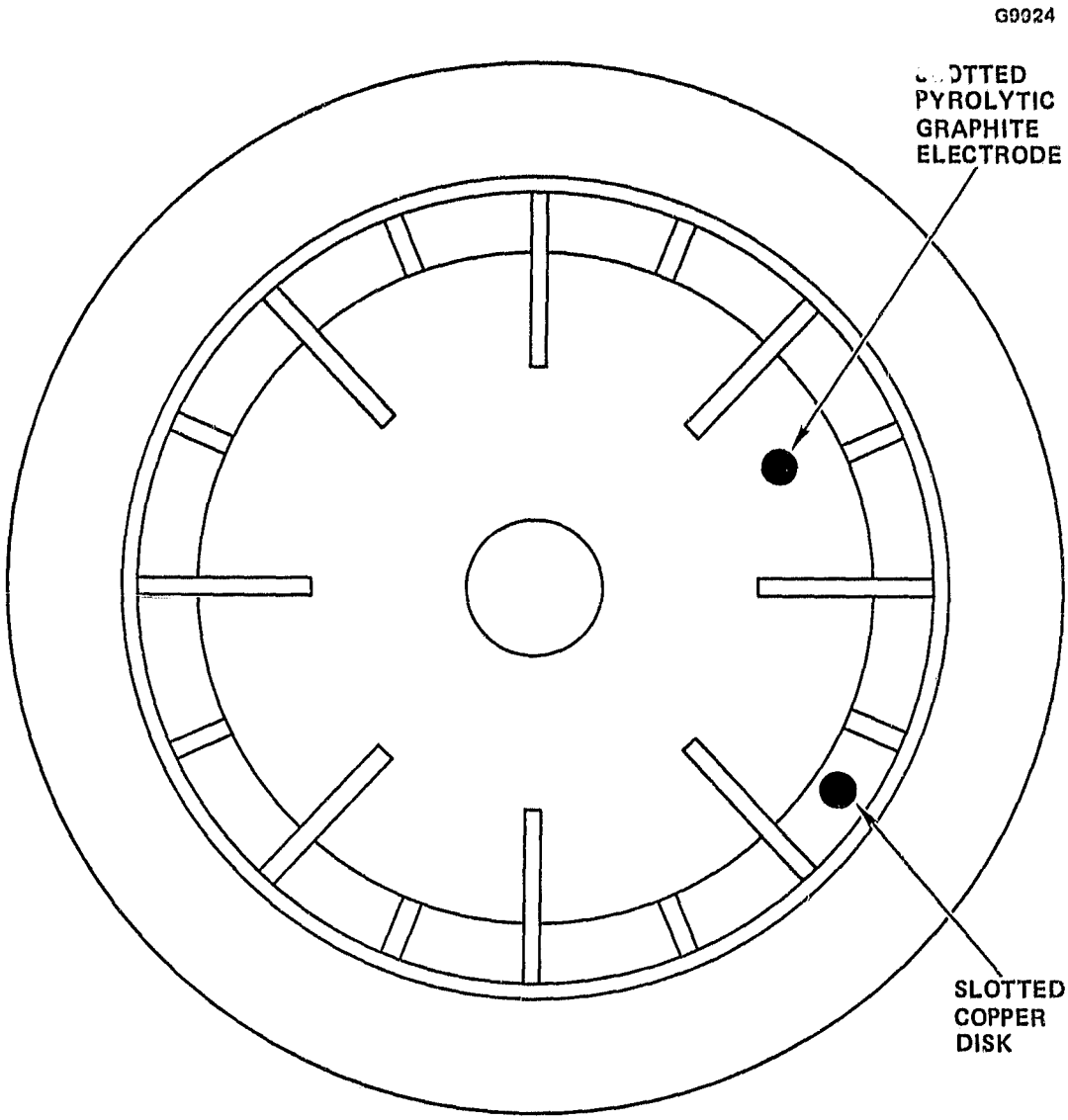

Figure 2.5-9 Pyrolytic graphite collector electrode configuration showing slots in electrode and disk.

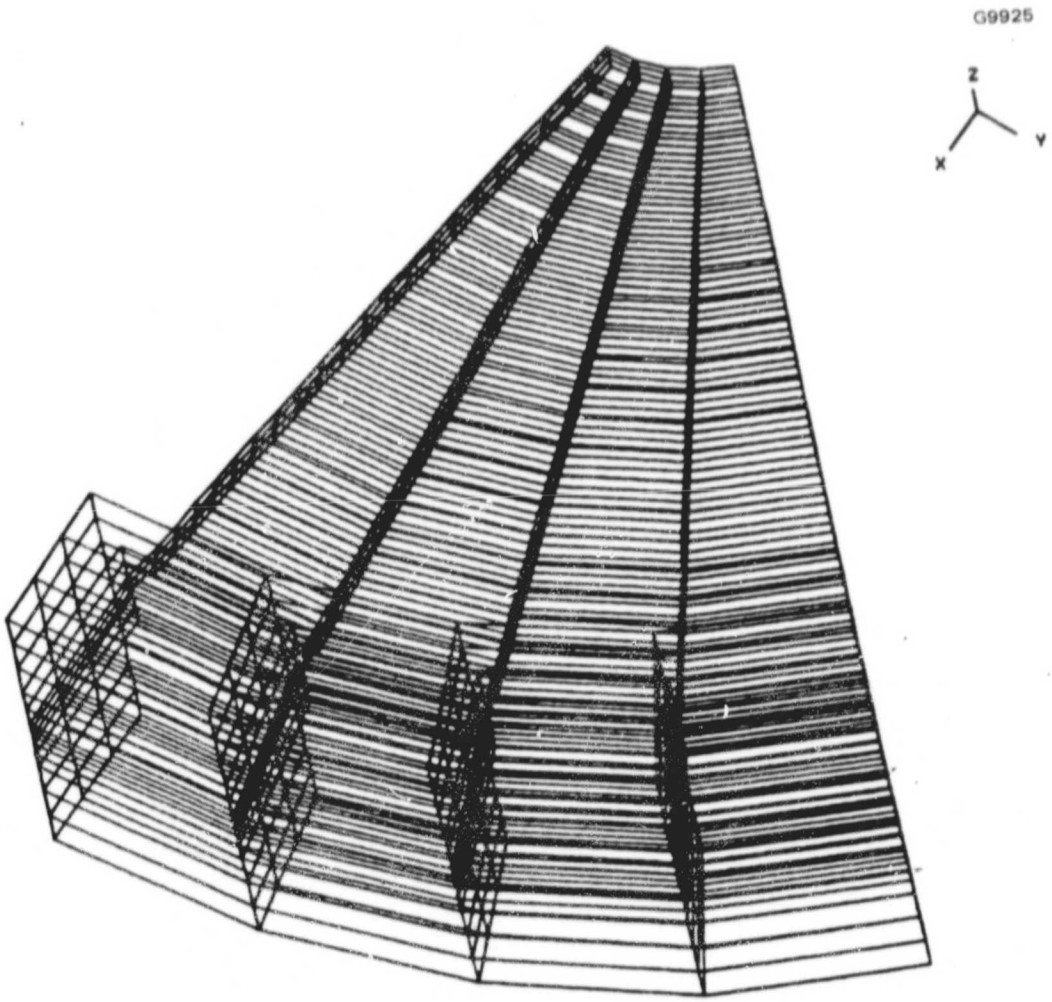

Figure 2.5-10 Finite element model of collector electrode assembly.

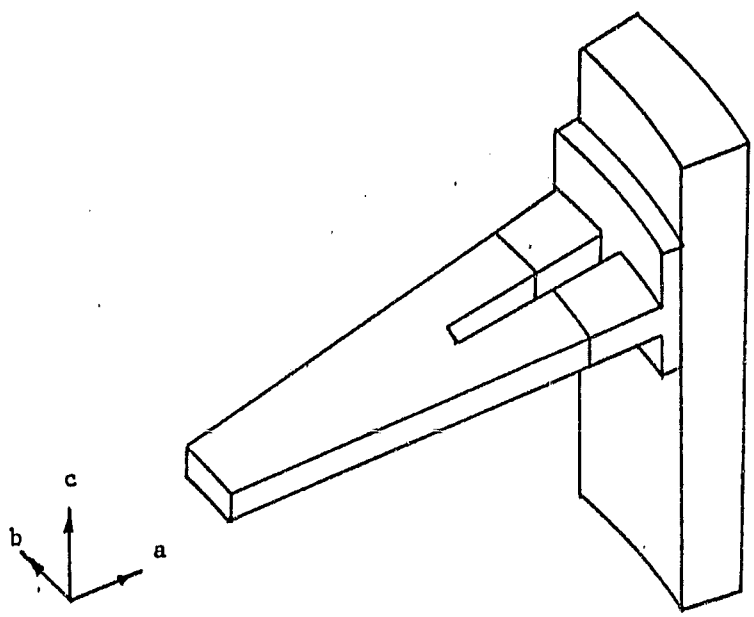

Figure 2.5-11 Representation of 22.5 degree slice finite element model.

The copper ring and alumina ceramic were considered to be isotropic materials. The pyrolytic graphite, however, was given its total anisotropic material characteristic. The material properties given in Table 2.5-2 should be referenced to Figure 2.5-12 for the directional characterization of the graphite. The "c" direction of the graphite is in the axis of the TWT collector. The "ab" plane is therefore made to conform to the radial and circumferential directions.

The particular material strengths of pyrolytic graphite, copper and alumina are given in Table 2.5-3. The important consideration that must be made is that the strength of the pyrolytic graphite depends on the type of load and its direction. The ultimate strength for this material is different in tension, compression and flexure for both its "ab" plane and "c" directions. For completeness, the stresses in the copper and alumina, though low, were still compared to their ultimate strengths in tension.

2.5.2.4 Results - Component stresses resulting from the assembly of the collector electrode via the brazing process are tabulated in Table 2.5-4. The corresponding margins of safety are also given as compared to the ultimate strengths of the materials. It should be noted that the pyrolytic graphite has definite limits in tension, compression and flexure for each of the directions. The "a" and "b" directions apparently have the same strengths; however, the "c" direction is much weaker in tension and fissure, and stronger in compression.

The stresses, in general, are probably pessimistic when one considers the boundary conditions of the model. The assembly was not allowed to expand or contract in the circumferential direction where the material is continuous. This in fact is not true; radial lines through the electrode should remain straight; however they would tend to translate in space as the object is heated up. This limitation was necessary to reduce the overall size and coat of the analysis. A two-dimensional analysis was not feasible because of the slots cut into the graphite and the copper.

TABLE 2.5-2

MATERIAL PROPERTIES

Pyrolytic Graphite

$E_a = E_b = 4.29 \times 10^6$ psi

$E_c = 1.55 \times 10^6$ psi

$\nu_{ab} = .15$ Transverse strain in planes due to stress along planes

$\nu_{ac} = .97$ Transverse strain across planes due to stress along planes

$\nu_{ca} = .35$ Transverse strain along planes due to stress perpendicular to planes

	TEMPERATURE (°C)		
	25	400	600
αa, αb in/in°C	0.8×10^{-6}	0.75×10^{-6}	1.0×10^{-6}
αc, in/in°C	20.0×10^{-6}	22.5×10^{-6}	24.2×10^{-6}

G_a, G_b 2.5×10^6 psi (Translaminar)

G_c 0.10×10^6 psi (Interlaminar)

Copper

	TEMPERATURE (°C)		
	25	400	600
E (PSI)	18.0×10^6	15.8×10^6	13.3×10^6
ν	0.328		
α in/in°C	17.0×10^{-6}	17.5×10^{-6}	18.5×10^{-6}

Alumina

	TEMPERATURE (°C)		
	25	400	600
E (PSI)	44.0×10^6		
ν	0.21		
α in/in°C	6.2×10^{-6}	6.8×10^{-6}	7.4×10^{-6}

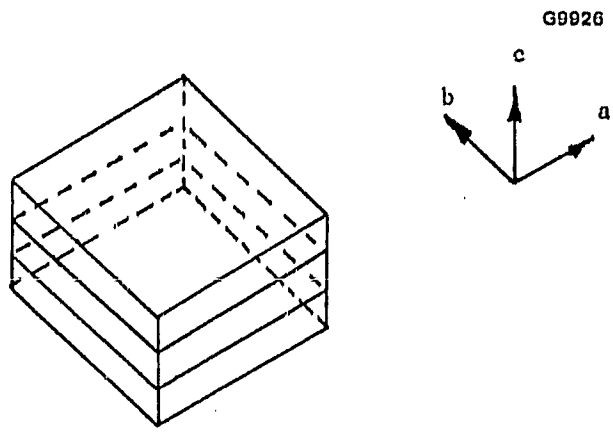

Figure 2.5-12 Material direction for pyrolytic graphite in collector electrode.

TABLE 2.5-3

MATERIAL STRENGTHS

Pyrolytic Graphite

	DIRECTION "ab"	DIRECTION "c"
Tensile (PSI)	16,000	400
Compressive (PSI)	14,000	45,000
Flexural (PSI)	24,000	1,880

Copper

Tensile (PSI)	32,000

Alumina

Tensile (PSI)	28,000

TABLE 2.5-4

MAXIMUM STRESSES
AND MARGINS OF SAFETY

Pyrolytic Graphite

	Tensile (PSI)	M.S.	Compressive (PSI)	M.S.	Flexural (PSI)	M.S.
"a" Direction	2,900	4.51	3,800	2.68	2,900	7.27
"b" Direction	4,000	3.00	10,500	0.33	4,100	4.85
"c" Direction	100	3.0	5,200	7.65	1,100	0.70

Copper

Tensile (PSI)	M.S.
5,800	4.51

Alumina

Tensile (PSI)	M.S.
5,400	4.18

2.5.3 Determination of the Best Mating Material for Pyrolitic Graphite

A thermal-structural analytical evaluation of brazing pyrolytic graphite to several materials was completed. It was first desired to determine which mating material would have the best match of coefficient of thermal expansion with the graphite. This was accomplished by a series of linear finite element model analyses. A simple two-dimensional test case, shown in Figure 2.5-13, was devised. The graphite material properties were given their transversely isotropic characteristics, while the mating material was considered to be purely isotropic. The individual material properties used are given in Table 2.5-5.

The SAAS III finite element model that was developed is shown in Figure 2.5-14. SAAS III is a finite element analysis computer program which specializes in axisymmetrics and plane solids with different orthotropic, temperature-dependent material properties in tension and compression. Three different linear analyses were performed on each of the four different mating materials. The four mating materials considered for evaluation were alumina, copper, kovar and molybdenum. The three analysis types studied were plane stress, plane strain and axisimmetric. With these analysis types the stress boundaries of each material characteristics could be evaluated.

The results of these analyses are listed in Table 2.5-6. Although these results are strictly linear, they still provide a valuable insight into the analytical material interactions during a brazing procedure. It appears that two of the mating materials, alumina and molybdenum, should be eliminated from further study. Their coefficients of thermal expansion are dramatically different from the "c" direction in the graphite. This is evidenced in the high tensile "Z" directional stresses. In real life this would tend to pull the graphite layers apart. When the stresses in the mating material are studied, thelinear analysis results are shown to be basically valid. The alumina ceramic is typically considered linear elastic until failure. Similarly the stresses in the molybdenum mating material were below the yield strength of the material, thereby also making the linear approximation valid.

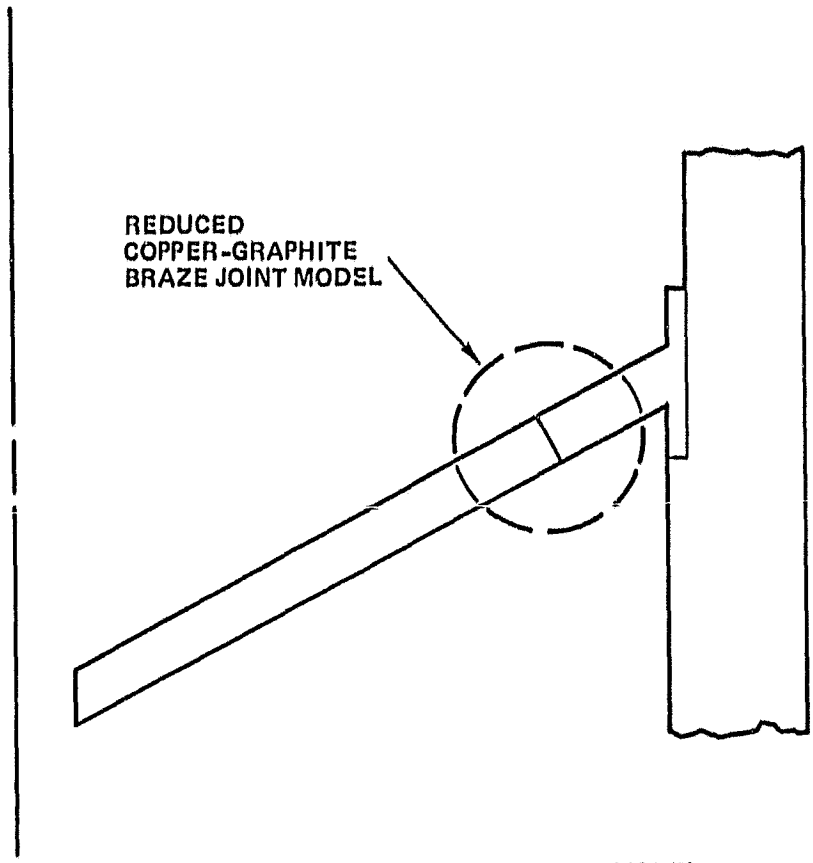

COLLECTOR ELECTRODE AND ISOLATOR MODEL

Figure 2.5-13 Proposed ANSYS models.

TABLE 2.5-5

MATERIAL PROPERTIES AT ROOM TEMPERATURE

	YOUNG'S MODULUS (PSI)	COEFFICIENT OF THERMAL EXPANSION (in/in $-^{o}C$)	POISSON'S RATIO
ALUMINA	44.0×10^{6}	8.2×10^{-6}	0.21
COPPER	18.0×10^{6}	19.9×10^{-6}	0.33
KOVAR	20.0×10^{6}	13.2×10^{-6}	0.32
MOLYBDENUM	43.9×10^{6}	6.5×10^{-6}	0.32
PYROLYTIC GRAPHITE			
Tension	4.29×10^{6}		
ab Direction			
Compression	4.19×10^{6}	1.5×10^{-6}	ab -0.15
Tension	1.55×10^{6}		cb 0.35
c Direction			
Compression	1.58×10^{6}	24.0×10^{-6}	

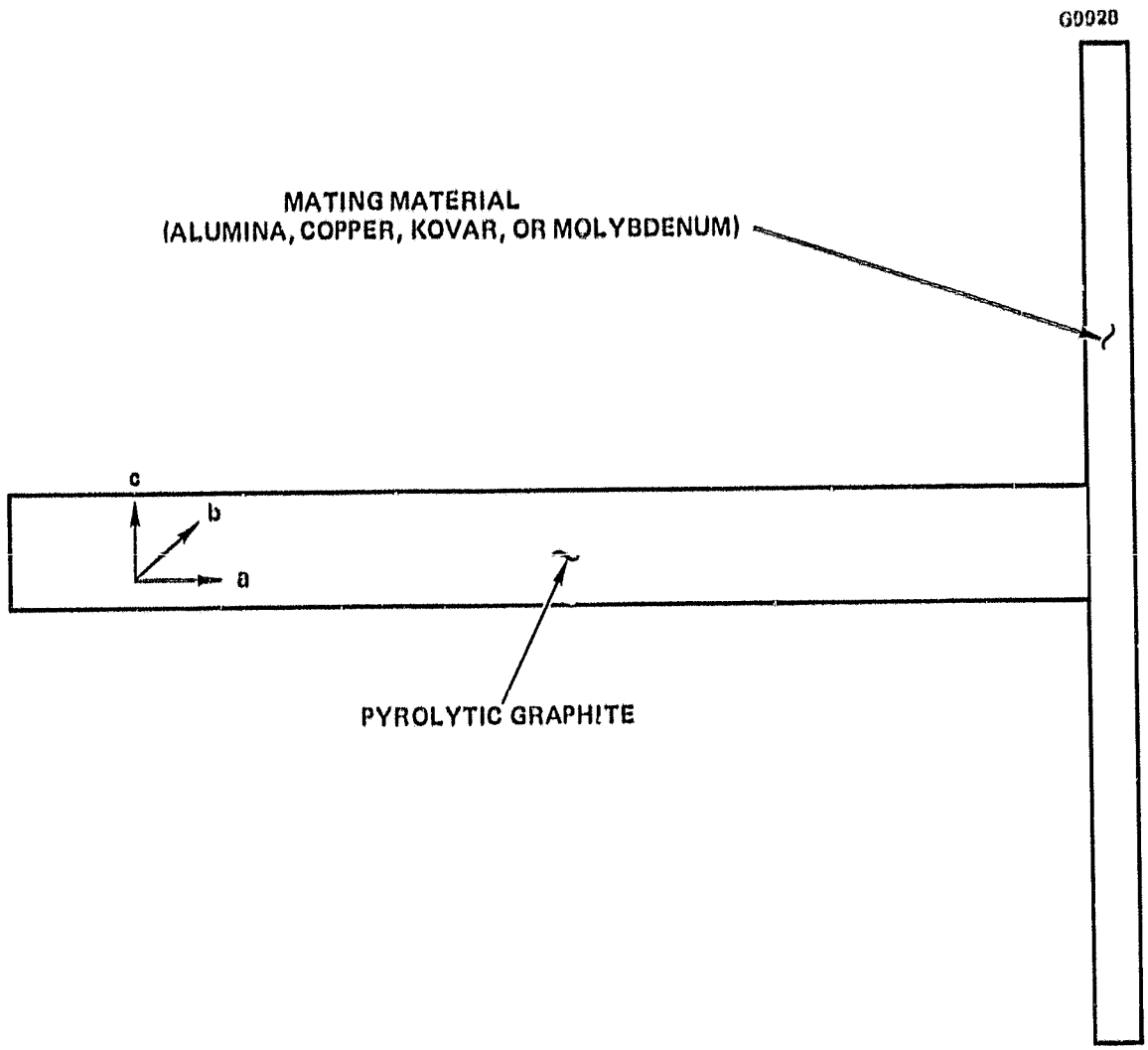

Figure 2.5-14 Sample two-dimensional test case.

TABLE 2.5-6 TWO-DIMENSIONAL STRESS RESULTS

WITHIN PYROLYTIC GRAPHITE

ATING ATERIAL		PLANE STRESS R (PSI)	PLANE STRESS Z (PSI)	PLANE STRESS T (PSI)	PLANE STRAIN R (PSI)	PLANE STRAIN Z (PSI)	PLANE STRAIN T (PSI)	AXISYMMETRIC R (PSI)	AXISYMMETRIC Z (PSI)	AXISYMMETRIC T (PSI)
ALUMINA	A	8053	20498	0.	7837	28475	32850	-19181	8626	- 6617
	B	-5902	18494	0.	-5903	26760	33249	-13142	11296	- 4526
	C	-4209	18804	0.	-3790	27407	33555	-10884	12186	- 3868
	D	-5920	18492	0.	-5913	26765	33255	-13122	11314	- 4513
	E	8013	20483	0.	7807	28457	32837	-19107	8651	- 6606
COPPER	A	1192	4799	0.	-268	-1613	4912	-67671	-50962	-71462
	B	-978	4431	0.	234	-1537	4910	- 3851	-33176	-62855
	C	-390	4523	0.	67	-1576	4897	- 1885	-30874	-60569
	D	-985	4431	0.	234	-1538	4910	- 3829	-33177	-62862
	E	1178	4792	0.	-264	-1610	4914	-67573	-50909	-71432
KOVAR	A	3413	12815	0.	2466	13563	19203	-39615	-17352	-32617
	B	-2760	11807	0.	-2071	12909	19251	- 6185	- 7579	-27544
	C	-1265	12044	0.	- 744	13229	19362	- 3719	- 6095	-26126
	D	-2776	11805	0.	-2086	12907	19251	- 6169	- 7669	-27539
	E	-3406	12811	0.	2448	13552	19196	-39534	-17315	-32598
MOLYBDENUM	A	9201	22856	0.	9028	31290	35392	-10253	17620	4879
	B	-6718	20592	0.	-6708	29356	35879	-12780	18438	6387
	C	-4894	20928	0.	-4534	30054	36228	-10448	19263	6942
	D	-6729	20594	0.	-6720	29361	35885	-12758	18460	6404
	E	9178	22846	0.	8980	31265	35375	-10182	17639	4885

The two remaining mating materials, however, deserve more consideration. The kovar stresses exceeded the yield strength of the material, making the linear approximation invalid in this area. The stresses in the kovar are specifically from 50% to 75% higher than the yield strength of the material. If the stresses in the graphite were linearly decreased by 75% as a first order approximation, the material would still be unacceptable overstressed.

The only remaining mating material worth consideration is copper. Although the graphite stresses in the axisymmetric analysis are quite high, the copper stresses were equally as high. The copper stresses, being an order of magnitude higher than its yield strength, would in reality tend to be much lower in a non-linear analysis. The stresses exhibited in the graphite in the plane stress and plane strain analyses show copper to be an excellent match for thermal expansion.

To further substantiate the use of copper as a mating material, a more sophisticated non-linear analysis must be performed. This analysis should include two different types of non-linear stress characteristics of the brazing process. The first of these is the non-linear stress versus strain versus temperature behavior of the copper. The second non-linear behavior is the path dependence of the braze cooldown procedure. One of the finite element programs capable of handling these non-linear type phenomena is ANSYS. ANSYS, ANalysis SYStem, is a large scale general purpose finite element program typically used for similar complex types of analyses.

Two finite element models are suggested for further study, see Figure 2.5-15. The first will detail an actual copper-graphite braze joint. The second will simulate the brazing of graphite, copper and alumina in a collector electrode and isolator type configuration.

2.5.4 Conclusions

As found in the earlier work, see Section 2.5.3, the material expected to best braze to the pyrolytic graphite is OFE copper. Other materials considered were alumina, kovar and molybdenum. It was found that the most important

ingredient to failure were the cross-grain or "c" directional stresses. These stresses can be reduced by using (1) a material with a coefficient of expansion close to "c" direction value; (2) a material with a low yield strength. The next phase of this study derived the residual component stresses produced in the current collector electrode configuration during its manufacture. A finite element model of the entire collector electrode assembly including the pyrolytic graphite electrode/copper disk and alumina isolator was made. The stresses in the area of a typical metal to graphite braze joint were studied. The calculated residual braze stresses produced acceptable margins of safety for all collector components. The components in the collector electrode assembly have not been designed to produce minimal residual brazing stresses. The final residual brazing stresses could probably be reduced by decreasing the outer diameter and/or the thickness of the pyrolytic graphite electrode.

The ease of manufacturability, with high reliability, will be hard to attain. The differences in the coefficients of thermal expansion for any mating material are dramatic. With the 850 to 900^{o}C change in temperatures during brazing, the fixturing and alignment of the electrodes could also be difficult in a complete collector assembly.

2.6 BRAZING TECHNIQUE INVESTIGATION

2.6.1 Material Selection

Fine braze alloys (Table 2.6-1) and six joint materials (Table 2.6-2) were selected for preliminary evaluation.

TABLE 2.6-1

SELECTED BRAZE ALLOYS

1.	Alloy name:	TICUNI
	Composition:	Ti-15% Cu-15% Ni
	Solidus/liquidus temperature:	910° to 960°C
	Supplier:	WESGO
2.	Alloy name:	TICUSIL
	Composition:	Ag-26.7% Cu-4.5% Ti
	Solidus/liquidus temperature:	830° to 850°C
	Supplier:	WESGO
3.	Alloy name:	NICROBRAZ - 30
	Composition:	Ni-19.0% Cr-10.2% Si
	Solidus/liquidus temperature:	1080° to 1135°C
	Supplier:	WALL COMONOY
4.	Alloy name:	NICROBRAZ - 35
	Composition:	Ni-19.5% Cr-9.8% Si-9.5% Mo
	Solidus/liquidus temperature	1080° to 1110°C
	Supplier:	WALL COLMONOY
5.	Alloy name:	NICKEL-TITANIUM EUTECTIC
	Composition:	Ti-71% Ni-28%
	Eutectic temperature (71.6 Ti):	950°C
	Supplier:	TITANIUM CORPORATION and INTERNATIONAL NICKEL COMPANY

TABLE 2.6-2

SELECTED JOINT MATERIALS

1. Aluminum Oxide
2. Metallized Alumina Oxide
3. Beryllium Oxide
4. Metallized Beryllium Oxide
5. Kovar (Fe-Ni-Co Alloy)
6. Molybdenum

A literature search was then began to determine the optimum brazing technique. Table 2.6-3 lists three important references cited in this section.

TABLE 2.6-3

REFERENCES

ITEM (1)	"The Brazing of Graphite," R.G. Donnelly and G.M. Slaughter, Welding Journal, May 1962.
ITEM (2)	"Welding and Brazing of Advanced Refactory Alloys," G.M. Slaughter, D.A. Canonico, and R.G. Donnelly, Society of Aerospace Material and Process Engineers, 1971, pp. 317-322.
ITEM (3)	"Recent Advances in Brazing," G.M. Slaughter, W.J. Werner, R.G. Gilliland, and J.P. Hammond, Society for the Advancement of Material and Process Engineering, 1973, pp. 115-123.

Item (1) indicates that brazing alloys containing the strong carbide-forming element, titanium and zirconium, as major constitutents are excellent general purpose material for fabricating graphite assemblies. Item (2) indicates that a number of compositions have been developed to satisfactorily braze refractory metal, alumina oxide, and graphite. Ti-25% Cu-21% V alloy is one of them. Item (3) indicates that a large number of brazing filler metals that wet and flow on ceramics have been developed.

These filler metals contain certain elements that have suitable atomic sizes and chamical properties to create an affinity for chemical bonding with ceramics. The 48% Ti-48% Zr-4% Be brazing alloy is one of them.

A vacuum furnace with a 6 inch diameter by 12 inch high resist heating element, and a vacuum pumping system consisting of an ion pump, sublimation pump, vacsorb pump, and mechanical pump was tested to determine the capability of carrying out the screening tests. The vacuum furnace was heated up to 1,200°C, the vacuum pressure was sustained at 12×10^{-6} torr in all the temperature ranges. The results indicate the furnace was satisfactory for the tests.

2.6.2 Pyrolitic Graphite to Alumina Ceramic Ticusil Braze Screening Tests

High purity alumina ceramics were selected for the first materials to be joined to graphite in the screening tests. The alumina ceramic rings of 4" ID and 6" OD were gritblasted per MPS 1-17-C, cleaned per MPS 1-25-F, and air fired per MPS 4-2-13.

Brazing alloy samples of Ticusil and Ticuni in 0.001" thick foil form supplied by Wesgo were used for the screening tests. A wettability of pyrolytic graphite test, a wettability on alumina ceramics test, a relative flowability on pyrolytic graphite to alumina ceramics test was performed in one furnace run for each braze alloy.

Both alloys have good wettability on pyrolytic graphite and alumina ceramics. Ticusil also shows promising results in the relative flowability and the T-joint brazing test. However, further testing was indicated in an attempt to reduce the thermal stress in the braze joint. The Ticuni joint between pyrolytic graphite and alumina ceramics failed because of brittleness. The effect of thermal cycles were to be studied further.

Two heating cycles (Table 2.6-4) were employed in an effort to reduce the thermal stresses developed in the previous screening tests.

TABLE 2.6-4
BRAZING CYCLES

I.	Heating Time:	10 Minutes
	Brazing Time:	10 Minutes
	Cooling Control:	Furnace Cool
	Vacuum Pressure:	2.0×10^{-6} to 10×10^{-7} Torr
	Brazing Temperature:	$880^{\circ}C$ to $922^{\circ}C$
II.	Heating Time:	170 Minutes
	Brazing Time:	20 Minutes
	Cooling Control:	55 Minutes cool to $515^{\circ}C$
	Vacuum Pressure:	1.4×10^{-5} to 0.8×10^{-7} Torr
	Brazing Temperature:	$880^{\circ}C$ to $893^{\circ}C$

The results of the two heating cycles did not indicate any significant difference. The heating cycle II was aimed at reducing the thermal stress in the braze joint. Very slight thermal cracks were observed in the brazed joints from both of the heating cycles.

The following five figures show the assembly before and after brazing according to heating cycle II (Figures 2.6-1 through 2.6-5).

E3628

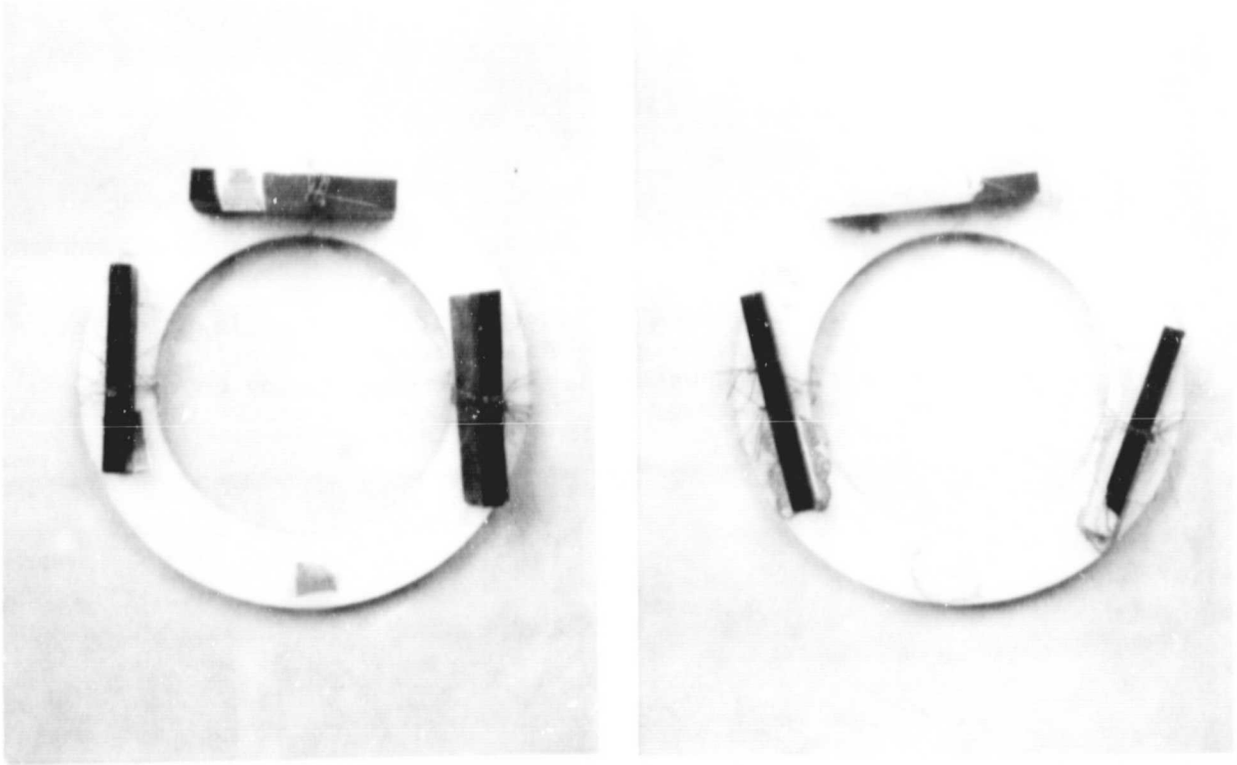

Figure 2.6-1 Left - as assembled combination braze evaluation sample. Right - sample after brazing. Mag. 1X.

E3629

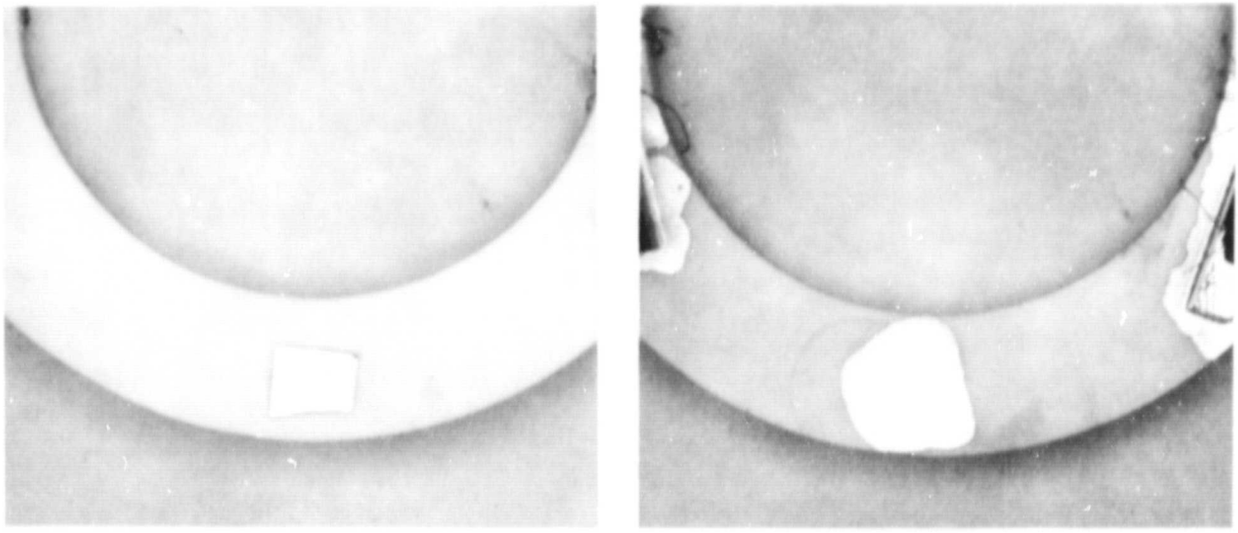

Figure 2.6-2 Left - Al_2O_3 - Ticusil weatbility sample prior to brazing. Right - After brazing indicating good flow and wetability of the braze alloy on the Al_2O_3. Mag. 2X.

E3630

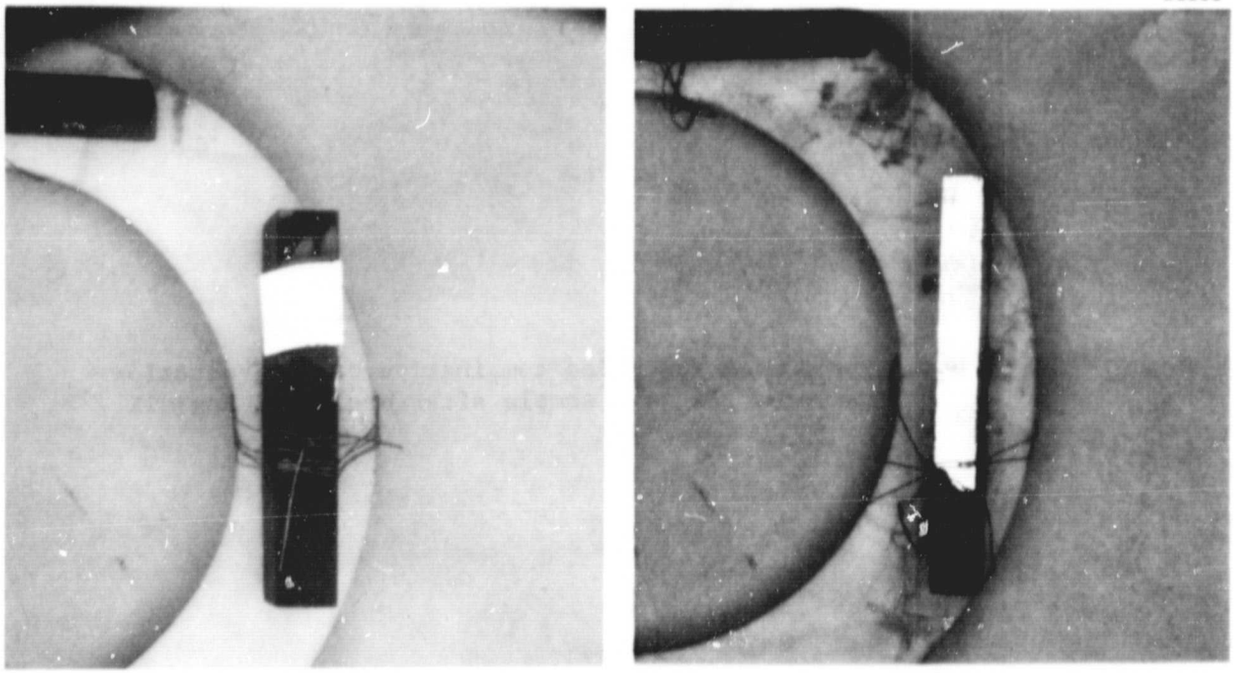

Figure 2.6-3 Left - PG-Ticusil wetability sample prior to brazing. Right - After brazing indicating good flow and wetability of the braze alloy on the PG. Mag. 2X.

E3631

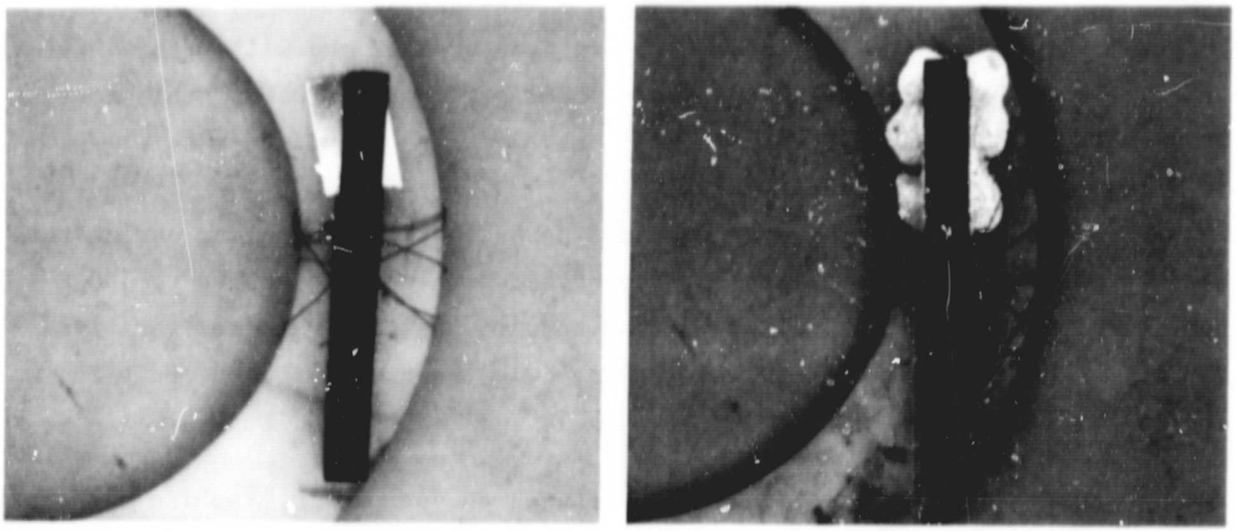

Figure 2.6-4 Left - Braze joint flowability sample prior to brazing. Right - After brazing indicating flow along the joint. Mag. 2X.

E3632

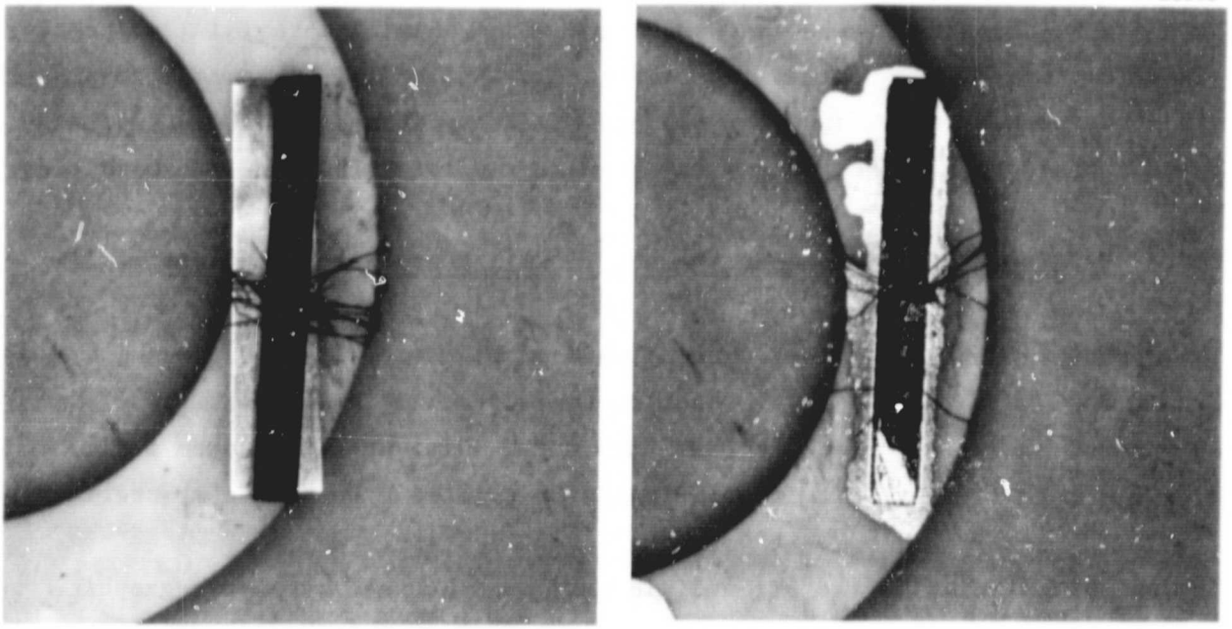

Figure 2.6-5 Left - T-joint sample prior to brazing. Right - After brazing indicating good flow and wetability along the entire joint. Mag. 2X.

From the Figures, the excellent flow of the brazing alloy can be observed. Thinner alloy sheet (0.003" thickness) has been ordered and will be used for the detail evaluation in place of the thicker alloy sheet (0.005" thickness) used in the screening tests.

To determine the durability of the brazed parts to thermal cycling during subsequent processing and application, the brazed samples were heated to 500°C held for 30 minutes, then cooled to room temperature, and repeated for five times. No detrimental effects were observed in the brazed joints after the thermal cycling.

Metallographic analyses of the T-joint between the pyrolytic graphite and alumina ceramics brazed with Ticusil are shown in Figures 2.6-6, 2.6-7, and 2.6-8.

A separation was noted along most of the length of the transverse section of the metallographically prepared joints. The gap observed did not appear to be a crack, and part of the gap was filled with mounting materials, suggesting a sample preparation problem. A crack in the AB-plane of the pyrolytic graphite was observed near the end of the gap and the start of the sound joint. This crack appears to be associated with stresses resulting from the gap condition.

2.6.3 Pyrolytic Graphite to Molybdenum Ticusil Braze Screening Test

The wettability of Ticusil on pure molybdenum was determined by placing a 0.25x0.25x0.005" Ticusil alloy sheet on the surface of a 1.5x0.75x0.090" molybdenum sheet, and brazed at 900°C±10°C for 10 minutes in vacuum 1.0 to 3.0×10^{-7} torr. Visual examination indicated excellent wetting characteristics.

The relative flowability of Ticusil in the joint between pyrolytic graphite and molybdenum was determined by placing a 0.25x0.25x0.005" Ticusil sheet at one end of a joint having a total length of 1.25", then, brazing at 900°C ± 10°C for 10 minutes in vacuum 1.0 to 3.0×10^{-7} torr. The flow length after brazing was 1.0"; four times the original length of braze alloy placed in the joint.

E3633

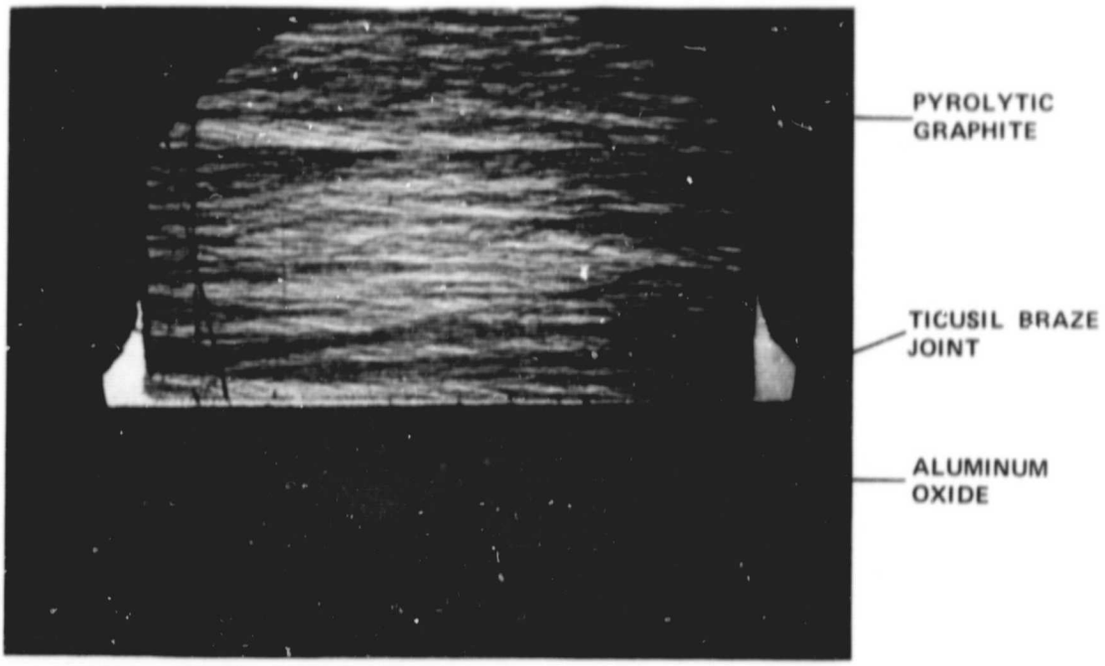

Figure 2.6-6 Transverse section through the T-joint sample. 25X MAG.

E3634

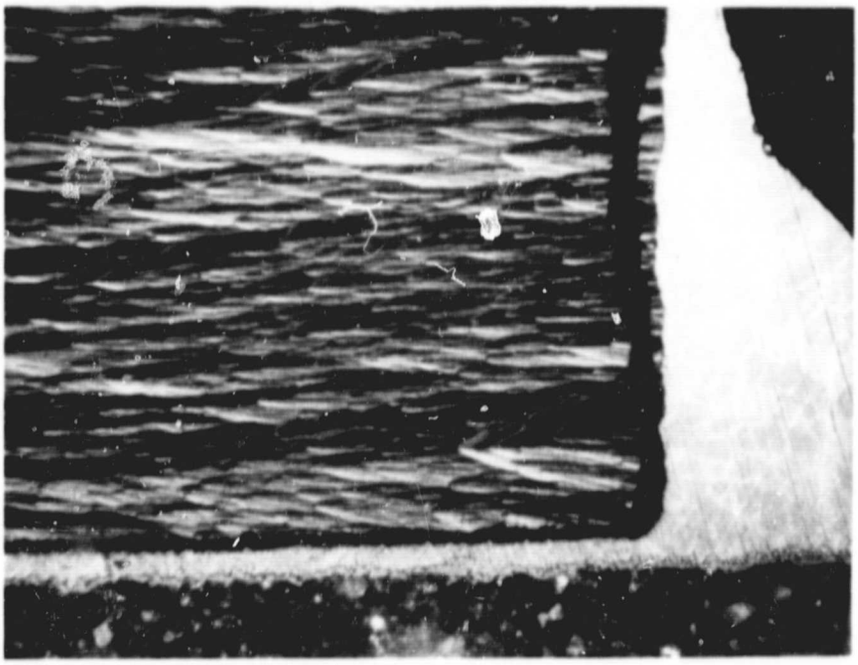

Figure 2.6-7 Enlarged view of the right side of the joint shown in Figure 2.6-6. The gap between the PG and the braze alloy is apparent along the length of the joint area shown. 160X MAG.

E3635

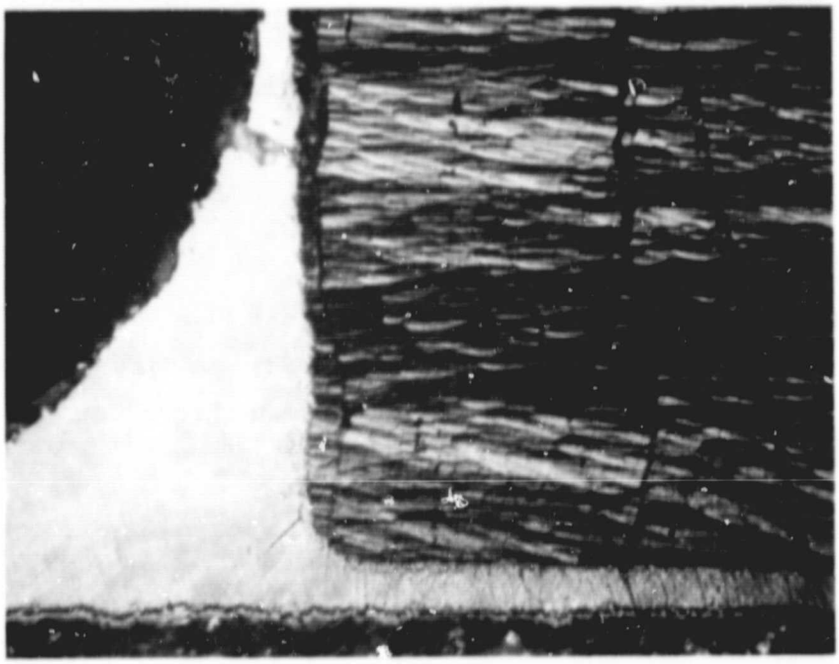

Figure 2.6-8 Enlarged view of the left side of the joint shown in Figure 2.6-6. The gap extends about half way along the length of the joint area shown. The dark angular line on the far right is a scratch from the polishing process, but the next line to the left emanating from the gap is a crack in the AB-plane of the PG. 160X MAG.

The T-joint bond evaluation was performed by placing a 0.15"x0.25"x0.005" Ticusil sheet between the T-joint of a 1.25"x0.5"x0.120" molybdenum sheet. The direction of the pyrolytic graphite sheet, i.e., the thickness of the sheet, was resting along the cross section of the molybdenum sheet. The T-joint assembly with Ticusil brazing alloy was secured with molybdenum wires, and brazed at $900^{o}C \pm 10^{o}C$ for 10 minutes in vacuum 1.0 to 3.0×10^{-7} torr.

Metallographic analysis of a transverse section of the T-joint showed a complete bond between the pyrolytic graphite sheet and the molybdenum sheet, but some cracks in the AB-plane of the pyrolytic graphite were observed. These cracks are believed to be caused by the thermal stress caused by the considerable differences in thermal expansion. Figures 2.6-9, 2.6-10, and 2.6-11 are photomicrographs of the bonded area.

2.6.4 Pyrolytic Graphite to Copper, Ticusil Braze Screening Test

Evaluation of copper to pyrolytic graphite brazed with Ticusil (Ti-Cu-Ag) was performed. Wettability, flow and T-joint brazes were performed at $900^{o}C$ for five minutes in a vacuum of 5×10^{-6} Torr. Copper strip, 0.078" thick, was used for the samples.

The wettability tests exhibited good wetting with very little flow. Since the braze alloy contains copper as one of its constitutents, the alloying reaction with the copper strip could be expected to raise the melting point and restrict the braze alloy flow. Because all previous braze tests with Ticusil exhibited extensive braze flow, concern had been developing that a stop-off material that could be applied to production items would have to be found to prevent excessive braze alloy flow. The apparent ability of the Ticusil to wet metals and non-metals alike made finding a stop-off material appear to be a sizeable task. However, the problem does not appear to exist with copper.

Visual examination of the T-joints indicated a sound joint was produced. A crack was observed in the pyrolytic graphite well above the braze joint and running in the general longitudinal direction. The copper strip had deformed in a concave direction away from the braze joint. The stress generated by

E3636

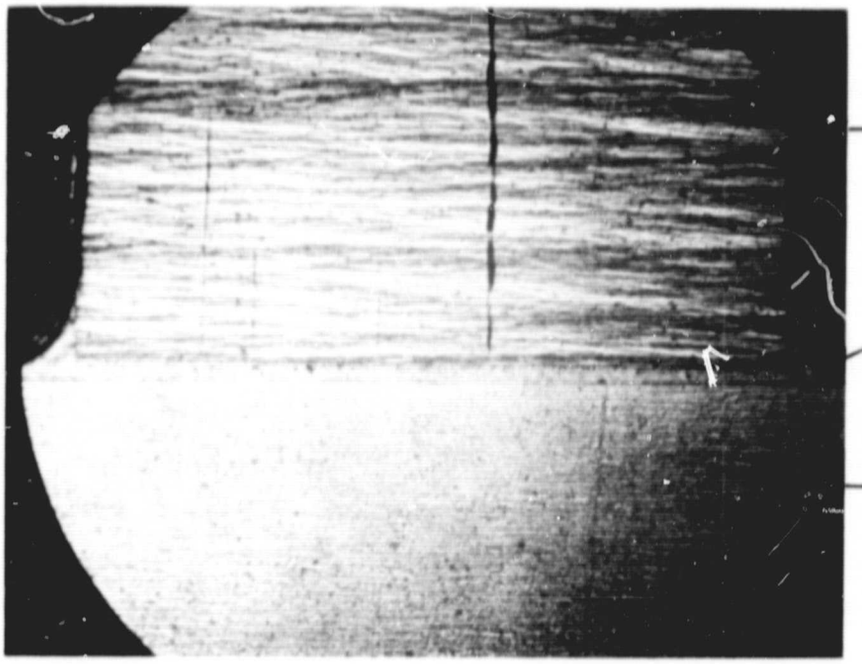

Figure 2.6-9 Transverse section through T-joint sample. Note cracks in the AB-plane of the pyrolytic graphite. 30X MAG.

E3637

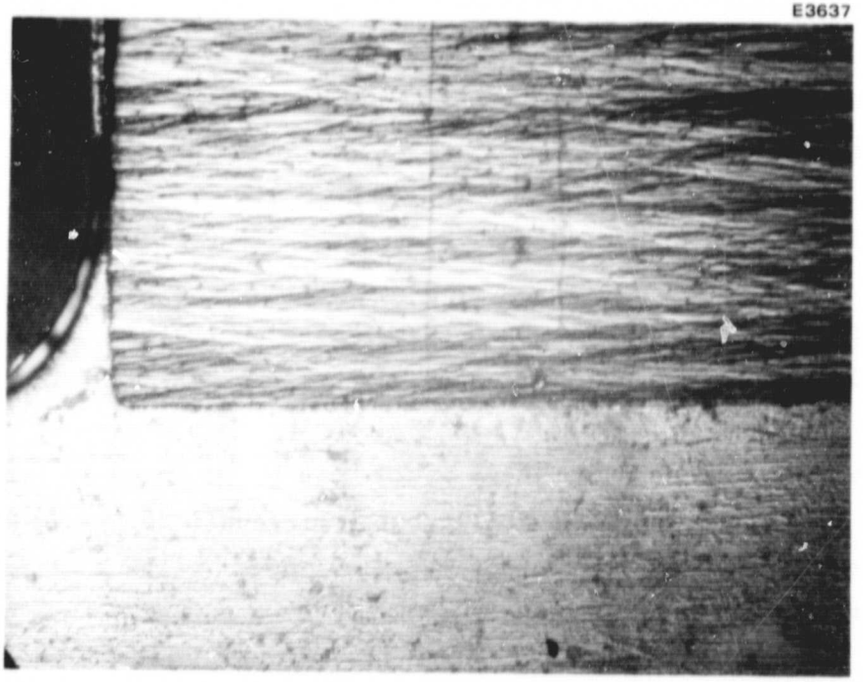

Figure 2.6-10 Enlarged view of the left side of the joint shown in Figure 2.6-9 and illustrating a complete, sound joint. 80X MAG.

C-2

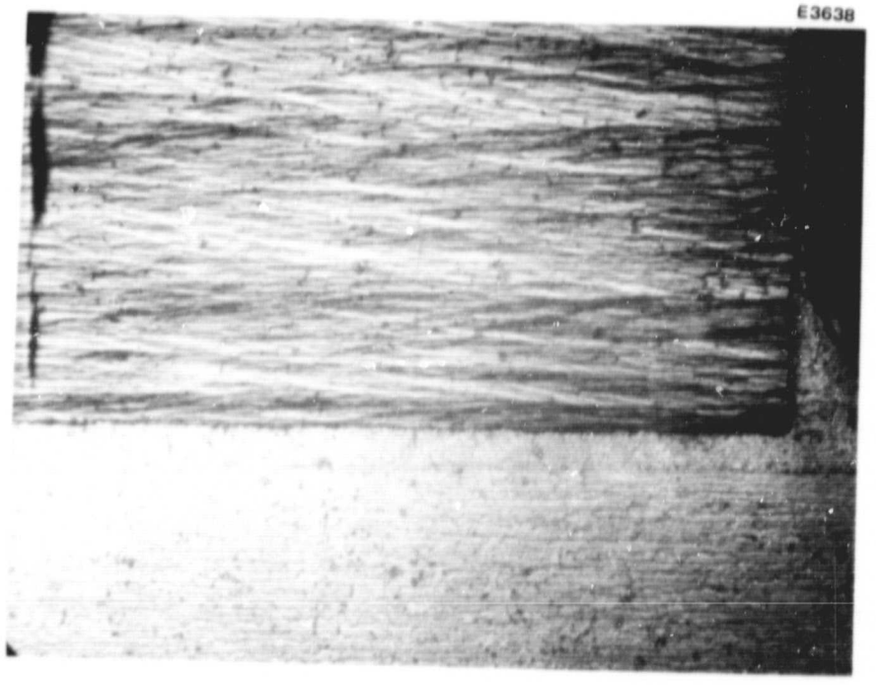

Figure 2.6-11 Enlarged view of the right side of the joint shown in Figure 2.6-9. Note that the crack does not emanate from the joint, but starts some distance from the joint suggesting that the compressive loads at the joint cause buckling in the graphite and cracking as a result of weak interlaminar bonds. 80X MAG.

the difference in thermal expansion between the copper and the pyrolytic graphite and concentrated in the braze joint was apparently relieved by the deformation of the copper and fracture in the pyrolytic graphite. The lack of any evidence of a failure in the joint indicates a mechanically strong joint was achieved.

The wetting and flow test of the Ticusil on copper indicated excellent wetting with a minimum amount of flow, Figure 2.6-12. The minimum flow is indicated by the wetted area being almost identical to the size of the original braze alloy form.

A T-joint of the pyrolytic graphite to copper brazed with Ticusil is shown in Figure 2.6-13. The longitudinal cracks in the PG above the braze joint was observed when the sample was removed from the brazing furnace. The cracks terminated about 1/4 inch from the end of the PG.

Because the copper has a significantly higher thermal expansion than the PG in the a, b directions, the originally flat copper strip bowed away from the PG during coolind and caused a stress in the PG above the braze alloy sufficient to cause the fracture. This type of cracking is not expected to be a problem in the collector design. The geometric configuration of the collector design will cause the stresses developed to translate into compressive loading of the PG, or they will be cancelled by adjusting the length of the two materials to produce an overall equivalent change in deminsion of both parts.

A transverse metallographic section through the joint, Figure 2.6-14 revealed an excellent joint between the copper and the PG. Unlike all other joints examined, there is no evidence of delamination between the a-b planes in the PG. Examination of the morphology of the braze alloy, Figures 2.6-15 and 2.6-16, indicates a complete metallurgical bond between the braze alloy and the PG as well as the copper. In some regions a platelet phase, Figure 2.6-17, formed in the braze alloy indicating a solutioning of the graphite by the braze alloy.

E3639

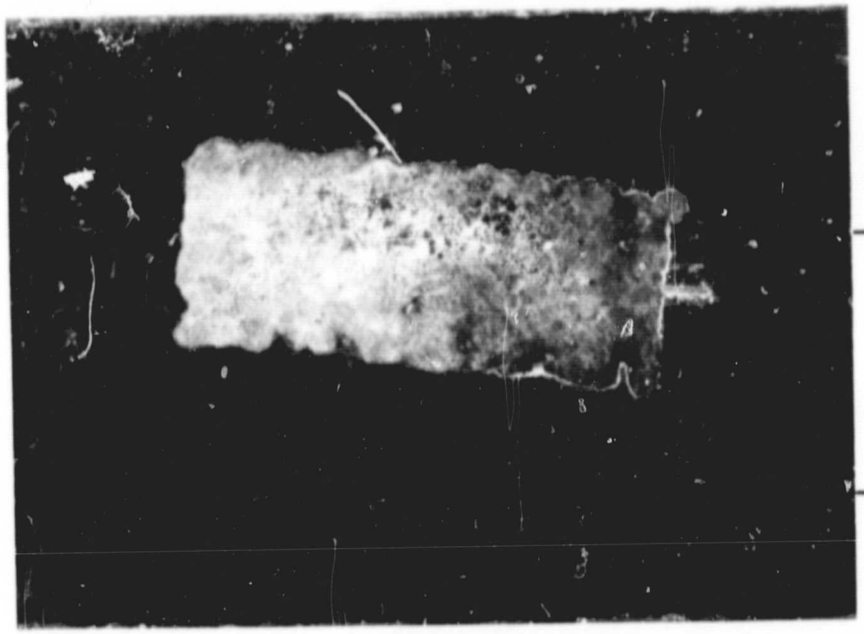

Figure 2.6-12 Wetting and flow test sample of Ticusil on OFE copper. Mag. 5X.

E3640

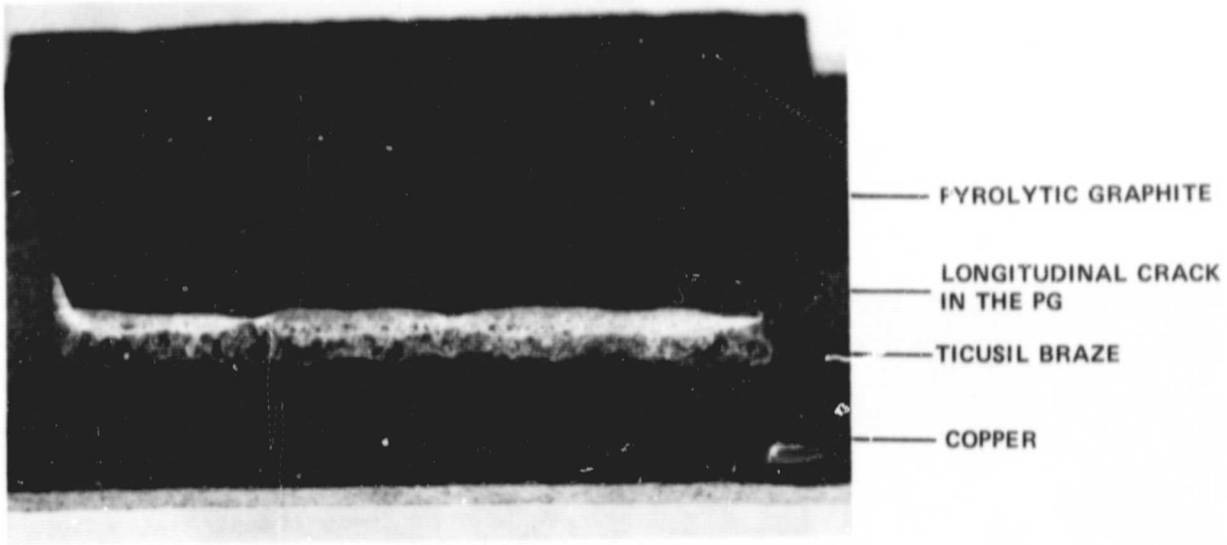

Figure 2.6-13 T-joint of PG to copper brazed with Ticusil. Mag. 4X.

E3641

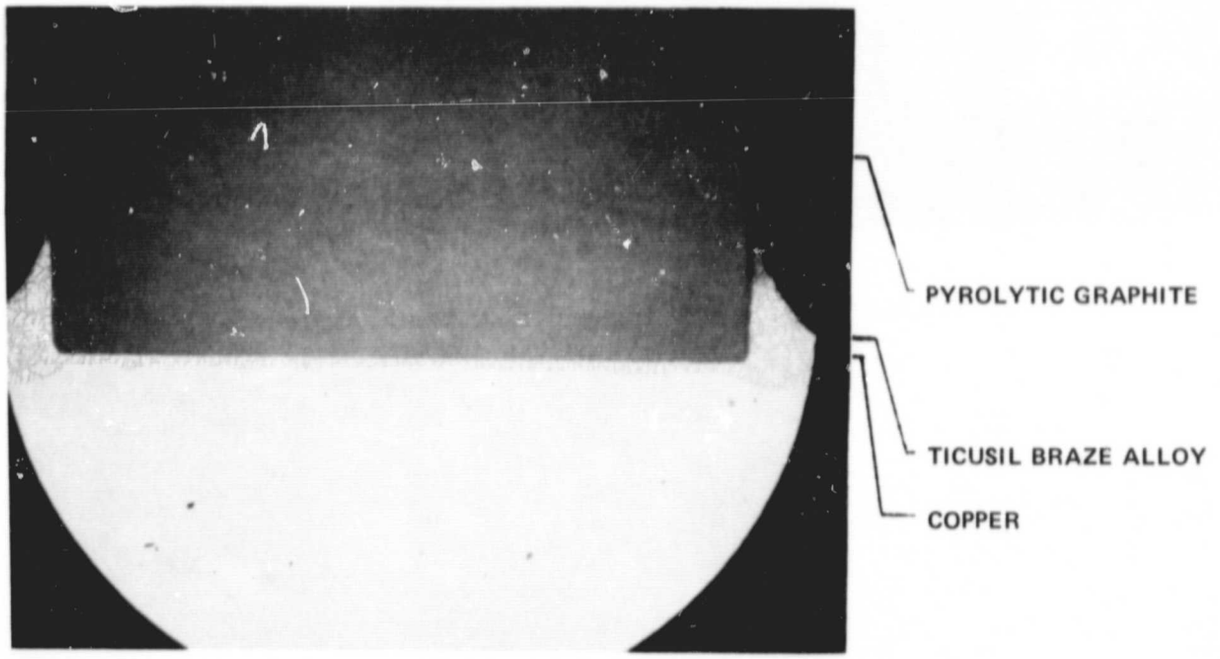

Figure 2.6-14 Transverse section of T-joint in Figure 2.6-13. Mag. 30X.

E3642

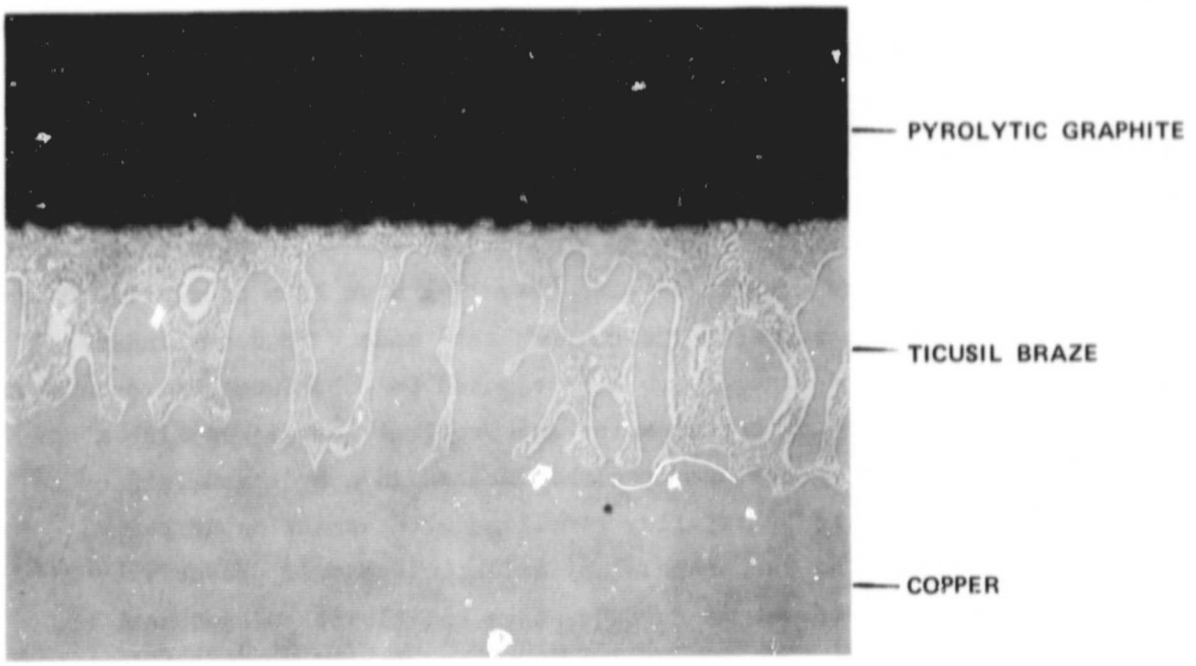

Figure 2.6-15 Enlarged view of braze joint in Figure 2.6-14. Mag. 400X.

E3643

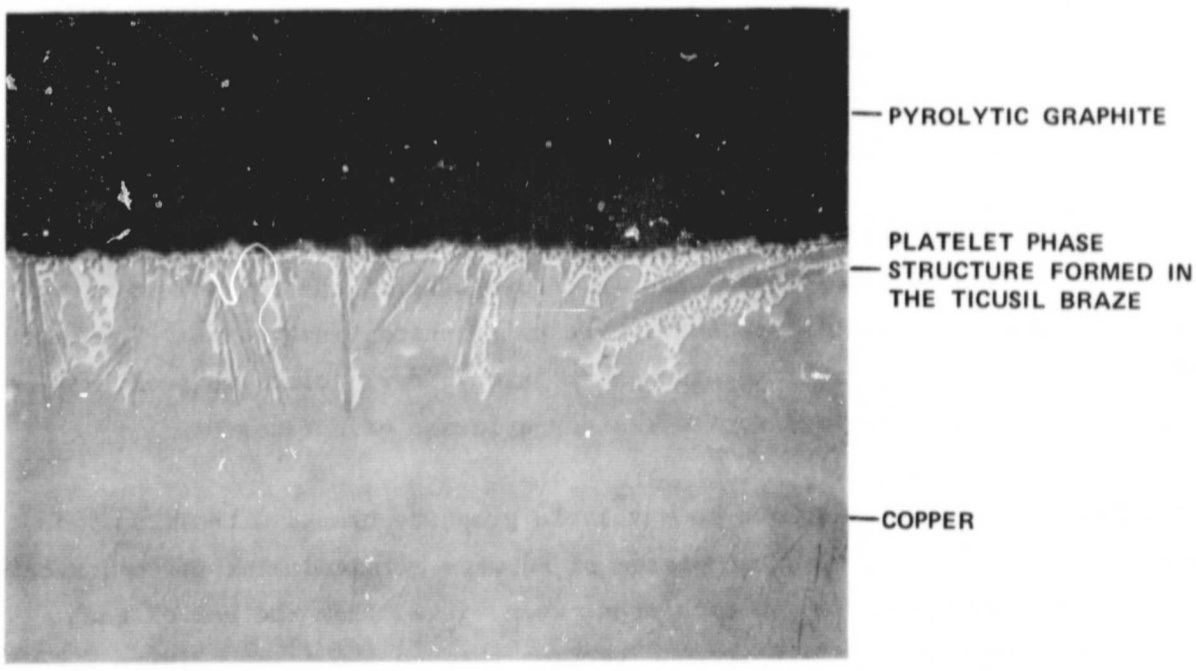

Figure 2.6-16 Platelet phase structure formed in some regions of the braze joint in Figure 2.6-14. Mag. 400X.

The ability of the brazed joint to transmit the stress caused by the difference in expansion between the materials being joined into the PG material at a level sufficient to cause it to fracture indicates that the joint itself is structurally sound.

To evaluate other factors associated with traveling wave tube production operations, additional PG to copper braze samples were made. To determine the compatibility of a brazed assembly to be subjected to subsequent hydrogen atmosphere brazing operations and to check for any problems associated with a possible lower remelt temperature, samples were heated in a hydrogen furnace to 950°C. No evidence of the braze alloy remelting or degradation of the PG was found. The surface of the braze alloy fillet discolored probably by the formation of titanium hydride. A subsequent vacuum firing removed most of the discoloration.

Based on the excellent quality of the joint produced between the pyrolytic graphite and copper using the Ticusil braze alloy, parts were designed and ordered for the fabrication of collector segment assemblies.

2.6.5 Pyrolytic Graphite to Pyrolytic Graphite, Ticusil Screening Test

Some conceptual MDC designs may require a PG to PG braze joint. Since previous tests have indicated the Ticusil wets and flows well on the PG, a T-joint was made to evaluate the quality of a graphite to graphite braze joint. The braze was performed at 900°C for five minutes at 5×10^{-6} Torr. joint. Visual examination of the joint did not reveal any evidence of defects.

A T-joint of pyrolytic graphite to pyrolytic graphite brazed with Ticusil is shown in Figure 2.6-17. The two pieces of PG were oriented with the c-direction of each piece perpendicular to each other when viewed from the end of the T-joint. A transverse metallographic section through the joint, Figure 2.6-18, revealed cracks or laminations between the a-b planes in both pieces of graphite. As expected, the cracks have propagated in each piece in a direction perpendicular to the c-direction. The difference in thermal expansion between the

E3644

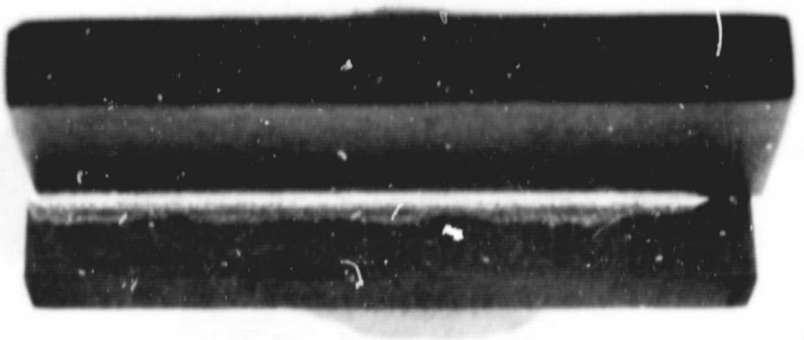

Figure 2.6-17 T-joint of pyrolytic graphite brazed to pyrolytic graphite with Ticusil. Mag. 4X.

E3645

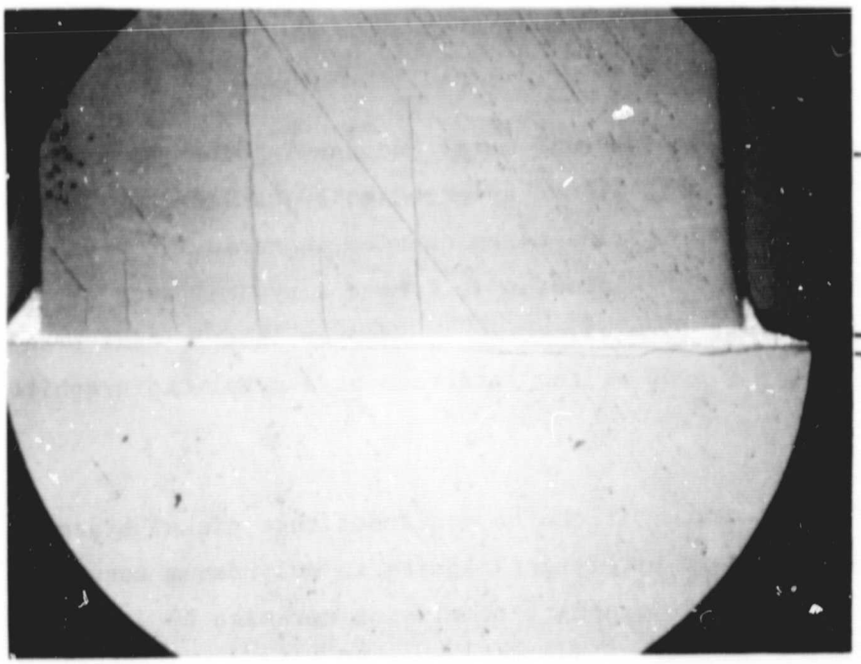

Figure 2.6-18 Transverse section of T-joint in Figure 2.6-17. Mag. 30X.

c and the a, b directions is apparently sufficient to cause the bond between the a-b planes to fail. A good metallurgical bond between the braze alloy and both pieces of graphite was achieved as shown in Figure 2.6-19.

2.6.6 Nicrobraz 35 and Nicrobraz 30 Screening Tests

Upon receipt of the brazing alloys, the screening tests for both were initiated to braze pyrolytic graphite to molybdenum metal and to braze pyrolytic graphite to alumina ceramics. Brazes were performed at 1175°C for 15 minutes in a vacuum of $1x10^{-4}$ torr for Nicrobraz 35. Brazes were performed at 1190°C for 15 minutes in a vacuum of $1x10^{-4}$ torr for Nicrobraz 30. Listed below is the breakdown of the alloys used.

Nicrobraz 35 - 19.34 Cr - 9.46 Si - 9.34 Mn - Ni
Powder Form, Mesh + 140 - 200

Nicrobraz 30 - 19.00 Cr - 10.20 Si - Ni Powder
Form, Mesh + 140 - 200

The wettability of both alloys on molybdenum metal and the T-joints of pyrolytic graphite to molybdenum for both alloys appeared to be satisfactory. The wettability test of both alloys on alumina ceramics were inconclusive and had to be rerun. The T-joint braze with Nicrobraz 35 formed a typical bond at the interface of a pyrolytic graphite alumina ceramic. However, the T-joint braze with Nicrobraz 30 did not form a bond at the interface of a pyrolytic graphite alumina ceramic.

As a result of these screening tests, it can be concluded that nickel braze brazing alloys can be used to braze pyrolytic graphite to molybdenum metal. The feasibility of brazing pyrolytic graphite to alumina ceramics by using nickel braze brazing alloys Nicrobraz 35 and Nicrobraz 30 needed additional evaluation.

The T-joints between pyrolytic graphite and molybdenum brazed with Nicrobraz 30 and Nicrobraz 35 alloys were examined metallographically. The Nicrobraz 30 joint exhibited excessive reaction and erosion of the molybdenum and voids at

E3657

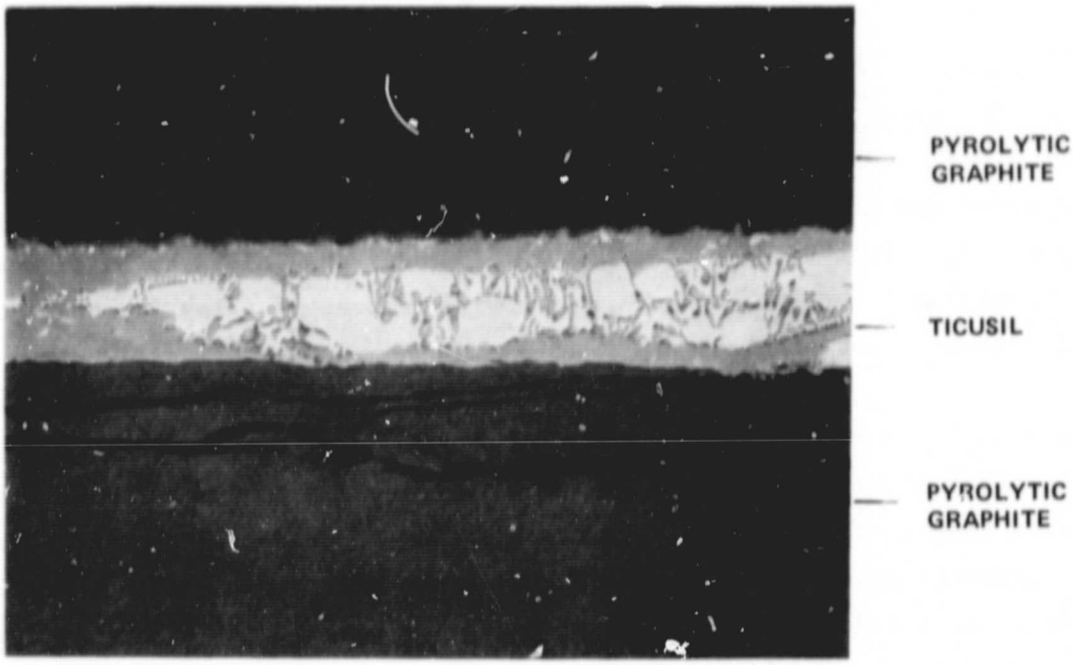

Figure 2.6-19 Enlarged view of braze joint in Figure 2.6-18. Mag. 400X.

the braze alloy - PG interface, Figures 2.6-20 and 2.6-21. The voids appear to be associated with the formation of new phase reactions with the graphite. The extent of the void formation varied significantly along the joint as indicated in Figure 2.6-22. Because control of the reaction and void formation would be difficult in production, further evaluation of Nicrobraz 30 alloy for this joint configuration is not planned.

The Nicrobraz 35 joint exhibited excessive cracking in the braze alloy and an intermittent poor quality bond between the braze alloy and thepyrolytic graphite, Figures 2.6-23 and 2.6-24. Although a reaction layer clearly formed between the graphite and the braze alloy, extensive fracturing of the reaction layer was observed. Since these conditions would render the joints to be of questionable reliability, further evaluation of the Nicrobraz 35 alloy for this joint configuration is not planned.

Attempst to braze pyrolytic graphite to aluminum oxide with the Nicrobraz 30 and Nicrobraz 35 alloys resulted in extensive cracking in the ceramic below the braze joint. The extent of the cracking was so extensive that the brazed parts separated under normal handling conditions. Apparently the bond between the braze alloy and the aluminum oxide was good, but the difference in thermal expansion of the braze alloy and the oxide caused high stresses in the ceramic below the braze joint. Although it may be possible to reduce the stress by reducing the thickness of the braze alloy joint, control would be difficult. Therefore, no additional evaluation is planned for these braze alloys in this joint configuration.

E3646

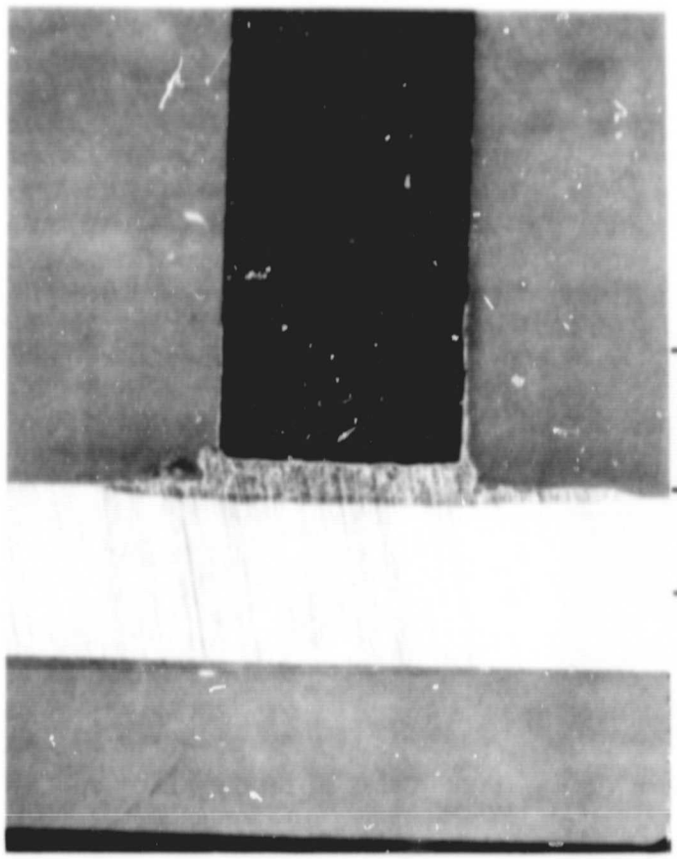

Figure 2.6-20 Transverse section of PG to molybdenum joint brazed with nicrobraz 30. Mag. 10X.

E3647

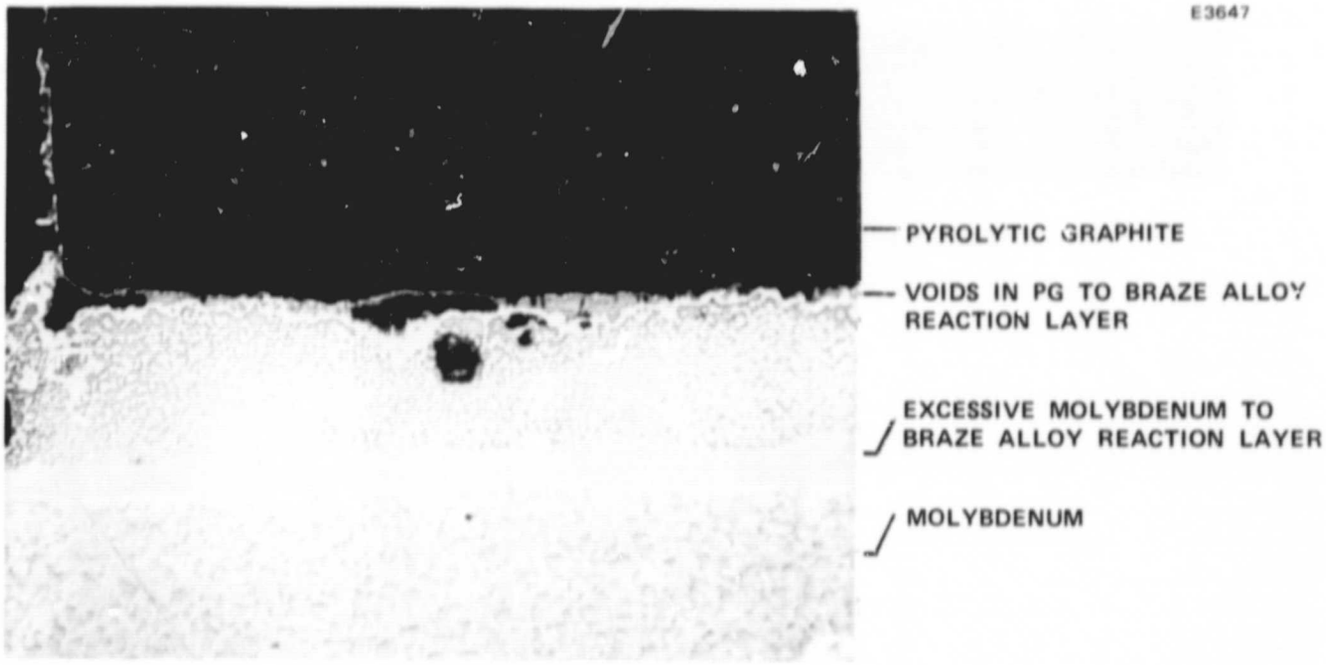

Figure 2.6-21 Enlarged view of braze join in Figure 2.6-20. Mag. 50X.

E3648

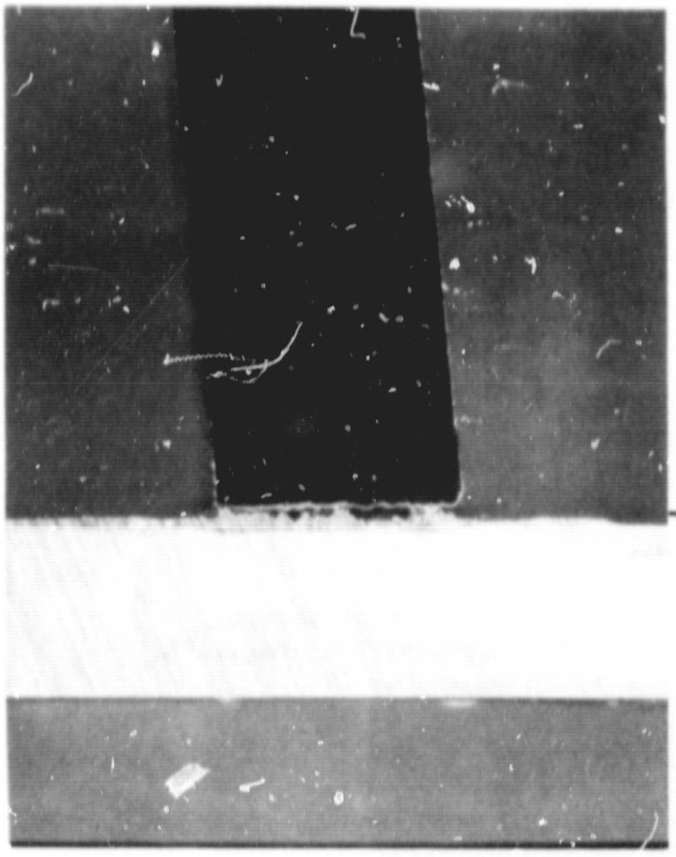

Figure 2.6-22 Similar to Figure 2.6-20 illustrating the extent of void formation at the PG to braze alloy reaction layer.

E3649

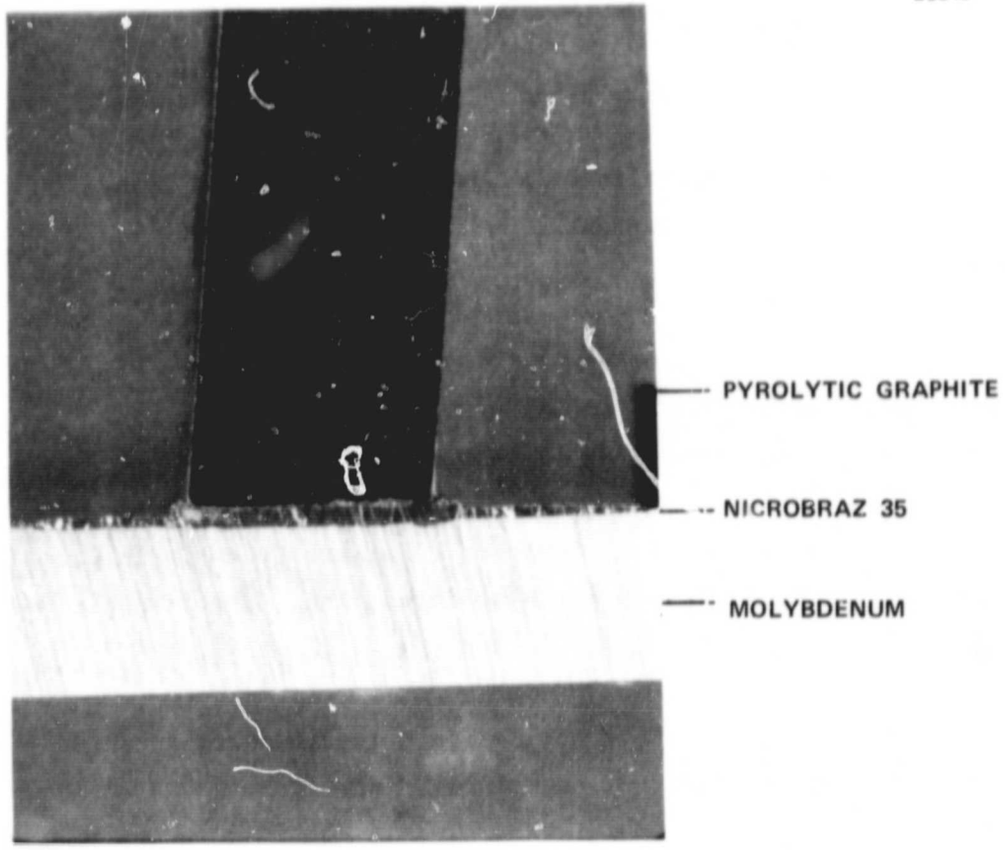

Figure 2.6-23 Transverse - section of PG to molybdenum joint brazed with nicrobraz 35. Mag. 10X.

E3650

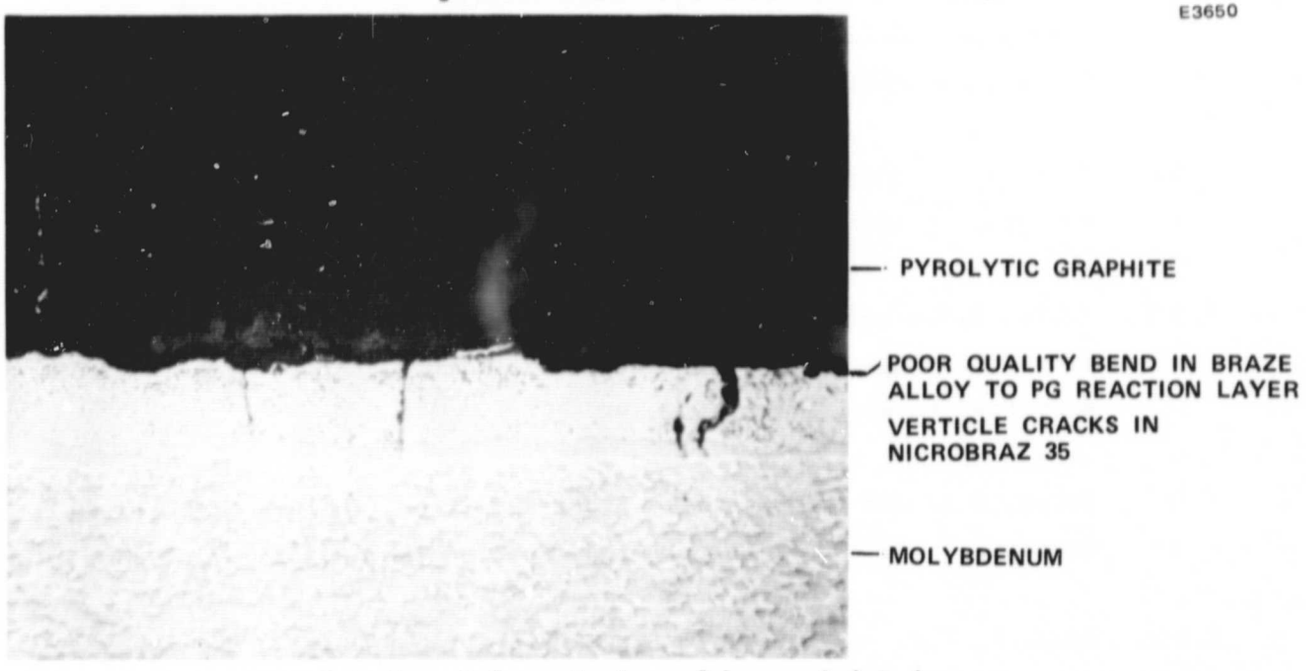

Figure 2.6-24 Enlarged view of braze joint in Figure 2.6-20. Mag. 50X.

REFERENCES

2.3-1. Buch, J.D. Structure-Properties Relationships in Advanced Carbon Materials. Aerospace Corporation, Report TOR-0079 (4726-04)-1, 25 September 1979.

2.3-2. Buch, J.D. "Mechanical Behavior Model for Graphites." Properties Related to Fracture Toughness, American Society for Testing and Materials, ASTM STP 605, 1976, pp. 124-144.

2.3-3. Buch, J.D., J.G. Crose, and E.Y. Robinson. Failure Criteria in Graphite Program. Prototype Development Associates, Inc., Report AFML-TR-77-16, March 1977.

2.3-4. Buch, J.D. Material Development and Design Guidelines for Advanced Graphite. Prototype Development Associates, Inc., Report PDA TR 1063-04-13, October 1976.

2.3-5. Jones, R.M. Nonlinear Multiaxial Modeling of Graphitic and Carbon-Carbon Materials. Air Force Materials Laboratory, Report AFML-TR-76-215, December 1976.

2.3-6. Fortner, J. Biaxial Tensile Fracture of ATJ-S Graphite. Air Force Materials Laboratory, Report AFML-TR-74-262, March 1975.

2.3-7. Pears, C.D., and H.S. Starrett. Polygraphites Subjected to Temperature Stress Loadings. Southern Research Institute, Report AFML-TR-73-59. Submitted to AFML March 1973.

2.3-8. Meyer, R.A. and J.E. Zimmer. Final Report on 'Failure Criteria in Graphite." Aerospace Corporation, Report ATR-74-(7425)-3, 10 May 1974.

2.3-9. Batdorf, S.B. A Polyaxial Stress-Strain Law for ATJ-S Graphite. Aerospace Corporation, Report SAMSO-TR-75-39, 28 January 1975.

2.3-10. Forney, D.M. Jr. (ed). Graphitic Materials for Advanced Re-entry Vehicles - Part I. Analytical Techniques and Materials Characterization. Air Force Materials Laboratory, Technical Report AFML-TR-70-133 (Part I), August 1970.

2.3-11. King, K.R., J.O. Bird, and J.R. Bohn. Thermal Stress Behavior of Polycrystalline Graphite - Part I. Air Force Materials Laboratory, Technical Report AFML-TR-71-152, July 1971.

2.3-12. King, K.R., J.O. Bird, and J.R. Bohn. Thermal Stress Behavior of Polycrystalline Graphite - Part II. Biaxial Fracture of ATJ-S. AFML-TR-71-152 Part II, December 1971.

2.3-13. Smith, W.H. and D.H. Leeds, "Pyrolytic Graphite." Modern Materials, Vol. 7, 1970, Academic Press, pp. 139-221.

2.3-14. Pyrolytic Graphite Specifications 101-B. Super-Temp Operations, B.F. Goodrich, 8 March 1972.

2.3-15. Warren, J.W. and R.M. Williams. "Isothermal Chemically Vapor-Deposited (CVD Processing." Fourth National SAMPE Technical Conference, Palo Alto, California, 17-19 October 1972.

2.3-16. "PG" Pyrolytic Graphite Grade HPG. Union Carbide Corporation, Carbon Products Division, Bulletin No. 442-212 II.

2.3-17. Canonico, D.A., N.C. Cole, and G.M. Slaughter. "Direct Brazing of Ceramics, Graphite, and Refractory Metals." Welding Journal, August 1977, pp. 31-38.

2.3-18. Fox, G.W. and G.M. Slaughter. "Brazing of Ceramics." Welding Journal, July 1964, pp. 591-597.

2.3-19. Shobert, E.I. "Carbon and Graphite." Modern Materials, Volume 4, pp. 1-99, Academic Press, 1964.

2.3-20. Coffin, L.F. Jr. "Structure-Property Relations for Pyrolytic Graphite." J. America Ceramics Society, Vol. 47, pp. 473-478, 1964.

2.3-21. Higgs, P.H. et al. "Studies of Graphite Deposited by Pyrolytic Processes." Wright Air Development Division, Technical Report No. TR-61-72, pp. 37, 82, 85. May 1964.

2.3-22. Pappis, J. "Mechanical Properties of Pyrographite." Mechanical Properties of Engineering Ceramics (W.W. Kriegel and H. Palmour, eds), Wiley (Interscience), New York, 1961.

2.3-23. Gebhardt, J. and J.M. Berry. "Mechanical Properties of Pyrolytic Graphite." J.AIAA, Volume 3, pp. 302-308, 1965.

2.3-24. Slack, G. "Anisotropic Thermal Conductivity of Pyrolytic Graphite." Physical Review, Volume 217, p. 3, August 1962.

2.3-25. Mantell, L.L. Handbook of Carbon and Graphite, Wiley (Interscience), New York, 1968.

2.3-26. Crose, J.G. and R.M. Jones. SAAS III - Finite Element Stress Analysis of Axisymmetric and Plane Solids with Different Orthotropic, Temperature-Dependent Material Properties in Tension and Compression. Aerospace Corporation, Report No. TR-0059 (S6816-53)-1, 22 June 1971.

2.3-28. Forman, R. "Secondary-Electron-Emission Properties of Conducting Surfaces with Application to Multistaged Depressed Collectors for Microwave Amplifiers." NASA Lewis Research Center, Cleveland, Ohio. NASA Technical Paper 1097, November 1977.

2.3-29. Curren, A.N. "Thermal Characteristics of the 12-Gigahertz, 200-Watt Output Stage Tube for the Communications Technology Satellite." NASA Lewis Research Center, Cleveland, Ohio. NASA Technical Paper 1344, October 1978.

2.3-30. Smith, W.H. and D.H. Leeds, "Pyrolitic Graphite." Modern Materials, Vol. 7, pp. 139-221. Academic Press, Inc., 1970.

2.3-31. "PG" Pyrolitic Graphite Grade HPG. Technical Information Bulletin No. 442-212II, Union Carbide Corporation, Carbon Products Division. (un-dated).

2.3-32. Canonico, D.A., N.C. Cole, and G.M. Slaughter. "Direct Brazing of Ceramics, Graphite and Refractory Materials," Welding Journal, pp. 31-38, August 1977.

2.3-33. Hammond, J.P. and G.M. Slaughter. "Bonding of Graphite to Metals with Transition Pieces." Welding Journal, Vol. 50, No. 1, pp. 33-40, January 1971.

2.3-34. White, J.L. and J.M. Poutelandolfo. "Hot-Worked Liquid Carbide (HWLC) Graphites Prepared by Hot-Working Extended Stock." Carbon, Vol. 6, pp. 1-6, 1968.

2.3-35. Gosset, P. and E.D. Maloney. "12 GHz TWT for TV Broadcasting." Microwave Journal, Application Note, pp. 47-48, July 1978.

2.3-36. Seunik, H., F. Hanf, and S. Wallender. "A 700 W 12 GHz TWT for TV Satellite Applications." Source unknown.

3.0 ELECTRODE SUBASSEMBLY FABRICATION

Upon receipt of the pyrolytic graphite electrodes and the copper support rings, development of the techniques for brazing the subassemblies was initiated. The first subassembly was made employing varying lengths of 2 mil thick Ticusil braze forms that were formed in a "C" shape and placed over the ends of the tabs formed by the slots in the copper rings (See Figure 3.0-1). Because the thermal expansion of the PG in the radial direction is significantly less than the copper, the joint design for a proper fit at the brazing temperature results in the PG part overlapping the copper at room temperature. During the heating part of the braze cycle, the copper expansion causes a sliding action between the PG and the braze alloy form. The varying length of the braze forms were employed to determine the braze form configuration that would withstand the translation of the parts and produce a satisfactory joint.

Since the first braze was primarily to establish the techniques for making the subassembly, a PG electrode that was only 20 mils thick and had a crack in the area of the beam hole was used. Also, the various braze forms were tack bonded to the copper ring with Lucite. The braze cycle involved heating in vacuum of 10^{-4} Torr to 890°C, holding for five minutes and cooling rapidly. It was noted that the Lucite contributed significantly to the outgassing during the heating up to 600°C.

The two shortest braze forms were dislodged and fell out of the joint as a result of the expansion of the parts during the heating cycle (See Figure 3.0-2). The other 14 joints were brazed, but several exhibited a dark residue believed to be from the Lucite. There was no evidence of any change in the crack after brazing. No other cracks formed in the PG even in the area where the PG was forced to return to the original copper overlap position where the braze forms had been dislodged.

Based on the favorable results of the first assembly, the second brazed subassembly was made using a PG electrode of the proper thickness (57 mil). The braze forms were all made large enough to assure that they would not be dislodged during the heating cycle, and Lucite was not used.

E3651

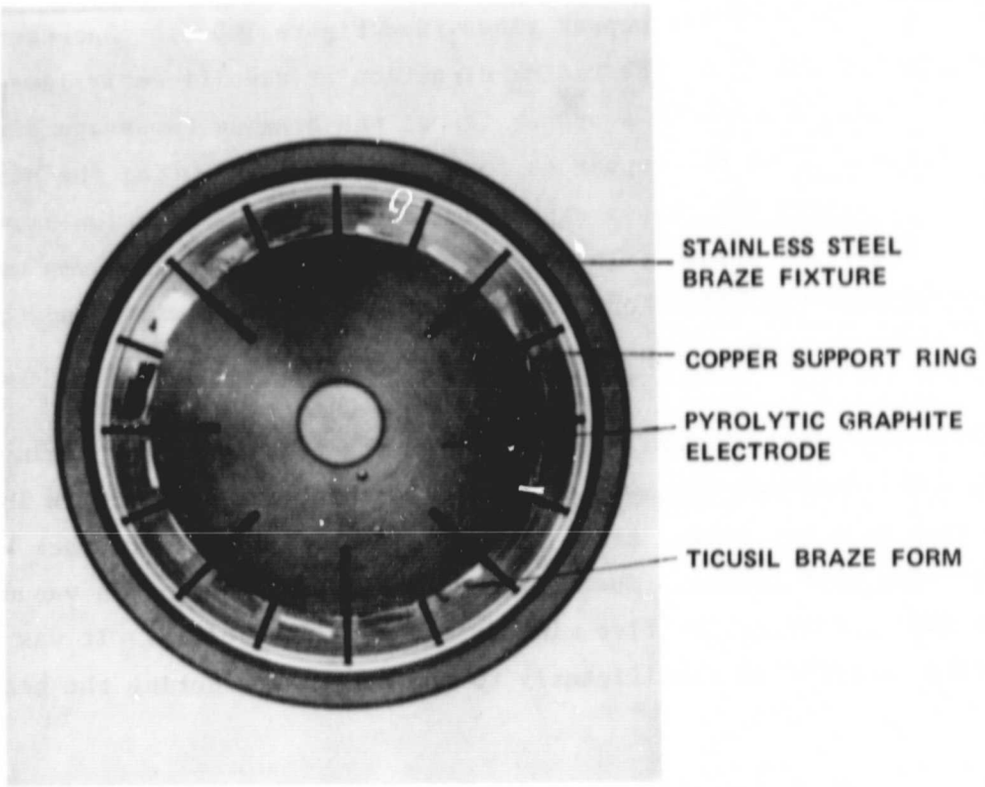

Figure 3.0-1 PG collector subassembly in braze fixture prior to brazing. Note: Varying braze form lengths on copper tabs of support ring. Mag. 1.1X.

E3652

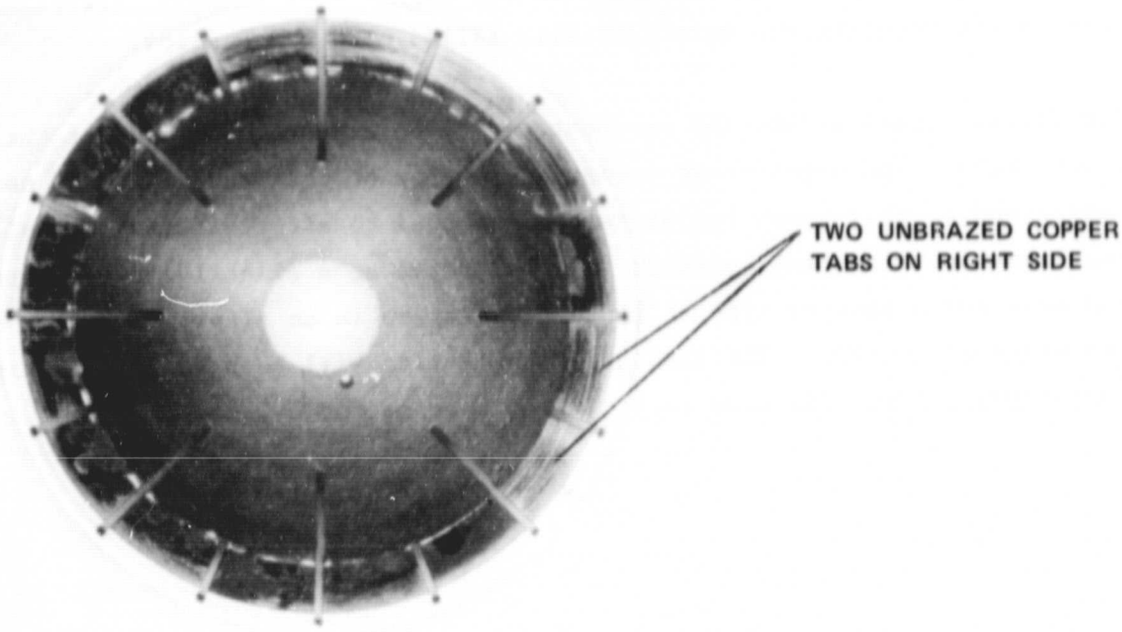

Figure 3.0-2 Top view of first brazed subassembly consisting of PG electrode (center) brazed to outer copper support ring with Ticusil braze alloy. Mag. 1.4X.

The braze cycle involved heating in a vacuum 10^{-4} Torr to 890°C, holding for five minutes, and cooling slowly. With the absence of the Lucite, significantly less outgassing was observed during the heating cycle.

All 16 tabs exhibited good braze joints, and there was no dark residue (See Figures 3.0-3 and 3.0-4). There was no indication of new crack formation in the PG electrode. Several of the slots in the copper that were not opposite to a slot in the PG electrode were partially filled with braze alloy.

The Ticusil braze alloy flow was observed to be extensive on some of the copper tabs. The significant variation in flow of the braze alloy is not understood at this time, but it is not expected to affect the functional requirements. The next assembly will be brazed at a slightly lower temperature and held for a shorter time at braze temperature in an effort to better control the braze alloy flow. The brazing subassemblies will be used to establish the techniques for brazing them into a ceramic collector cylinder.

E3653

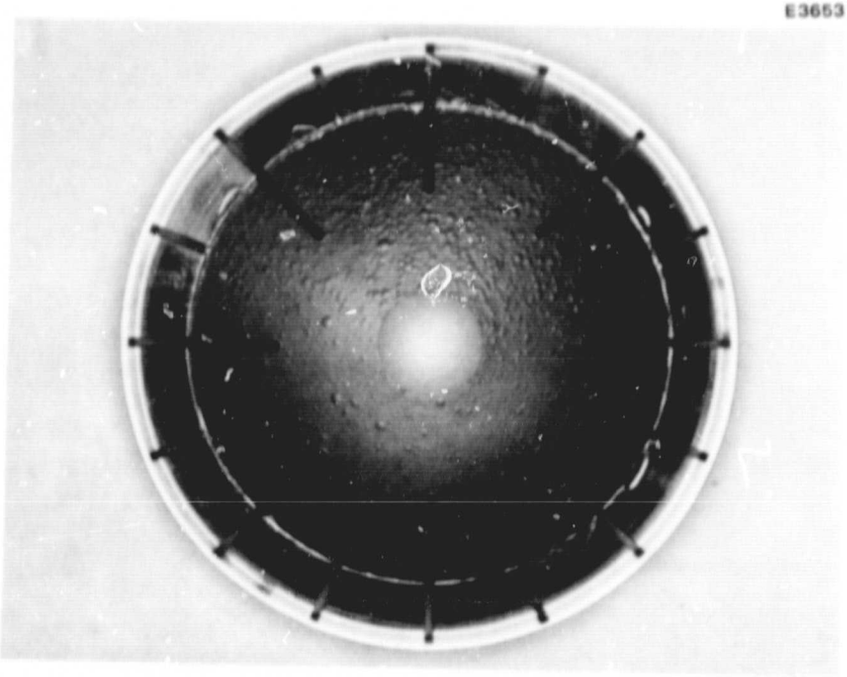

Figure 3.0-3 Top view of second brazed subassembly illustrating braze joints between the PG electrode and the 16 copper tabs on the copper support ring. Mag. 1.4X.

E3654

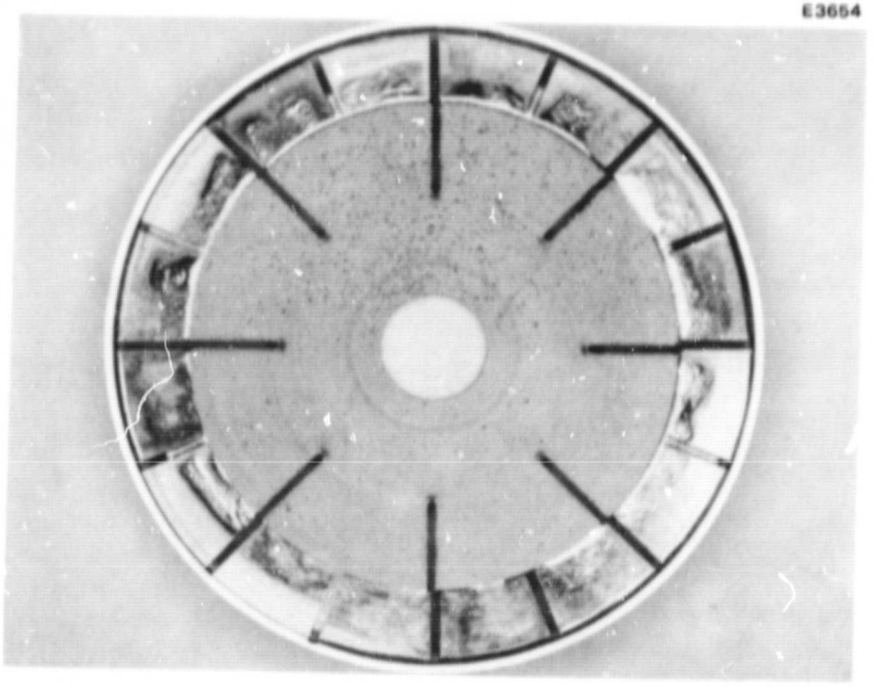

Figure 3.0-4 Bottom view of subassembly shown in Figure 3.0-3. Mag. 1.4X.

4.0 CONCLUSIONS

The purpose of this program was to investigate the important physical properties of pyrolitic graphite, to formulate the necessary design criteria and to develop effective fabrication techniques for use of this material in multi-stage depressed collectors.

The program objectives were all satisfactorily met and subassemblies of a typical multi-stage collector were successfully fabricated using vacuum brazing with Ticusil.

The pyrolitic graphite electrodes were fabricated to the desired configuration by Super Temp Co. using their standard manufacturing methods. Some difficulty was encountered in the final machining of these electrodes, particularly cutting the stress relief radial slots. This machining operation caused material cracks and delamination in some of the electrodes.

Vacuum brazing using Ticusil, an alloy comprised of 26.7% Silver, 4.5% Copper, Titanium was found to produce excellent brazed interfaces between the pyolytic graphite and the copper supports. The brazing time/temperature schedules and assembly techniques were perfected after only 3 attempts. Circumferential cracks were noticed on one of the assemblies but did not appear in subsequent units.

The brazed collector subassemblies were subjected to several thermal cycles with excursions in excess of 600^{o}C. No significant degradation was observed in any of the assemblies.

Limited vibration tests were performed on the subassemblies with no deleterious effect observed. NASA Lewis has performed extensive vibrational analysis of P.G. subassemblies with no major problems occuring.

In conclusion pyrolitic graphite appears to be an excellent material for electrodes in multi-stage depressed collector.

5.0 RECOMMENDATIONS

As a result of the investigations carried out on this program, Hughes EDD makes the following recommendations for further work:

1. Additional work should be performed to eliminate the stress relief slots in the pyrolitic graphite electrodes. This would reduce both both the cost of the electrodes and the possibility of cracking and delamination of the material. Some modification of the copper supports may be required.

2. A study of alternate pyrolitic graphite to ceramic interface designs should be undertaken. HEDD has been successful in brazing copper electrodes into ceramic cylinders using an "offset wave fin" configuration. This approach may also be applicable to pyrolitic graphite electrodes with a resulting cost savings and improved reliability with thermal cycling.

3. Work on improving the purity and reproduceability of pyrolitic graphite electrodes should be continued.

4. A complete multi-stage collector assembly using brazed pyrolitic graphite electrodes should be fabricated and evaluated on a working TWT to demonstrate the total feasability of the design. A life test with on/off cycles should also be performed.